Summer 7-27-2017

A Numerical Investigation of the Implications of Altered Channel-Floodplain Connectivity on Hydrodynamic Flood Wave Processes

Colin F. Byrne
University of New Mexico - Main Campus

Colin Francis Byrne
Candidate

Civil Engineering
Department

This dissertation is approved, and it is acceptable in quality and form for publication:

Approved by the Dissertation Committee:

Mark Stone, Chairperson

Julie Coonrod

Ricardo González-Pinzón

Grant Meyer

i

**A NUMERICAL INVESTIGATION OF THE IMPLICATIONS
OF ALTERED CHANNEL-FLOODPLAIN CONNECTIVITY
ON HYDRODYNAMIC FLOOD WAVE PROCESSES**

by

COLIN FRANCIS BYRNE

B.S., Zoology, University of Wisconsin-Madison, 2006
M.S., Biological Systems Engineering, University of Wisconsin-Madison, 2009

DISSERTATION

Submitted in Partial Fulfillment of the
Requirements for the Degree of

**Doctor of Philosophy
Engineering**

The University of New Mexico
Albuquerque, New Mexico

December, 2017

DEDICATION

To all teachers who have helped me learn, grow, and achieve.

ACKNOWLEDGEMENTS

A NUMERICAL INVESTIGATION OF THE IMPLICATIONS OF ALTERED CHANNEL-FLOODPLAIN CONNECTIVITY ON HYDRODYNAMIC FLOOD WAVE PROCESSES

by

Colin Francis Byrne

B.S., Zoology, University of Wisconsin-Madison, 2006

M.S., Biological Systems Engineering, University of Wisconsin-Madison, 2009

Ph.D., Engineering, University of New Mexico, 2017

ABSTRACT

With severely altered rivers throughout the developed world, hydrodynamic processes and floodplain connectivity have changed drastically. The research presented here focuses on quantification of two hydrodynamic processes: flood wave attenuation and channel-floodplain fluxes. Objectives of the three research chapters were to (1) evaluate how the ecosystem service of flood wave attenuation has changed with the implementation of river engineering practices as well as contemporary river restoration efforts, (2) describe the sensitivities of flood wave attenuation to contemporary and altered conditions, and (3) characterize channel-floodplain connectivity through lateral flux metrics. All chapter objectives were met using high-resolution, two-dimensional hydrodynamic modeling techniques conducted on the Rio Grande, New Mexico, USA. Models were created for historical, pre-restoration, contemporary, and altered conditions. Chapter 1 results indicate that historical conditions provided more attenuation than contemporary conditions. Sudden storage of water creates attenuation and alters flood wave shape. Chapter 2 results suggest that attenuation is most sensitive to total area for flow and area available for water storage while also displaying differences in process between topographic and roughness alterations. Chapter 3 flux results show differences in mass and momentum flux due to anthropogenic impacts and inset floodplain feature types provide greater and more heterogeneous lateral connectivity. Results presented here have

implications for both anthropogenic flood control strategies and potential application to a myriad of ecological issues based in river connectivity and process-based science. Contributions of the dissertation include new methods for two-dimensional hydrodynamic modeling, improved metrics for attenuation research, and spatiotemporal description of channel-floodplain flux dynamics.

TABLE OF CONTENTS

LIST OF FIGURES

LIST OF TABLES

Chapter 1

Introduction

3.1. Motivation and Objectives

River science is defined by contributions from interdisciplinary fields including hydrology, geomorphology, and ecology. Seminal work in river science has sought to describe the linked nature of these systems through the connectivity of systems [*Junk et al.*, 1989; *Ward*, 1989; *Tockner et al.*, 2000; *Amoros and Bornette*, 2002; *Opperman et al.*, 2010; *Covino*, 2017], quantification of processes often for the purpose of river restoration [*Palmer et al.*, 2005; *Kondolf et al.*, 2006; *Beechie et al.*, 2010; *Wohl et al.*, 2015], and the economic importance of natural processes through the understanding of ecosystem services [*Costanza et al.*, 1997; *Brauman et al.*, 2007; *Costanza et al.*, 2014]. These topics in river science are inherently linked. Human needs have been at the forefront of river management for centuries and only relatively recently have efforts been made to understand ecological demands. Therefore, many river systems have been subjected to substantial alteration of connectivity and process leading to decreased ecosystem services. Quantification of river processes in the context of altered river hydrology, geomorphology, and ecology can provide context for historical and contemporary conditions and inform integrated anthropogenic- and ecologic-influenced river management strategies.

Lateral channel-floodplain connectivity drives exchange of water and associated hydrodynamic processes. While qualitative assessment of connectivity and associated processes has been described and refined for decades, quantification of these connectivity processes has typically been in the form of intense feature and reach field efforts [*Lane and Richards*, 1997; *Babaeyan-Koopaei et al.*, 2002; *Jones et al.*, 2014; *Scott et al.*, 2014], laboratory description of process [*Shiono and Knight*, 1991; *Myers et al.*, 2001; *Yang et al.*, 2007; *Vermaas et al.*, 2011], or modeling efforts with simplified river morphology [*Bousmar and Zech*, 1999; *Cao et al.*, 2006]. The combination of continued improvement in computational power, hydrodynamic models, and improved resources for

topographic and vegetation data acquisition improves modeling capabilities to describe both local feature and reach length processes. The applicability of two-dimensional hydrodynamics has been expressed in a number of ecological scenarios usually under steady flow conditions or time-series analysis [*Crowder and Diplas*, 2000; *Lacey and Millar*, 2004; *Crowder and Diplas*, 2006; *Jacobson and Galat*, 2006; *Daraio et al.*, 2010; *Carnie et al.*, 2016; *Stone et al.*, 2017]. While unsteady modeling further increases computational demands, there is compelling relevance to contemporary ecological strategies such as short term environmental flows and biogeochemical flood processes. Unsteady flow dynamics within modeled rivers are often ignored in favor of simpler, steady flow conditions. However, the dynamics with which floods interact with the floodplain geomorphology and ecology are of critical importance.

Incorporation of improved channel-floodplain dynamics is often the focus of contemporary integrated river management with the idea that floodplain storage of flood flows is an integral part of the attenuation process and essential to floodplain ecology [*Hudson and Middelkoop*, 2015]. Flood wave attenuation, an ecosystem service [*Brauman et al.*, 2007], is a reach scale process that accrues as a flood wave travels downstream. Previous research indicates the strong influence of water storage on the process of attenuation, but research is dominated by simplified conditions and one-dimensional modeling strategies [*Wolff and Burges*, 1994; *Woltemade and Potter*, 1994; *Jaffe and Sanders*, 2001; *Acreman et al.*, 2003; *Sanders et al.*, 2006; *Sholtes and Doyle*, 2010; *Fong et al.*, 2016]. New research indicates that floodplain connectivity has a substantial impact on flood wave shape [*Fleischmann et al.*, 2016]. This finding from gage analysis in combination with the call from previous work for two-dimensional hydrodynamic modeling in the process of flood wave attenuation displays a scientific need [*Wolff and Burges*, 1994; *Ghavasieh et al.*, 2006; *Sholtes and Doyle*, 2010]. Further, with high-resolution two-dimensional modeling now accessible, local feature scale processes which contribute to reach and basin scale attenuation can be analyzed as well.

Due to the applicability of attenuation and connectivity processes research in contemporary river management strategies, the goal within this dissertation was to quantify the hydrodynamics associated with short duration flood waves with a focus on how processes have changed through time due to both anthropogenic and climatic

alterations. Therefore, three specific objectives were set for each of the following three chapters:

1. Evaluate how the ecosystem service of flood wave attenuation has changed with the implementation of river engineering practices in the name of flood protection and water use as well as contemporary river restoration efforts
2. Describe the sensitivities of flood wave attenuation to contemporary and altered conditions representative of historical river manipulation
3. Characterize channel-floodplain connectivity through lateral connectivity metrics important in the consideration of biogeochemical processes

The following three chapters describe the research conducted to address each of the specific objectives. Each chapter was written as a standalone paper to be submitted to a scientific journal for publication. All chapter objectives were achieved using two-dimensional hydrodynamic modeling methods. Chapter 2 describes the impact of river engineering and restoration strategies on flood wave attenuation with a focus on three representative time periods within the Middle Rio Grande: a pre-engineered historical system, an engineered pre-restoration system, and a contemporary system including recent river restoration strategies. Chapter 3 focuses on statistically describing flood wave attenuation sensitivities to contemporary channel-floodplain conditions and understanding how specific alterations to the Rio Grande have impacted hydrodynamic processes. Chapter 4 switches focus from attenuation to local hydrodynamic processes to quantify mass and momentum flux at the channel-floodplain interface, and to compare lateral and longitudinal flow characteristics in a contemporary setting.

3.2. Broad Contribution of Research

With motivation for this research driven by fields of river science which focus on channel-floodplain connectivity, process-based understanding of river hydrodynamics, and ecosystem services important to anthropogenic river management strategies; the research presented here addresses each of these topics and extends the body of knowledge in each respective field. The contributions of the following three chapters are in the form of modeling methodologies, quantifiable hydrodynamic metrics, and new strategies for incorporating large-scale spatial and temporal analysis of processes.

The methods used were chosen to both inform river science within the Middle Rio Grande and improve methods for further study in other rivers as well. All portions of the dissertation were completed using two-dimensional hydrodynamic modeling techniques. Methodologies were implemented to create high-resolution computational meshes to represent the complexities of channel-floodplain connectivity and floodplain topography. With continually improving computational power, these types of hydrodynamic models have the ability to inform process on a local scale, but can now be run over considerably larger distances than in the past. Linking local feature dynamics with watershed and regional dynamics is critical to linking scientific understanding of hydrologic processes [*Harvey and Gooseff*, 2015], so the ability to model large areas, yet retain feature resolution, can drive this science forward and is displayed within this research.

While no model will ever completely replicate natural processes, the measurement of hydrodynamics along rivers in both time and space is extremely difficult at small spatiotemporal scales. Numerical simulation can complement empirical river science to a great degree [*Covino*, 2017]. Therefore, improvement and advancement of computational techniques must continue. Specific to this research, the implementation of scripting techniques to extract information at key locations of interests can help solve some problems arising from computational storage demands and thus inform specific questions of interest. In addition, this research displays the ability of high-resolution, two-dimensional modeling to capture hydrodynamic channel-floodplain processes that are not expressed in lower-resolution, two-dimensional models or one-dimensional, hydrodynamic models. While other modeling strategies are suitable for other topics such as flood mapping, quantifying hydrodynamics appropriately should use the more data-intensive techniques displayed here.

The research within this dissertation also presents metrics novel to flood wave attenuation. The attenuation metrics are complementary in that they help explain the processes which cause attenuation through the context of historical modeling (Chapter 2) and modeling of alterations to contemporary conditions (Chapter 3). Comparison of attenuation ratios and statistical analyses conducted within the attenuation chapters indicate the same processes occurring but from different quantification approaches. Therefore, the ratio metrics are valuable in the future application to other river systems

which will provide further context for flood wave management. Understanding of attenuation processes may be critical as integrated floodplain management and environmental flow implementation continue to be pursued. Unsteady flows are critically important to rivers, thus understanding of the processes impacting flood waves should be pursued for these interdisciplinary reasons.

Finally, the research informs hydrodynamic processes key to floodplain connectivity science. The novel approaches for both local and integrated mass and momentum flux represent new approaches for quantifying lateral channel-floodplain connectivity (Chapter 4). These flux metrics have been expanded in one approach to analyze lateral and longitudinal discharge relationships, however, the metrics have applicability to countless hydrologic, geomorphic, and ecologic studies. For example, quantification of lateral sediment and nutrient fluxes are critical to floodplain ecosystems, thus the addition of focused channel-floodplain flux quantities could prove to be extremely helpful in other fields.

3.2.1. Conceptual Model of Linked Nature of Dissertation

The three chapters of research presented here quantify hydrodynamic processes occurring along various scales during unsteady flow events. Along reach-scales, flood wave attenuation is dependent on the transfer of water and the dissipation of momentum as the unsteady pulse moves downstream. These reach-scale hydrodynamic processes are the result of the integrated local and feature-scale flux of mass and momentum. Figure 1.1 displays the topics of each chapter in relation to greater fields within river science. Flood wave attenuation and mass and momentum fluxes are dependent on lateral floodplain connectivity, which stems from hydrologic, geomorphologic, and ecological processes. In addition, attenuation and fluxes are influenced by the way in which rivers are managed, both historically and at present. In the context of broader fields of river science, flood wave attenuation is considered an ecosystem service in that natural mechanisms provide flood control for downstream locations. While mass and momentum flux accrue to create flood wave attenuation, upstream flood wave attenuation will also likely decrease downstream lateral fluxes. These hydrodynamic fluxes are important to biogeochemical processes occurring in the channel-floodplain system. Thus, each chapter has

applicability to, and improves understanding of, other fields of river science beyond the specific application. In addition, the techniques used for quantification of hydrodynamic processes within my dissertation advance computational methodologies in river science.
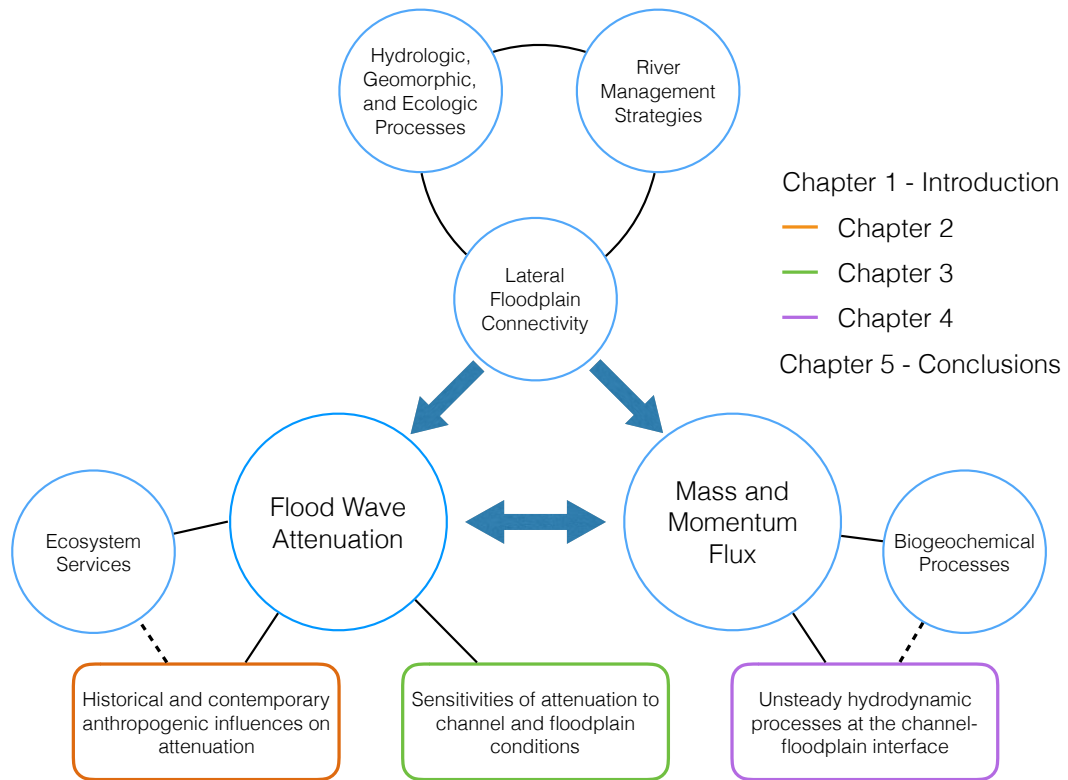
Figure 1.1. Conceptual model of dissertation research.

3.3. Modeling Environment

3.3.1. Deltares' D-Flow Flexible Mesh

All two-dimensional hydrodynamic modeling was conducted using the Netherlands-based Deltares' new D-Flow Flexible Mesh (D-Flow FM) [*Deltares*, 2015]. While several fully two-dimensional models now exist, D-Flow FM was chosen for a few reasons. First, the model has been verified as using appropriate and highly efficient numerical techniques to compute water depths and velocities. At the time this research began, we became beta testers in agreement with Deltares and were given access to both

a Windows graphical user interface (GUI) and Linux source code. The Windows GUI was used for mesh and boundary fabrication as well as runs of smaller models while the Linux source code was built on a supercomputer at the University of New Mexico's Center for Advanced Research Computing (CARC).

The availability of the source code was another reason D-Flow FM was chosen. While no alterations were ultimately made to the code, we were interested in the possibility that we could manipulate the code to only give model outputs in areas of interest, thus saving on computational storage with the large datasets produced by hydrodynamic models with high spatial and temporal resolution. While the source code was not manipulated, the availability of the source code allowed for improved understanding of how the model calculates hydrodynamics and the building of the model on university supercomputers.

The ability to partition a mesh and use parallel computing resources was the final reason that D-Flow FM was chosen over other available two-dimensional models. The goal of the modeling methodology was to implement modeling techniques in the fields of attenuation research and connectivity processes that captured large spatial and temporal scales. Therefore, high-resolution models were created which averaged 25 m^2 in element area. This produced contemporary models with nearly 800,000 computational elements and a historical model with nearly 3,900,000 computational elements. Main channel elements were curvilinear in form to promote efficient calculation of longitudinal discharge, and floodplain elements were predominantly triangular in shape to describe the complex topography of the floodplain. Main channel elements were curvilinear in form to promote efficient calculation of longitudinal discharge, and floodplain elements were predominantly triangular in shape to describe the complex topography of the floodplain and improve complex inundation dynamics.

The D-Flow FM solver techniques are driven by the fundamental shallow-water equations based upon conservation of mass and momentum. These equations are depth-averaged as the spatial and temporal horizontal scales are much larger than vertical scales and hydrostatic pressure distribution is assumed within D-Flow FM [*Deltares*, 2015]. The continuity equation, or conservation of mass, is defined by Equation 1.1, while Equations 1.2 and 1.3 represent the conservation of momentum in the x- and y-directions

[*Chaudhry*, 2007]. Within these equations h represents water depth, t is time, u is depth-averaged velocity in the x-direction, and v is depth-averaged velocity in the y-direction, g is the gravitational constant, S_{Ox} and S_{Oy} are the channel bottom slope in the x- and y-directions, respectively, and S_{fx} and S_{fy} are the friction slope in the x- and y-directions, respectively.

$$\frac{\partial h}{\partial t} + \frac{\partial (uh)}{\partial x} + \frac{\partial (vh)}{dy} = 0 \tag{1.1}$$

$$\frac{\partial u}{\partial t} + \frac{1}{2}\frac{\partial u^2}{\partial x} + \frac{\partial uv}{\partial y} = -g\frac{\partial h}{\partial x} + g[S_{Ox}\text{-}S_{fx}] \tag{1.2}$$

$$\frac{\partial v}{\partial t} + \frac{\partial uv}{\partial x} + \frac{1}{2}\frac{\partial v^2}{\partial y} = -g\frac{\partial h}{\partial y} + g[S_{Oy}\text{-}S_{fy}] \tag{1.3}$$

Within D-Flow FM, these equations are solved using finite-volume techniques implementing established k-ε turbulence closure methodology [*Deltares*, 2015]. With latitude, longitude, elevation, and roughness defined by the user, output data at each element includes h, u, and v. For calculation of friction losses, Manning's roughness coefficients were chosen for bed and vegetation roughness description with vegetation mapping and hypothetical conditions defining the spatial extents. One-meter topographic digital elevation models were interpolated to D-Flow FM mesh nodes using values nearest to mesh nodes. The mass and momentum equations were solved using a time-step dependent on a maximum Courant number of 0.7 (Eqn. 1.4), which allows for time-steps to vary based upon flow conditions. More specific description of mesh smoothing and orthogonalization methods and finite-volume mathematical techniques can be found in the D-Flow FM User Manual [*Deltares*, 2015].

$$0.7 \geq u\Delta t/\Delta x \tag{1.4}$$

3.3.2. Parallel Computing at CARC

The benefits of D-Flow FM would not have been achievable without collaboration from CARC. The supercomputers at CARC allow for research across all disciplines with a support staff that helps facilitate computational techniques. The staff at CARC built D-Flow FM allowing me to focus on the modeling methodologies. The D-Flow FM model was built on Ulam, a supercomputer at CARC which allows for tightly-coupled parallel computing. The parallel computing of a D-Flow model involves the partitioning of the entire model domain into smaller domains. These domains then simultaneously solve the

defining physical equations while overlapping in small areas to produce contiguous results.

The D-Flow FM GUI interface allows for the partitioning of a model into any number of domains. At the beginning of the modeling enterprise, a benchmarking study was implemented to determine the number of domains at which the models ran most efficiently. That is, at some point, small gains in computational speed may not support increased computational resources in the further partitioning of the models. Additionally, users on Ulam are limited to the number of computational nodes. Each node on Ulam has 8 individual processors. Substantial decreases in computational time were found by using up to 8 nodes (64 processors or model partitions). To most efficiently use Ulam nodes in addition to considerations about queue time in regard to node limitations, the majority of models were run on 4 nodes or 32 partitions. The exception was the historical model in Chapter 2 which was run on 8 nodes (64 partitions) due to the substantially greater number of elements in that model compared to contemporary models because of much greater lateral extents.

1.3.3. Model Validation and Uncertainty

To determine if the contemporary model used in Chapters 2 through 4 was appropriate for unsteady conditions within the reach of study, an unsteady hydrograph from September 13 – 18, 2013 was modeled. In addition, 1, 1.5, and 3-day segments of model results starting on September 13th were used to investigate the appropriateness of the contemporary topographic and roughness conditions on similar time-scales to those investigated in this research (Fig. 1.2). Topographic data was defined with 2010 and 2012 light detection and ranging data. Vegetation and Manning's roughness relationships from prior studies involving hydrodynamic modeling were utilized on the floodplain [*Mussetter Engineering*, 2002; *Adair*, 2016], while a channel roughness of 0.025 was defined. More specific contemporary model methodology is defined in Chapter 2 and topographic methods included in Appendix B. Using the Nash-Sutcliffe Efficiency (NSE), percent bias (PBIAS), and root mean square error-standard deviation ratio tests (RSR) [*Moriasi et al.*, 2007], the model returned satisfactory results for stage when compared to data recorded 14 river kilometers downstream at USGS 08330000

(Albuquerque gage) under all durations (Table 1.1). These results provided confidence for the modeling of short duration flow events within this dissertation. While having more events to validate the model would have been beneficial, events such as the September 2013 storm are rare, thus other storms were not of the same magnitude and less appropriate for validation.
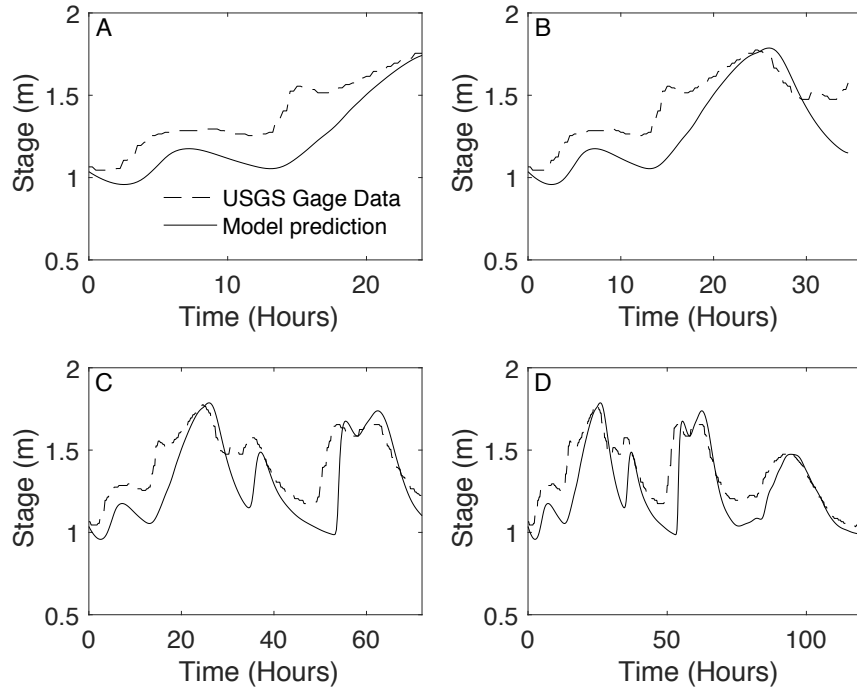
Figure 1.2. Unsteady flow validation of contemporary model for (A) 1-day, (B) 1.5-day, (C) 3-day, and (D) 5-day durations.

Table 1.1. Statistical results of contemporary model validation for four durations beginning on September 13, 2013.

	1-day	1.5-day	3-day	5-day
NSE	0.53	0.59	0.52	0.65
PBIAS	11.85	9.64	8.13	6.62
RSR	0.69	0.64	0.70	0.59

The validation of this contemporary model was deemed an acceptable level of performance for two reasons: (1) the gage data used for the upstream discharge boundary and downstream for statistical evaluation are subject to the uncertainty discussed in sand-bed river gaging strategies [*Isaacson and Coonrod*, 2011], and (2) the modeling

conducted in this research is predominantly theoretical in its application to river science, as opposed to a specific practical event. While any method of data collection is prone to error, the uncertainties associated with the computational modeling method must be addressed. Topographic uncertainty is likely highest within the main channel where one-dimensional cross-section elevation data were used to interpolate two-dimensional elevation data. Roughness uncertainty is inherent to two-dimensional, hydrodynamic modeling as roughness becomes an all-encompassing momentum dissipation mechanism due to the direct interpolation of latitude, longitude, and elevation information [*Lane and Richards*, 1998; *Morvan et al.*, 2008]. However, validation suggests methodology used within this dissertation creates topographic and roughness conditions suitable for addressing unsteady processes within the reach.

Uncertainties and sources of error were minimized as best as possible by utilizing the most detailed data available. With the contemporary model performing appropriately, historical and altered model scenarios were created with the same methodology where possible. No validation data were available for these events, however, the similarity in mesh creation techniques should provide appropriate results for era and alteration comparisons conducted within Chapters 2 through 4. A sensitivity analysis of the relationship between microtopography and roughness was conducted in Appendix A to better understand the relationship these factors have with unsteady flow modeling.

1.4. The Middle Rio Grande

The work presented in this dissertation focuses on a 32-km stretch of the Middle Rio Grande (MRG) which runs through Albuquerque, NM, and is known as the Albuquerque Reach. The Albuquerque Reach provides an excellent setting for research dealing with historical and contemporary influences on hydrodynamic processes as the river has been subjected to substantial alterations during the past century under the name of flood control, water use, and river restoration. As each chapter of the dissertation was written as a standalone scientific paper for publication, each includes a section with relevant facts about the MRG to place the chapter research into context.

While specific findings presented within this research will be most applicable to semi-arid, snowmelt driven river systems, the methods presented within the dissertation

are highly applicable to all river systems. Further, the quantification of the presented attenuation and flux metrics in other systems will be beneficial to the further understanding of how processes are both similar and different in various other types of systems.

Chapter 2

Implications of anthropogenic river alterations on the ecosystem service of flood wave attenuation

2.1. Introduction

River systems have provided important landscapes for societal growth throughout human history. However, the expansion of human land use, including agriculture and urbanization, and the methods employed for flood protection and water use (e.g. dams, levees, etc.) along river corridors have been to the detriment of ecological systems [*Baxter*, 1977; *Ligon et al.*, 1995; *Birkland et al.*, 2003]. Functioning environmental systems are known to provide ecosystem services, otherwise known as the benefits and economic value of environmental systems functioning with little to no human disturbance [*Costanza et al.*, 1997; *Daily*, 1997]. More specifically, economic benefits of terrestrial systems involving water are referred to as hydrologic services and include water supply, water quality, water damage mitigation, and cultural significance [*Brauman et al.*, 2007]. A floodplain, most often characterized as terrestrial land but often inundated during high river discharges, has been described as one of the most valuable terrestrial ecosystems [*Costanza et al.*, 1998, 2014]. Therefore, it is vital to put value on the consequences of human influence on floodplain ecosystems and river-floodplain processes.

Ultimately, the extent of hydrologic services and value associated with floodplains is based on periodic inundation of the floodplain. A river system with the ability to transport water onto the adjacent floodplain is said to have lateral floodplain connectivity [*Ward*, 1989]. This lateral connectivity is important in providing ecosystem services along any stretch of river. Because ecosystem services are based upon the idea that healthy ecosystems have a monetary value, ecological function and ecosystem services are inherently linked. An ecologically functioning floodplain has been characterized by three elements including connectivity as well as flow regime and a sufficient spatial scale for dynamic processes to occur and for benefits to accrue to meaningful levels [*Opperman et al.*, 2010]. Examples of ecological benefits on a well-connected, large-

scale floodplain subject to varying flows include fish recruitment [*Welcomme*, 1979; *Graaf*, 2003; *Balcombe and Arthington*, 2009], fish refugia [*Beesley et al.*, 2012], and riparian plant recruitment [*Corenblit et al.*, 2007; *Morrison and Stone*, 2014]. In turn, the same well-connected, large-scale floodplain would also produce quantifiable ecosystem services. Quantification of a single ecosystem service may therefore act as one indicator of floodplain connectivity and ecosystem health. Changes to the elements required for an ecologically functioning, heterogeneous floodplain (i.e. connectivity, flow regime, and sufficient spatial scale), will no doubt influence the ecosystem services provided as well.

One ecosystem service associated with floodplain connectivity and important for economic interests and public safety is flood wave attenuation [*Brauman et al.*, 2007]. Flood wave attenuation, or the process in which a flood wave is dampened and elongated as the wave moves downstream, has been linked to processes involving channel morphology, floodplain ecosystem conditions, and hydrologic regime of a system [*Woltemade and Potter*, 1994]. Physically, the process of flood wave attenuation entails momentum transfer through eddies at the main channel and floodplain interface, mass and momentum transfer from areas with different roughness characteristics, and floodplain water storage [*Archer, D. R.*, 1989; *Knight and Shiono*, 1990; *Helmiö*, 2004; *Vermaas et al.*, 2011]. Abrupt changes in topography, vegetation, and bed material at the channel-floodplain interface and complex floodplain topography indicate that lateral processes are crucial to flood wave attenuation processes. Geomorphic and ecological changes to river systems will no doubt influence both the local hydrodynamics and processes such as flood wave attenuation which are representative of the integration of these processes at longer river distances.

Anthropogenic alteration of river systems has existed along rivers for thousands of years. Prior to European settlement of North America, impoundments, diversions, and flood protection strategies were likely minimal in scale, thus having effects on local river dynamics, but less influence on longer reaches of river. However, large scale manipulation of river systems in the twentieth century, most notably through the construction of levees and dams [*Dynesius and Nilsson*, 1994; *Tobin*, 1995], has led to significant alteration of river hydrology and hydrodynamics [*Dynesius and Nilsson*, 1994; *Graf*, 1999], channel-floodplain geomorphology [*Syvitski et al.*, 2005; *Graf*, 2006],

14

biogeochemical exchange [*Thoms*, 2003], and river-floodplain ecology [*Ligon et al.*, 1995; *Shankman*, 1996; *Marston et al.*, 2005]. In addition, although motivation for river engineering is often based on flood control in the longitudinal and lateral directions, classic engineering approaches can be detrimental to environmentally-driven flood wave attenuation. Upstream channelization has been shown to produce greater flood peaks at downstream cross-sections than previously existed [*Acreman et al.*, 2003], while also causing downstream aggradation of channels, thus lowering flow capacity and increasing flood potential [*Shankman and Samson*, 1991]. Further, urbanization of river systems can increase flood peaks and shorten time to peak discharge [*Turner-Gillespie et al.*, 2003]. More recently, river restoration and rehabilitation strategies have become common and widespread in developed nations with improved understanding of natural processes along river corridors. While hypothetical rehabilitation of headwater streams has suggested greater attenuation is achieved with these strategies [*Liu et al.*, 2004], studies of rehabilitation along river corridors suggest that restoration and rehabilitation projects are not typically on a large enough scale to influence attenuation [*Sholtes and Doyle*, 2010]. With shifting strategies of river management from historical to contemporary time periods and attempts to alter historically degraded systems, understanding the impacts that river alterations have on flood wave attenuation can be a key indicator of the degree to which river process has changed through time.

Quantification of flood wave attenuation under historical river conditions is a difficult task due to a lack of data comparable to contemporary sources. Due to attenuation occurring on the scale of kilometers to hundreds of kilometers, modeling studies have mainly focused on methodologies that use cross-sectional information. Empirical studies have used stage and discharge measurements from gauged sites along rivers to study attenuation, including how changing river conditions influence attenuation [*Wong and Laurenson*, 1983; *McCartney and Naden*, 1995; *Jacobson et al.*, 2015]. While empirical studies benefit from real-time data and real-world measurements, this type of research is also inherently impacted by unquantifiable hydrologic inputs, hydrologic outputs, and the heterogeneity of river systems. Numerical modeling methods make assumptions and simplifications about highly dynamic environments, but modeling can also isolate surface water processes under a quantifiable framework. One-dimensional

(1D) modeling approaches have dominated numerical attenuation research [*Garbrecht and Brunner*, 1991; *Wolff and Burges*, 1994; *Anderson et al.*, 2006; *Cao et al.*, 2006; *Di Baldassarre et al.*, 2009; *Sholtes and Doyle*, 2010; *Fong et al.*, 2016]. However, 1D modeling simplifies channel-floodplain connectivity due to interpolation between cross-sections. Channel-floodplain interactions captured within two-dimensional (2D) modeling environments may provide more insight into flood wave attenuation than those captured under 1D conditions and 2D model performance has been found to be superior to 1D performance in predicting attenuation [*Ghavasieh et al.*, 2006].

Two-dimensional model applications to flood wave attenuation are rarer and predominant applications have been in hydrologic response and theoretical engineered attenuation research [*Jaffe and Sanders*, 2001; *Turner-Gillespie et al.*, 2003; *Ghavasieh et al.*, 2006; *Sanders et al.*, 2006]. Di Baldassarre et al. [2009] was successful in predicting historical inundation using a 2D model, however, this condition simulated a historic levee breach. It is our belief that a two-dimensional application has not been made in the context of how pre-engineering and contemporary anthropogenic changes to river morphology influence attenuation. High resolution two-dimensional, historical models, with computational elements on the order of meters, have been created for other applications to river science. For example, historical channel conditions have been studied to estimate changes in shallow-water habitat [*Jacobson and Galat*, 2006]. While high resolution, 2D meshes require substantial computational power, new numerical models and parallel computing power can provide the required resources for long lengths of river required for attenuation studies. With important processes occurring in both the longitudinal and lateral directions, it is believed a 2D modeling environment can provide important information for flood wave attenuation science.

The objective of this research was to better understand the influence of human alterations along the Rio Grande on the ecosystem service of flood wave attenuation. More specifically, this study quantified the impact of both historical river engineering strategies and more recent river restoration approaches on the flood wave attenuation metrics of discharge, river stage, inundated area, celerity, and hydrograph shape. To achieve these goals, three different periods of time along the Rio Grande, New Mexico were modeled: (1) a historical condition representing pre-engineered river conditions 80

to 100 years before present, (2) a pre-restoration condition representing river conditions 15 to 20 years before present, and (3) a contemporary condition. Hypothetical flood waves were modeled with normalized attenuation metrics that are applicable to rivers beyond the modeled system. A historical flood wave scenario was also modeled to better understand contemporary impacts to such a flood. Cutting-edge modeling methodology was implemented, especially in the description of topography with high mesh resolutions and parallel-computing techniques. Therefore, the methods and results quantified here can inform contemporary river science which has begun to focus on comprehensive strategies that include both classic river engineering approaches and natural processes which provide ecosystem services.

2.2. Site Description

Modeling for this study was conducted within the Albuquerque Reach of the Middle Rio Grande (MRG). As the name of the reach implies, this stretch of the Rio Grande passes through the city of Albuquerque (Fig. 2.1). Thus, the reach is the most heavily urbanized stretch of the river in New Mexico. The MRG has sustained concentrated Pueblo populations since the 1300s, however, only since the late 19th-century have anthropogenic alterations to the MRG and its associated watershed been of large enough scale to substantially alter natural river processes [*Scurlock*, 1998]. River engineering, here referred to as any human induced river alteration in the name of flood control or water use, in combination with a changing climate has led to significant channel narrowing, channel incision, and diminished accessible floodplain in the Albuquerque Reach [*Scurlock*, 1998; *Richard and Julien*, 2003; *Swanson et al.*, 2011]. More recently, human manipulations to the MRG and its floodplain have come in the form of river restoration projects. In this study, river restoration is in reference to strategies to improve ecological habitat, predominantly in the name of the endangered Rio Grande silvery minnow (*Hybognathus amarus*) and other endangered species [*Tetra Tech EM Inc.*, 2004]. Historical and contemporary changes to the MRG are therefore the focus of this paper. The MRG provides an optimal setting to address the continued call for quantification of river processes and ecosystem services as data are available dating back to nearly the time in which river engineering began.

17

The MRG lies in the semi-arid, southwestern United States where Rio Grande flow is in most years predominantly driven by snowmelt occurring in the mountainous regions of northern New Mexico and southern Colorado. The distinctive snowmelt pulse, historically occurring between April and June, produced numerous flooding occurrences throughout the Rio Grande valley now home to Albuquerque [*Scurlock*, 1998]. While the flood waves associated with the most severe floods are derived from snowmelt pulses along the river, these flood events take place over weeks and months and are unlikely to be attenuated within the reach of focus. More likely to be attenuated are shorter duration events either occurring on top of the snowmelt pulse or during the late summer months when monsoonal moisture creates short but intense storm events. Therefore, these shorter duration events were the focus of this research.

2.3. Methods

2.3.1. Model Overview

Hydrodynamic modeling was conducted with the Deltares' D-Flow Flexible Mesh (D-Flow FM) modeling program. The two-dimensional application of D-Flow FM is based on flexible, or unstructured, mesh development to describe the land surface. This allows for curvilinear, triangular, and polygon-shaped mesh cells to be included in the same mesh, which benefits the description of a river system. Selection of D-Flow FM was based on partitioning capabilities within D-Flow FM on Linux operated systems and parallel computing of developed modeling scenarios. Parallel computing was conducted on a super computer at University of New Mexico's Center for Advanced Research Computing (CARC). The ability to run models in parallel provides for a significant decrease in computational time. This allowed for large historical floodplains to be modeled in reasonable amounts of time but retain fine resolution mesh sizes. All meshes, introduced subsequently, were created to be comprised of approximately 40 m^2 sized elements (Table 2.1).

2.3.2. Historical Mesh Development

Historical model development consisted of data collection, processing, and integration from various historical sources in the city of Albuquerque. Floodplain contours from 1918, at a vertical distance of two feet, were collected from the U.S. Bureau of Reclamation (USBR) while limited 1936 and 1937 channel cross-section information was found from the Soil Conservation Service [*Adair*, 2016]. These two data sources were used in the creation of a digital elevation model (DEM). Although these data sources represent different years, the goal of the historical model development within this study was to create a representation of historical conditions prior to significant MRG river engineering rather than a specific year in history. River engineering refers to all anthropogenic features within the MRG, including levees, diversion dams, flood control dams, tributary dams, and river training devices that were constructed or installed in the name of flood control and water use. While the Rio Grande has been used for centuries for agricultural purposes and European settlement began in the 1500's [*Scurlock*, 1998], large scale river engineering to deliberately impact river flows and floodplain connectivity started shortly (~1930) after the acquisition of data (~1918) used in this study. It also must be noted that the hydrology and geomorphology of the Rio Grande had already been altered by land use changes within the greater watershed, although changing climate also likely had significant impact on hydrology and geomorphology as well [*Phippen and Wohl*, 2003; *Swanson et al.*, 2011; *Friedman et al.*, 2015]. With the arrival of the railroad in 1880, logging and grazing greatly altered the headwater landscapes within the MRG and is thought to have contributed to increases in runoff and sediment supply to the river. Due to these hydrologic and geomorphic processes, it may be that the historical condition presented in this study represents a condition with more lateral floodplain connectivity than was typical prior to landscape changes within the watershed. However, we believe the study of a historical condition prior to river engineering practices and the comparison of present conditions can raise important findings about quantified flood wave attenuation. The historical elevation DEM was interpolated to a mesh encompassing the entire historical floodplain, here referred to as the Historical Contour model (HC) (Fig. 2.1).

2.3.3. Pre-Restoration and Post-Restoration Mesh Development

Pre- and post-restoration mesh elevations were informed using 2010 light detection and ranging (LiDAR) data sourced from the Mid-Region Council of Governments. These data were acquired in the form of a one-meter DEM. The DEM was then manipulated in three ways to produce three different meshes for modeling: a pre-restoration mesh with floodplain topography based upon LiDAR data, a post-restoration mesh with floodplain topography based upon LiDAR data, and a post-restoration mesh with floodplain topography based upon smoothed 2010 elevations. These mesh boundaries are of more limited extent compared to the historical model as levees and bounding topography make the current accessible floodplain considerably smaller than the historical floodplain (Fig. 2.1). All channel bathymetry was produced using the same methods as those used for the historical mesh. In this case, USBR channel cross-sections from 2014 were used to interpolate channel bathymetry elevations. Lateral bounds of all three of these models are defined by either natural topography that was substantially higher than the active floodplain, or by levees or man-made berms. This research assumes a fixed bed and therefore does not address whether these man-made features would fail during the modeled flood waves.

The pre-restoration mesh was created using ESRI's ArcMap 10.1. First, boundaries of habitat restoration sites were acquired from the database of the Middle Rio Grande Endangered Species Collaborative Program. The habitat restoration sites of focus were those areas in which excavation or earth moving practices had been implemented. Along the bounding line, vertices were created and elevations were interpolated from the DEM. These elevations exist at a pre-restoration elevation. A triangulated irregular network (TIN) was created linking these bounding elevations creating an estimation of pre-restoration elevations. The TIN was then converted to a DEM and mosaicked into the 2010 DEM to produce a representative surface for a Pre-restoration, LiDAR condition (PL) which was then interpolated to the two-dimensional mesh nodes.

Post-restoration models were developed from the combination of 2010 and 2012 LiDAR DEMs, the latter also of one meter resolution. Because the 2010 LiDAR did not include several restoration sites constructed between 2010 and 2012, the DEM was supplemented with elevations from the 2012 DEM at those locations by extracting 2012

elevations within restoration bounds and creating a mosaic with the 2010 DEM. The resulting topography was interpolated to the same mesh as the pre-restoration mesh to study the influence of restoration sites on flood wave attenuation. This model is referred to as the Contemporary, LiDAR condition (CL).

A fourth mesh was created for comparison to the historical mesh to understand how river engineering practices have impacted attenuation. Because the historical topography was created from a two-meter contour map, the representative DEM lacked microtopography that would influence the calculated depth and velocity of water on the floodplain. Therefore, post-restoration topography was adjusted to represent present day conditions in a similar way to historical floodplain topography. To remove microtopography from the DEM, a 30-meter focal average was calculated for floodplain points within the bounding topography. In this way, levees and defining topography were not lowered, but the accessible floodplain surface was effectively smoothed to produce a more gradual surface characteristic of the historical mesh. The focal-average floodplain surface was combined with channel bathymetry and interpolated to the mesh with present day channel alignment and bounds to create a model comparable to the historical model. This model is referred to as the Contemporary Contour condition (CC).
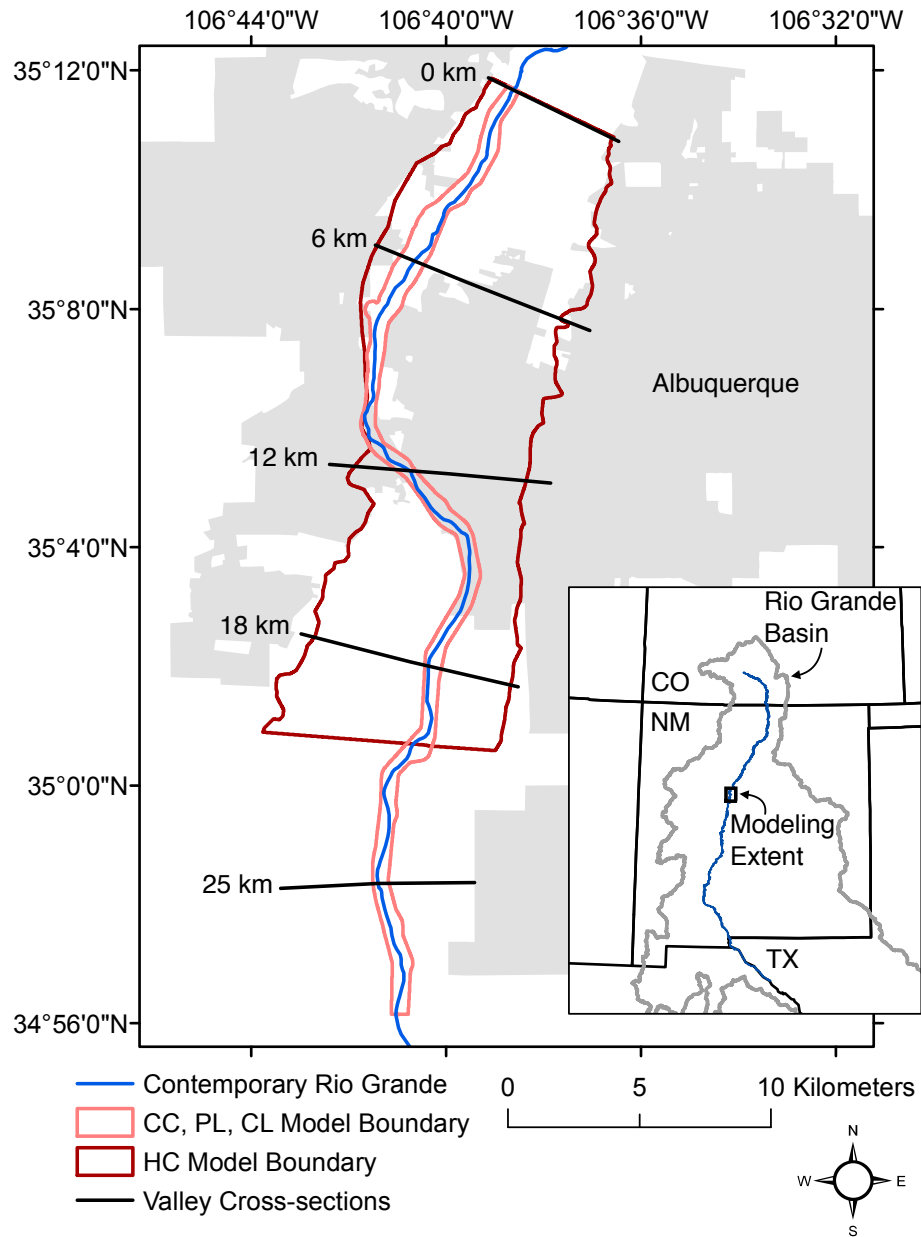
Figure 2.1. Mesh boundaries for historical (HC), pre-restoration (PL), and contemporary (CC, CL) models along the Albuquerque Reach of the Middle Rio Grande.

2.3.4. Modeled Hydrology

Hypothetical flood waves representative of discrete precipitation events were focus of this research. Three durations of flood waves, 1, 1.5, and 3 days, were modeled for two

initial conditions. Moderate flood conditions are defined by an initial flow of 30 m^3 s^{-1} and represent late summer monsoonal events on top of a wetted main channel. Major flood events are defined by greater initial conditions of 150 m^3 s^{-1} and represent a storm event occurring when the main channel is full and portions of the floodplain area already connected. This scenario would likely occur during spring snowmelt. Flood magnitude was set at 150 m^3 s^{-1} above initial conditions, resulting in 180 m^3 s^{-1} and 300 m^3 s^{-1} upstream flood peaks for the moderate and major flood events, respectively. Flood magnitudes are approximately representative of 5- and 50-year recurrence interval flood events.

In addition to the hypothetical flood waves, results are presented within this study for a historical flood event that occurred in 1942. The floods of the early 1940's are considered the last major floods within the Rio Grande valley as subsequent river engineering prevented more substantial flooding within the reach. Daily mean discharge data is used to represent the upstream flood hydrograph for this event. All modeled upstream flood waves are plotted alongside results for downstream flood waves.

2.3.5. Boundary, Initial, & Roughness Conditions

Upstream and downstream boundary conditions and initial inundation conditions were needed for unsteady, hydrodynamic modeling. Upstream boundary conditions were defined by the six hypothetical and 1942 historical flood waves. Because no rating curve existed for historical or contemporary downstream boundaries, downstream boundary conditions were set at a water surface elevation relative to the upstream peak flow conditions. In reality, this condition would be a dynamic stage-discharge relationship. Instead, the most downstream two kilometers, measured in valley length, of model results were removed. Results at this distance upstream were not impacted by changes in downstream water surface elevation. Initial inundation conditions for the unsteady flow events were set by steady flow simulations.

Roughness values for each model were spatially distributed. The two contemporary and pre-restoration models used roughness maps, which related to vegetation maps developed from both ground and aerial surveys [*Hink and Ohmart*, 1984; *Callahan and White*, 2004]. Manning's roughness values were then approximated

based upon the defining vegetation in conjunction with previous literature [*Chow*, 1959; *Mussetter Engineering*, 2002], and are recorded in previous literature [*Adair*, 2016]. Distributed historical roughness was defined by mapped 1918 land use and land type [*Bloodgood*, 1930; *Van Cleave*, 1935; *Adair*, 2016]. These land use, land types were then converted to Manning's roughness values using the same methods as the contemporary model.

Table 2.1. Summary of all models created for comparison of historical, pre-restoration, and contemporary Rio Grande conditions.

	Floodplain Topography	Channel Topography	Roughness Data Source	Hydrograph Distances (Figs. 2.2, 2.8)	Attenuation Ratio Distances (Figs. 2.4, 2.6-2.8)
Historical Contour (HC)	1918 contours (0.61 m)	1936-1937 cross-sectional surveys	1918 land use classification	18 km	18 km
Contemporary Contour (CC)	30-m focal-averaged smooth 2010 LiDAR with added 2010-2012 restoration site elevations	2014 cross-sectional surveys	Contemporary floodplain vegetation maps	18 km	18 km
Pre-restoration LiDAR (PL)	2010 LiDAR with raised 2000 - 2010 restoration site locations	2014 cross-sectional surveys	Contemporary floodplain vegetation maps	18 km	25 km
Contemporary LiDAR (CL)	2010 LiDAR with added 2010-2012 restoration site elevations	2014 cross-sectional surveys	Contemporary floodplain vegetation maps	18 km	25 km

2.3.6. Hydrograph Analysis

Hydrographs, perhaps the most common flood metric in the quantification and description of flood waves, were plotted at 18 km downstream for all flood waves and modeled scenarios. A distance of 18 km was used for all flood waves as it was the most downstream distance applicable for historical modeling outputs and thus provides a uniform means of comparison amongst all flood waves. Quantification of recorded peak discharge (Q_P), time to peak discharge (t_{Qp}), average celerity (c_{AVG}), and change in flood wave skewness (ΔS) was conducted for all flood wave scenarios. While peak discharge, time to peak, and celerity are all common flood wave metrics, changes in flood wave skewness were assessed to quantify changes to flood wave shape. As skewness has been been introduced as a metric of floodplain and wetland influence on hydrograph form [*Fleischmann et al.*, 2016], it was the goal of this metric to compare upstream and downstream hydrograph shape under the different river time period conditions. Methods for quantifying skewness are found in Fleischmann et al. [2016], and change in skewness, in this research, is defined by the difference between downstream (S_{DS}) and upstream (S_{US}) skewness values (Eqn. 1). The lowest one percent of flows above initial conditions were removed from skewness calculations in this research.

$$\Delta S = S_{DS} - S_{US} \tag{1}$$

2.3.7. Metrics of Attenuation

To quantify the impact of anthropogenic changes to the Middle Rio Grande on the ecosystem service of flood wave attenuation, three dimensionless metrics are included in this research. These metrics focus on peak discharge, peak stage, and inundated area associated with a flood event. Because it is important to understand how these metrics change when compared to other floodplain scenarios and for multiple flood events, the metrics in this study are normalized to steady flow conditions of the upstream boundary flood peak. Previous studies have discussed relative downstream attenuation or percent attenuated in terms of discharge [*Wolff and Burges*, 1994; *Sholtes and Doyle*, 2010], however normalization with steady peak flow conditions within this research allows for normalized comparison of attenuated stage and inundated area, in addition to discharge.

26

The normalization of peak discharge, peak stage, and inundated area produce what will be referred to in this paper as attenuation ratios for each metric and can be examined for various flood wave events and scenarios. The discharge attenuation ratio (QAR) and stage attenuation ratio (SAR) are presented in Equations 2 and 3, respectively.

$$QAR = Q_{p,i}/Q_{p,u} \tag{2}$$

Here $Q_{p,i}$ is the measured peak discharge ($m^3 s^{-1}$) at a defined distance downstream from the upstream boundary, while $Q_{p,u}$ is defined as the flood peak at the upstream boundary. In the case of floods presented here, $Q_{p,u}$ was either 180 m^3 s^{-1} or 300 m^3 s^{-1} depending on the flood wave modeled. For the historical flood wave, $Q_{p,u}$ was 583.4 m^3 s^{-1}.

$$SAR = \left(h_{p,i} - z_{min,i}\right)/\left(h_{S,i} - z_{min,i}\right) \tag{3}$$

Here $h_{p,i}$ is the water surface elevation of the flood wave at a defined downstream cross-section, i, $h_{S,i}$ is the water surface elevation under steady peak flow conditions at a defined downstream cross-section, and $z_{min,i}$ is the local minimum channel elevation at the cross-section.

To calculate the discharge and stage attenuation ratios, cross-sections and observation points recorded data within D-Flow FM. Because the Rio Grande channel has shifted between historical and contemporary conditions, in addition to the disconnection of a substantial portion of the historical floodplain through levee construction, downstream channel cross-sections and observation points would not be directly comparable between historical and present systems if measured at the channel center. Therefore, the data presented in this research records measurements based upon the locations of cross-sections plotted across the historical floodplain at 250-meter increments, referred to here as valley cross-sections. Observation points were located along these valley cross-sections at the middle of the respective channel of interest (i.e. historical or contemporary). Cross-sections measured discharge while observation points measured water surface elevation at ten minute increments during model runs. Due to the

availability of historical data, HC and CC data are presented through 18 kilometers downstream while CL and PL data are presented through 25 kilometers.

In contrast with discharge and stage metrics which are a function of distance downstream, inundated area is a two-dimensional property based upon distance downstream and lateral inundation. Therefore, calculations needed to be performed in a different manner. Data requirements are substantially greater in the collection of temporal inundation information, as a record of all mesh elements must be recorded instead of a select number of observation points or cross-section points. Thus, time steps of inundation outputs were of one hour from the point in time when the flood peak entered the reach to five hours after the flood wave left the reach. The purpose of the extra five hours was to give time for water to move across portions of floodplain further downstream. Total areas were then calculated based upon whether each element was inundated at any of the hourly time-steps. Area analysis was conducted based upon the locations of valley cross-sections. Inundated areas between cross-sections were assigned to the downstream cross-sectional distance at the same 250-meter increments. Flood wave inundation was then compared to inundation during steady model runs of upstream peak flow, 180 m^3 s^{-1} or 300 m^3 s^{-1}, to calculate an inundation attenuation ratio (IAR).

$$IAR = I_{p,i}/I_{p,u} \qquad\qquad\qquad (4)$$

Here $I_{p,i}$ is defined as the total inundated area for a specified cross-section at some distance downstream, while $I_{p,u}$ is the area inundated associated with steady upstream boundary peak flow conditions within the same cross-sectional area.

2.4. Results

Flood waves under HC conditions were attenuated to the greatest extent in all flood scenarios in comparison with the CC conditions (Fig. 2.2). The HC flood waves were attenuated between 1.2 and 2.1 times more than the CC flood waves at eighteen kilometers downstream. In combination with lower peak discharge, flood peaks under HC conditions also took longer to travel 18 km than flood waves under CC conditions. Specific flood wave timings and discharges are recorded in Table 2.2 to quantify the

28

differences in flood wave discharge, timing, and average celerity (c). On average, flood waves under HC conditions arrived 3.14 hours after CC modeled waves for all flood wave scenarios. Flood wave times were delayed to the greatest degree for short duration, moderate flood events; while increases in flood duration and magnitude led to more similar flood wave timing. As flood waves in the HC model were subjected to a substantially greater floodplain area, both the reduction in peak magnitude and the delay in peak discharge arrival result are intuitive with distributed floodplain flow. The CL and PL conditions display very similar results for both discharge and time to peak discharge for all flood wave scenarios, indicating that restoration features do not greatly influence downstream hydrographs. Average flood wave celerity over the 18 km distances was also calculated for all model conditions and flood wave scenarios (Table 2.2). Differences in HC and CC conditions were greatest for the short duration moderate event with average celerity 1 km hr^{-1} slower for HC conditions. However, for all flood waves average celerity was greater than 0.5 km hr^{-1} faster under contemporary conditions when compared with historical conditions. Average celerity was relatively unaffected with the inclusion of restoration sites throughout the reach.

In addition to quantifiable differences in flood peak and flood timing, flood wave shape is the last observable characteristic at 18 km. During moderate flood events, historical models display a distinct point of inflection on the rising limb, with 18-kilometer discharges rising at a slower rate earlier in the flood event than closer to peak discharge. This slower rising flood rate appears to be produced by the creation of a shoulder caused by floodplain storage. To further illustrate the alteration in historical shape, hydrographs are presented at various downstream distances for the 1-day, moderate flood event (Fig. 2.3). Shoulders have been documented in previous flood wave studies as a result of floodplain storage [*Garbrecht and Brunner*, 1991; *Wolff and Burges*, 1994; *Snell et al.*, 2004; *Costabile and Macchione*, 2012; *Fleischmann et al.*, 2016]. In contrast to many of the studies that report shoulders in downstream hydrographs, the shoulders here are much less defined and the form of these shoulders and hydrographs continue to adjust as the flood wave moves downstream. This can be attributed to the heterogeneity of the floodplain and channel-floodplain connections. However, the same process of the exceedance of an inundation threshold and the correlated instantaneous

29

inundation likely create these small shoulders only with more dynamic channel-floodplain interaction. The flood magnitude to which the main shoulder rises decreased and the time to the end of the shoulder increased with increased flood duration. The shoulder disappears altogether for major flood events.

Because only the HC, moderate flood events display extreme alteration of hydrograph shape, floodplain impact on hydrograph shape was also assessed by calculating the difference in skewness between upstream and 18 km downstream flood waves and documented in Table 2.2. The largest changes in hydrograph shape in terms of skewness value were strong positive changes produced in the HC, moderate flood scenarios. The CC model does not display substantial changes to the skewness value, while PL and CL models show positive skewness changes for 1 day events but minimal change for 1.5 and 3 day events. These results support the idea that skewness is representative of floodplain influence on hydrograph shape as HC conditions contain the most floodplain area and short duration flood waves should be the most susceptible to floodplain effects.
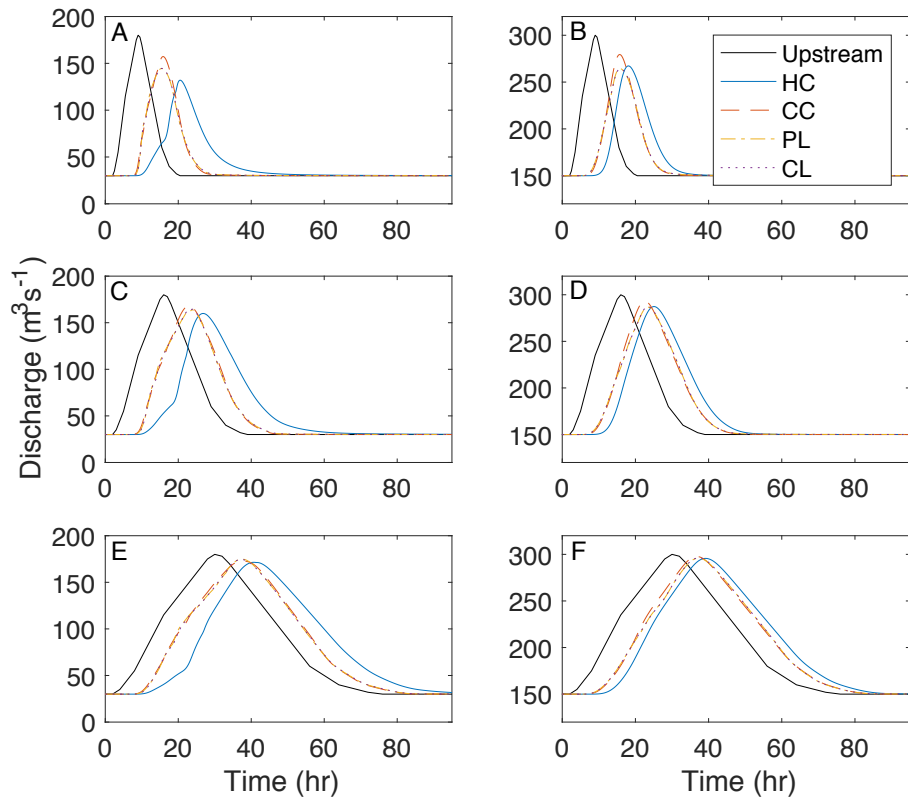
Figure 2.2. Upstream and 18-km hydrographs under all modeled scenarios for (A) 1-day, moderate, (B) 1-day, major, (C) 1.5-day, moderate, (D) 1.5-day, major, (E) 3-day, moderate, and (F) 3-day, major flood events.

Table 2.2. Recorded peak discharge (Q_p), time to peak discharge (t_{Qp}), average celerity (c_{AVG}), and change in flood wave skewness (ΔS) for all model conditions (HC, CC, PL, CL) and flood scenarios at 18 km downstream.

		Moderate Floods			Major Floods		
		1 day	1.5-day	3-day	1 day	1.5-day	3-day
Historical Comparison at 18 km	Q_pHC	132.0	159.9	171.5	267.2	287.3	295.7
	Q_pCC	157.3	168.0	173.0	279.4	293.0	297.7
	%ΔQ_p	16.1	4.8	0.9	4.4	1.9	0.7
	$t_{Qp}HC$	11.5	10.8	10.7	9.0	9.0	9.2
	$t_{Qp}CC$	6.8	7.0	7.5	6.7	6.5	6.8
	$\Delta t_{Qp}H\text{-}C$	-4.7	-3.8	-3.2	-2.3	-2.5	-2.3
	$c_{AVG}HC$	1.6	1.7	1.7	2.0	2.0	2.0
	$c_{AVG}CC$	2.6	2.6	2.4	2.7	2.8	2.6
	ΔS_{HC}	0.29	0.22	0.11	0.18	0.09	0.05
	ΔS_{CC}	0.05	0.00	-0.01	0.08	0.03	0.00
Restoration Comparison at 18 km	Q_pPL	144.5	163.8	174.9	264.5	286.7	295.9
	Q_pCL	144.6	164.5	174.5	264.1	287.3	296.2
	%ΔQ_p	0.1	0.4	-0.2	-0.1	0.2	0.1
	$t_{Qp}PL$	6.5	7.8	7.5	6.8	7.3	7.2
	$t_{Qp}CL$	6.5	7.8	7.2	6.8	7.5	7.3
	$\Delta t_{Qp}P\text{-}C$	0.0	0.0	-0.3	0.0	0.2	0.2
	$c_{AVG}PL$	2.8	2.3	2.4	2.6	2.5	2.5
	$c_{AVG}CL$	2.8	2.3	2.5	2.6	2.4	2.5
	ΔS_{PL}	0.15	-0.03	0.00	0.10	-0.03	-0.02
	ΔS_{CL}	0.16	-0.02	0.02	0.10	-0.03	-0.02
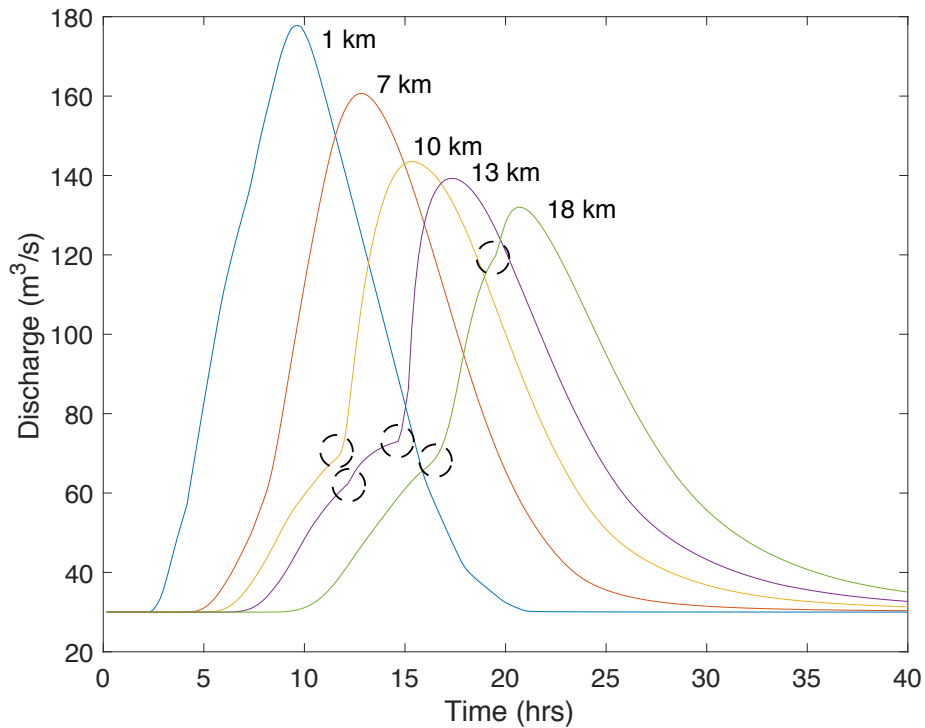
Figure 2.3. Historical model hydrographs at five cross-sections for the 1-day, moderate flood event. Circles mark notable points of inflection and shoulders along each hydrograph.

In comparison to temporal discharge at a fixed station downstream, QARs were plotted to describe changes to flood wave discharge as a function of distance downstream (Fig. 2.4). Discharge attenuation ratios for HC conditions at 18 km downstream ranged from 0.73 for the short duration, moderate flood event to 0.99 for the long duration, major flood event. As expected, moderate flood scenarios were more greatly attenuated than major flood events for all model conditions. While attenuation of discharge at 18 km was found to be greatest under historical conditions for all flood waves in comparison to CC conditions, the degree to which attenuation differs between the HC and CC scenarios is highly dependent on location within the reach. For example, in Figure 2.4C, the flood wave is attenuated to a greater extent under CC conditions than HC conditions between 6 and 8.5 km downstream. Fundamental to QAR dependence on downstream location, are stretches of river with substantial increases in attenuation. These greater rates of

33

attenuation are evident in the stepped decreases in QAR. In the short duration, moderate flood event (Fig. 2.4A), attenuation in the HC model occurs at high rates between two and three kilometers downstream and again between eight and ten kilometers. This attenuation becomes less clear with increasing duration and magnitude; however, the patterns do remain observable. In addition, while total attenuation decreases between moderate and major flood scenarios under the CL and PL scenarios, localized high rates of attenuation are observed to achieve similar magnitudes in both flood magnitudes. In Figure 2.4B, flood peak is reduced by more than 6% within a span of two kilometers. These high rates of attenuation are likely due to activation of the floodplain near peak discharge and in conjunction high rates of floodplain storage. This process is further described with stage and area attenuation metrics as well as spatial analysis of inundation.

Attenuation ratios were not impacted greatly by the implementation of habitat restoration scenarios. In fact, under moderate duration events, PL conditions created more attenuation than CL conditions, albeit by a very minimal margin. Although perhaps counterintuitive to initial hypotheses, this could be explained by the idea that restoration areas are constructed for inundation at a design discharge. If that design discharge is far enough below the flood peak, the feature will inundate before the flood peak arrives. Therefore, the feature will not provide storage during the highest flood discharges. In contrast, the pre-restoration surface may be raised to an extent in which it newly activates at or near the flood peak and therefore contributes to floodplain storage during the flood event. The addition of floodplain storage at or near the peak discharge appears to be most influential floodplain characteristic in the attenuation of flood waves along the MRG.

Figure 2.4. Discharge attenuation ratios (QAR) for all modeled conditions for (A) 1-day, moderate, (B) 1-day, major, (C) 1.5-day, moderate, (D) 1.5-day, major, (E) 3-day, moderate, and (F) 3-day, major flood events. The shaded downstream distances of the CL condition in 4B are investigated spatially in Figure 2.5.

To further describe the high rates of attenuation along certain lengths of the modeled reach, channel and floodplain depths were plotted at consecutive hourly time steps. Figure 2.5 displays both hydrographs and spatial inundation for kilometers 5 through 7 of the CL condition displayed in Figure 2.4B. The spatial inundation plots display the movement of the flood wave downstream and the downstream right floodplain becoming inundated with increasing time. It was the purpose of these spatial inundation plots to help explain the stepped decreases in QAR at localized stretches of river. Therefore, inundation at consecutive times are mapped to show the influence of floodplain storage on attenuation. Downstream distance of the flood peak is noted for each time step. The downstream right floodplain is not connected under initial conditions and only inundates as the flood peak moves through the sub-reach. Also evident is that inundation of much of the floodplain occurs after the flood peak has moved through the

35

reach. Furthermore, much of the bankline is predicted to remain dry during all time steps. Thus, the water inundating the area is being sourced from an upstream connection that only activates at flow levels near peak flow. All of this information suggests that the floodplain feature is acting similarly to a diversion off of the main channel. The flood water then travels at a slower rate on the floodplain due to floodplain topography and roughness and is stored on the floodplain until it ultimately reconnects with the main channel via a downstream connection. Flood hydrographs confirm the spatial findings as the floodplain pulse of water arrives at 7 kilometers after the bulk flow peak. In short, the very peak of the flood wave is essentially being removed off the top and diverted onto the flood wave. Because kilometers six and seven are disconnected at lower flows, the remainder of the flood wave moves through the main channel. Similar processes have been recorded in studies involving levee breaching for the purpose of downstream flood control [*Jaffe and Sanders*, 2001; *Sanders et al.*, 2006]. This study indicates that streambank levees may create channel-floodplain disconnection that ultimately leads to floodplain storage and flood wave attenuation when water surface elevations eclipse these surfaces at high flows.
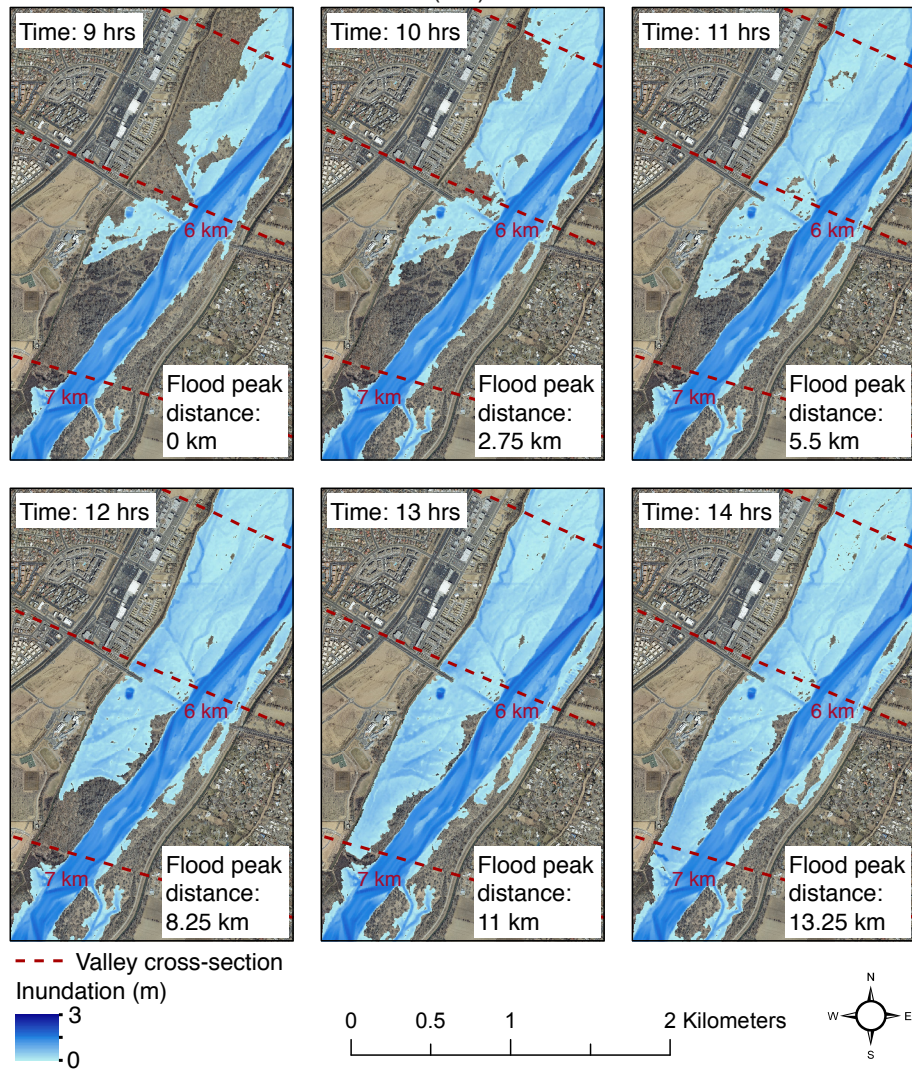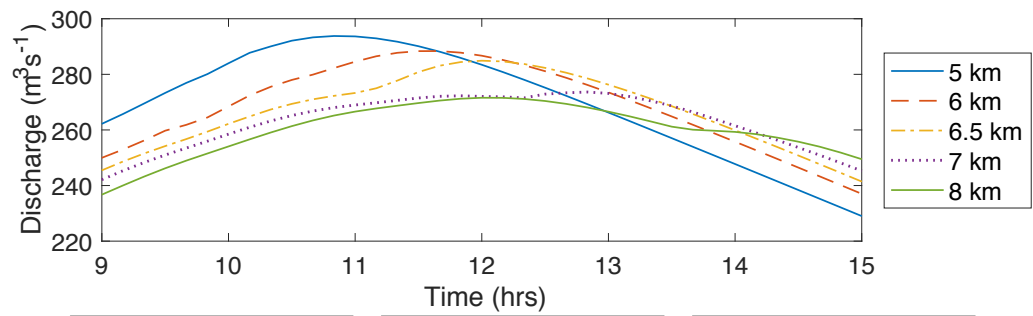
Figure 2.5. Spatial inundation of the 1-day, major flood event approximately 5 to 7 valley kilometers downstream in combination with hydrographs recorded at the same distances downstream.

The SARs for the six hypothetical flood scenarios were plotted as a function of downstream distance (Fig. 2.6). Two patterns are immediately observable in the SAR plots. First, SAR trends differ from QAR trends in that values do not decrease consecutively. That is to say, water surface elevation values are also dependent on local channel and floodplain characteristics leading to fluctuating SAR values as the flood wave moves downstream. Even with this relationship to the defining topography, SARs display trends under moderate and major flood conditions. Moderate flood conditions show an observable decreasing trend in SAR, but that trend is less observable as flood duration increases and thus discharge attenuation decreases. In comparison, under major flood conditions, attenuation of stage is more dependent on local attenuation of discharge. For example, in Fig. 2.6B, the LiDAR models exhibit large reductions in SAR at the same location where discharge was also attenuated greatly (Fig. 2.4B and Fig. 2.5). Second, while values have a tendency for spikes and troughs, the general trends accumulated over the entire reach show that water surface elevations are attenuated to a similar degree under HC conditions than CC conditions with the exception of the 1-day, moderate event. The fact that water surface elevations are not impacted to the same degree as discharge may be logical as the historical model has a far greater lateral floodplain, likely leading to smaller changes in water surface elevation as discharge is attenuation. In addition, the substantial discharge attenuation which occurs in the LiDAR models drives accompanied water surface elevation attenuation. The implication is that contemporary water surface elevations are altered to a lesser degree in the channelized, confined conditions and that microtopography is again important to modeling attenuation processes.
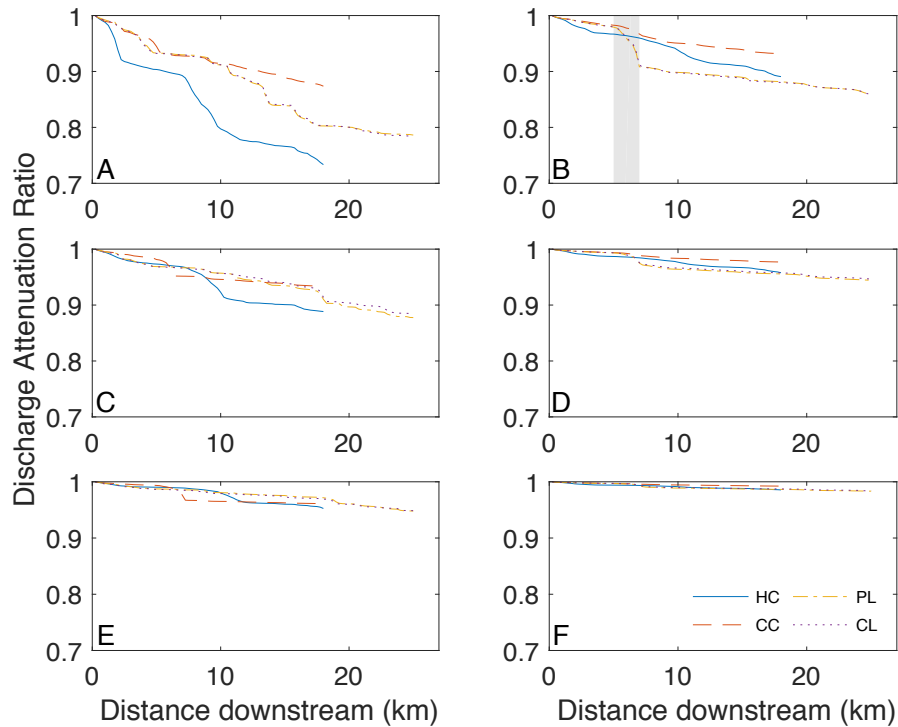
Figure 2.6. Stage attenuation ratios (SAR) for all modeled conditions for (A) 1-day, moderate, (B) 1-day, major, (C) 1.5-day, moderate, (D) 1.5-day, major, (E) 3-day, moderate, and (F) 3-day, major flood events.

The fraction of total inundated area under each flood wave to peak flow inundation, or IAR, is plotted in Figure 2.7. An IAR equal to one describes a floodplain area which inundates to the same extent that it would under steady upstream peak flow conditions. In all modeling scenarios, even those in which substantial discharge attenuation is occurring, certain lengths of the floodplain exhibited this characteristic. There are two possibilities to explain this phenomenon: (1) the portion of the floodplain connects at flows lower than peak discharge and thus has time to inundate during the flood wave, or (2) the floodplain is disconnected to an extent that it is minimally flooded at both peak discharge and during the flood wave. A reduction in IAR from one thus indicates that while areas of the floodplain will inundate under peak flow conditions, they do not inundate during the flood event. The lack of inundation is due to the lack of necessary time at the highest water surface elevations. In conjunction with the discharge and spatial attenuation analysis, it is these stretches of river that are to be expected to

39

contribute to attenuation to the greatest extent as the floodplain in these areas provides more area for active water storage at flood peak. The other possibility is that the flood wave has been attenuated to a degree in which the attenuated peak will no longer inundate the floodplain. These areas may then no longer contribute to further attenuation as connectivity has been removed by the attenuation process. Comparing plots in each respective column of Figure 2.7, increasing duration leads to less extreme decreases in IAR values, which arises from the increased in time to peak and thus allows for more area to become inundated.

The IARs for all flood scenarios in Figure 2.7 are most notably highly dependent on local floodplain connectivity in addition to attenuation of the flood wave. During moderate flood events (Fig 2.7A, C, & E), IARs for all modeling scenarios are highly variable. This suggests that the floodplains are actively connecting in some portions of the reach while other portions of the reach remain disconnected. It is likely more common during moderate flood events that values near one are representative of the condition in which the floodplain does not inundate under flood wave nor peak flow conditions. It is under these moderate flood conditions when floodplains within the reach are just beginning to connect. In comparison, during major flood conditions the opposite is to be expected to be true, in that the majority of available floodplain surfaces are already inundated when the flood peak arrives, thus the total amount of inundated area does not change. The IAR values also appear to be influenced by attenuation of discharge and, in conjuction, water surface elevation, at least for moderate flood events. While in the upstream portion of the reach, IAR values for moderate flood events rebound to one, at the most downstream portion of the reach, values appear to trend in a decreasing direction. The decreasing trend is less great as flood duration increases. This supports the idea that IAR values are being attenuated when QAR and SAR values display the same characteristic. In terms of process, the attenuation of discharge leads to decreases in water surface elevation, thus further limiting the extent of inundation beyond local topographic controls. Major flood events do not display this decreasing IAR trend, likely because the degree of flood wave attenuation is minimal.

Differences in IAR values between model conditions help describe differences in floodplain characteristics. While moderate flood conditions display the greatest changes

in IAR, there remain certain lengths of river that actively connect within the flood reach in all model conditions during major flood events. In the comparison of HC and CC conditions, it is apparent in decreased IAR values that the historical floodplain still has substantial lengths of river that do not inundate during the major flood events. These changes to IAR are of similar magnitudes to those recorded during moderate flood events. The substantially greater available floodplain area, observable in Figure 2.1, is also likely indicative of greater topographic heterogeneity on the floodplain. Therefore, even at major flood magnitudes, portions of the floodplain are still actively inundating. The CC models present minimal decreases in IAR for major flood events, indicating that much of the contemporary floodplain is inundated when a major flood event travels through the reach.

When the microtopography associated with improved topographic description (LiDAR) is included in the PL and CL conditions, IAR values display some magnitude of change along short distances of the reach. The heterogeneity associated with improved topographic description inherently will create more complex flow paths and thus more dynamic inundation patterns. Approximately a kilometer of the reach (~ 8 km downstream) is unable to fully inundate during major flood conditions, while the majority of floodplain is at or near an IAR value of one for both PL and CL conditions. While the general trends of IAR for the PL and CL conditions are similar, IAR values do display more notable differences between these two conditions than do QAR and SAR values. This is logical as topographic adjustment of the floodplain is likely to impact inundation patterns and timing. There are examples of both the PL and CL conditions having lower IAR values. A lower IAR value under PL conditions would suggest that the higher pre-restoration surface inundates at a higher discharge than the restoration site. Lowering topography as is done along the Rio Grande may also lead to connections to other portions of the floodplain thus allowing inundation of those areas at lower discharges as well. Therefore, relatively large differences in pre- and post-restoration inundation timing may occur. An example of this is likely evident in the major flood scenarios (Fig. 2.7B, D, F). In comparison, a lower IAR for CL conditions likely indicates that a restoration feature and connected areas activate near peak discharge, but do not fully inundate due to a lack of sufficient flood duration. Higher surfaces (PL conditions) would inundate to a

41

lesser extent under flood conditions, thus having values closer to one. Examples of this phenomena are evident in the moderate flood events at 9 km downstream (Fig. 2.7A, C, E). As duration increases in these plots, differences between PL and CL IAR values decrease, supporting this explanation of the driving process.
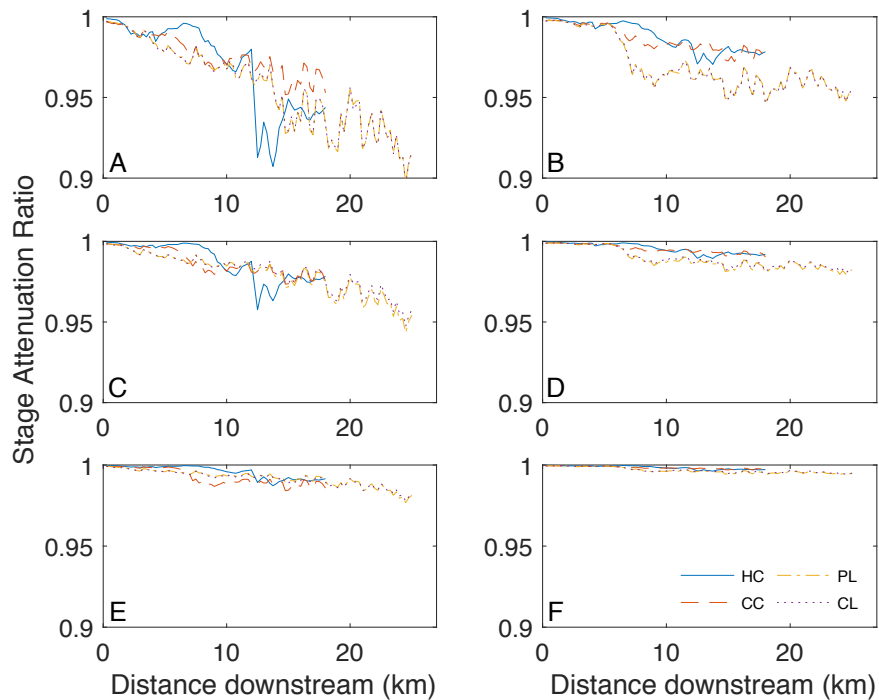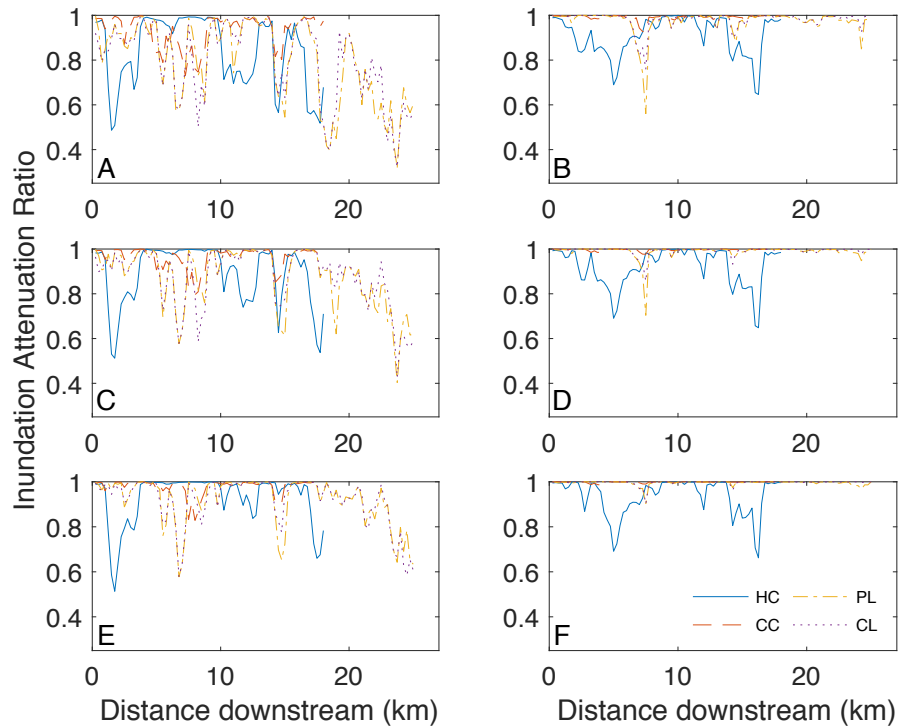

Figure 2.7. Inundation attenuation ratio (IAR) for all modeled conditions for (A) 1-day, moderate, (B) 1-day, major, (C) 1.5-day, moderate, (D) 1.5-day, major, (E) 3-day, moderate, and (F) 3-day, major flood events.

While hypothetical flood waves provide valuable information about flood wave attenuation processes, modeling of a major historical flood event and the comparison between systems provides valuable context for this research. Figure 2.8 displays the modeled results of the 1942 flood event using the same metrics presented for hypothetical flood waves. Flood wave attenuation was greatest for all metrics under HC conditions with the exception of SAR. Again, with flow distributed across a greater floodplain width, the lack of stage attenuation under historical conditions is expected. The

42

magnitude of attenuation for all metrics was smaller than hypothetical flood waves with the exception of HC model QAR and IAR values. A smaller magnitude of attenuation was expected as the 1942 flood magnitude was nearly twice that of the major hypothetical flood waves, but HC QAR and IAR ratios show greater attenuation than those resulting from the major, 3-day hypothetical flood wave. Calculation of QARs display low rates of attenuation for CC, PL, and CL conditions with approximately 1% decrease in peak discharge over the 18-km distance. While the HC model displays consistently lower QAR values, a sharp 1% decrease in QAR is also evident at 17 km downstream. The HC model also displays decreases in IAR in the downstream portion of the reach which likely contributes to the attenuation of discharge. All other model conditions display less than 5% decreases in IAR. These data promote the idea of a heterogeneous historical floodplain in that there are newly activating surfaces even at very large discharges which have the ability to attenuate flood waves. These results further suggest that under pre-restoration and contemporary conditions, storage effects on attenuation are inconsequential and hydraulic processes drive attenuation rather than geomorphic influences [*Åkesson et al.*, 2015]. For contemporary models, kilometers 5 through 8 were once again most influential to SAR. However, it should be noted that these changes are an order of magnitude smaller than those plotted for hypothetical flood waves in Figure 2.6. Thus, while kilometers 5 through 7 still have the most influence on SAR, the changes to water surface elevation were very small.

Discharge, time to peak, average celerity, and skewness are quantified in Table 2.3. Peak discharge under HC conditions was only slightly lower than CC conditions and time to peak in HC conditions was delayed to a smaller degree. Flood waves at 18 km downstream display similar shape to the upstream hydrograph and quantified changes in skewness were low. Celerity was increased in all model conditions from the hypothetical flood waves but remains almost a kilometer per hour slower under historical conditions compared with contemporary speeds. All changes in flood wave metrics are driven by the increased magnitude of the 1942 flood event. As this event occurred during the spring snowmelt pulse, even historical conditions had minimal impacts on attenuation of this event.
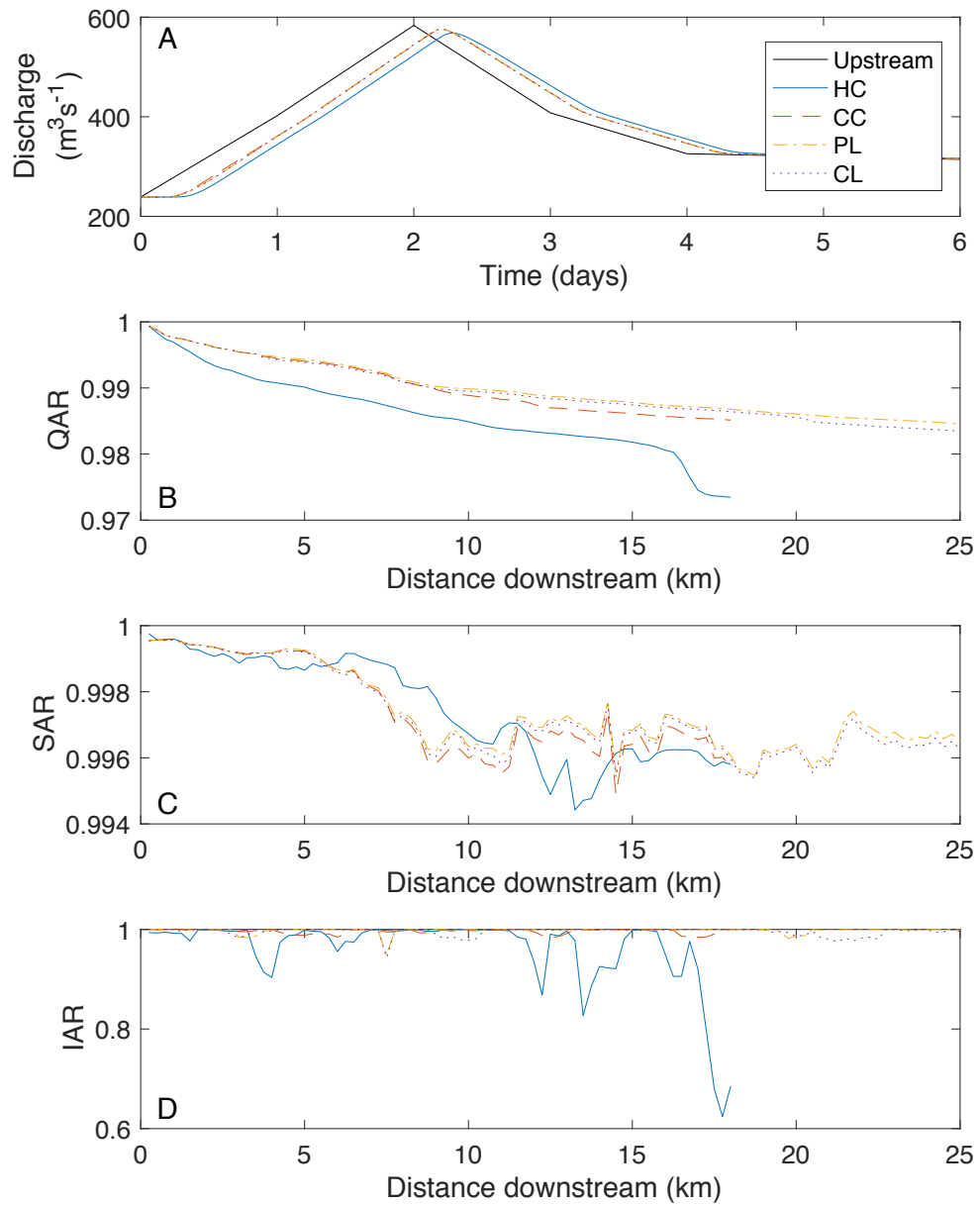
Figure 2.8. Downstream hydrographs and attenuation ratios for the 1942 flood event under all model conditions.

Table 2.3. Recorded peak discharge (Q_p), time to peak discharge (t_{Qp}), and average celerity (c_{AVG}) for all model conditions (HC, CC, PL, CL) under 1942 flood conditions.

		1942 Flood
Historical Comparison at 18 km	Q_pHC	568.2
	Q_pCC	575.0
	$\%\Delta Q_p$	1.2
	$t_{Qp}HC$	6.8
	$t_{Qp}CC$	5.0
	$\Delta t_{Qp}H\text{-}C$	-1.8
	$c_{AVG}HC$	2.6
	$c_{AVG}CC$	3.6
	ΔS_{HC}	0.03
	ΔS_{CC}	0.02
Restoration Comparison at 18 km	Q_pPL	576.0
	Q_pCL	575.7
	$\%\Delta Q_p$	-0.1
	$t_{Qp}PL$	4.8
	$t_{Qp}CL$	4.8
	$\Delta t_{Qp}P\text{-}C$	0.0
	$c_{AVG}PL$	3.7
	$c_{AVG}CL$	3.7
	ΔS_{PL}	0.03
	ΔS_{CL}	0.03

2.5. Discussion

Within this study, flood wave attenuation was quantified using normalized attenuation metrics to inform the influence of anthropogenic alterations along the MRG. Floodplain influences on Rio Grande attenuation have decreased with the implementation of historical river engineering as evident in flood wave shape, discharge, and timing at 18 km. As expected, discharge was attenuated to a greater extent under historical conditions than contemporary conditions. While attenuation of discharge decreased by a factor

between one and two under contemporary conditions, this leads to substantial decreases in discharge at downstream locations. Attenuation of stage was locally dependent on channel topography; however general trends indicate that water surface elevation was not attenuated to the same degree under historical conditions likely due to wide lateral floodplain connections and a less sensitive relationship between discharge and water surface elevation. The IAR results describe the heterogeneous topographic nature of the historical floodplain in comparison with the contemporary floodplain. While floodplain inundation is similar for moderate flood conditions, historical IAR results retain heterogeneity for major flood events, including the 1942 event, while the contemporary floodplain is almost uniformly inundated. As portions of the historical floodplain become newly connected during major flood events, those systems are likely to be of a different geomorphic and ecological characteristic than portions inundated at moderate flood levels. The attenuation metrics are presented as downstream ratios in the hope that such metrics can be applied to other systems. While alternative river systems will no doubt have different physical conditions leading to differences in process, the attenuation metrics may provide insights into how various reach or river characteristics influence attenuation. Rates of attenuation are modeled here for a heavily manipulated, sand-bed river flowing through a semi-arid landscape. Differences in hydrology, geomorphology, and ecology are likely to have significant influence on attenuation in combination with the scale of other rivers.

Discharge and stage attenuation are thought to be most greatly impacted by available storage on the floodplain. However, available area for inundation on the floodplain does not always produce substantial attenuation of a flood wave. This is evident for major flood events in the comparison of historical IAR values, flood wave hydrographs, and QAR values during major flood events. The IAR values for historical conditions indicate that there is storage available on the floodplain during major flood events. However, flood wave discharge, while attenuated to a greater extent in HC conditions than CC conditions, does not display the same magnitude of attenuation even with substantial area available. This is most likely because these areas are of the greatest hydrologic distance from the flow paths of greatest discharge (i.e. the main channel or a secondary floodplain channel). Because water surface elevations are attenuated to a

46

smaller degree, results predict that these small changes are likely to influence inundation of large areas as flood waves were historically attenuated. While the same areas will inundate under longer duration flood events than those of focus in this research, the areas contribute very little to attenuation. While not as important to the process of attenuation, these areas were likely still of ecological importance during the late-spring, early-summer flood pulse when elevated discharge can last for weeks to months. This further displays the topographic heterogeneity of the historical floodplain as portions of the floodplain activate continuously under dynamic conditions. Results here are complementary to qualitative descriptions of the historical Rio Grande floodplain which describe the floodplain as an environment with a myriad of ecosystems including wetlands and a channel subject to relatively frequent avulsions [*Scurlock*, 1998], a system drastically different than the cottonwood dominated contemporary floodplain.

Changes in historical hydrograph shape present the importance of floodplain heterogeneity in attenuation processes as the exceedance of inundation thresholds on certain floodplain surfaces provide physical storage, an important mechanism for attenuation. Previous research on flood wave shape has focused on compound channels with uniform geometry [*Garbrecht and Brunner*, 1991; *Wolff and Burges*, 1994; *Cao et al.*, 2006; *Ghavasieh et al.*, 2006; *Costabile and Macchione*, 2012; *Fleischmann et al.*, 2016]. The models presented here were constructed to retain channel-floodplain heterogeneity and floodplain complexity, even when microtopography data did not exist. This means that floodplain connectivity is highly dynamic both spatially and temporally depending on the defining hydrology. Results suggest that this heterogeneity is responsible for the multiple points of inflection and shoulders that are formed in the various downstream hydrographs presented in Figure 2.3. For example, at 13 km downstream, there appear to be two points of inflection, with one displaying shoulder attributes. However, as the flood wave moves further downstream, that shoulder becomes less evident, or washed out. Further, there is a new point of inflection at this location at a higher discharge. Research under uniform channel conditions suggests that shoulders are produced when discharge increases above bankfull discharge and flood volumes are stored instantaneously [*Garbrecht and Brunner*, 1991; *Costabile and Macchione*, 2012; *Fleischmann et al.*, 2016]. The small shoulders produced here are examples of the

exceedance of an inundation threshold and immediate storage of water on the floodplain. In contrast, gradual inundation of the floodplain creates negatively skewed hydrographs [*Fleischmann et al.*, 2016].

Skewness results in this research differ from those found in Fleischmann et al. [2016] in that the model with the greatest floodplain area has the greatest positive change in skewness rather than negative changes. This may be a result of the lack of floodplain microtopography in the HC model to create more permanent floodplain storage, or wetlands, during periods of flood recession. In addition, positive changes in skewness during 1-day events for PL and CL conditions are likely a result of minimal large-volume storage areas within the confined contemporary floodplain. It is also likely that flood wave shape would be more greatly impacted for a longer reach of river. If HC data were available, it may be that instead of the rising limb containing a gradual rising shoulder, the rising limb becomes more gradual for the entire rising duration. This would create the negative skewness observed in large floodplain systems. In complex, heterogeneous systems, there is likely a combination of instantaneous and gradual dynamics. It may be that if the historical model created in this research covered a longer portion of the river, floodplain inundation dynamics would create negatively skewed hydrographs due to both gradual inundation and instantaneous storage on the floodplain. Even without that information, these data do display that loss of heterogeneity in terms of channel-floodplain connectivity and floodplain topography, have had a substantial impact on the alteration of flood waves in terms of dynamic spatial and temporal influence along the MRG.

Differences in historical and contemporary flood wave attenuation in the MRG have implications for river management strategies and floodplain derived ecosystem services. While the floodplain connectivity under historical conditions modeled in this study was likely greater than pre-railroad settlement due to landscape changes such as logging and grazing in combination with climate-driven landscape processes [*Scurlock*, 1998; *Phippen and Wohl*, 2003; *Swanson et al.*, 2011; *Friedman et al.*, 2015], it was confirmed that floodplain influences on hydrology were greater under historical conditions, especially in terms of the lateral extent of floodplain surfaces within the MRG. Contemporary changes to floodplain connectivity in the form of topographic

48

lowering do not impact flood wave shape to an observable extent. However, the restoration conducted within this heavily urbanized stretch of river has been conducted within the levee and topographic boundaries. It should also be noted that historical changes have occurred over a period of 100 years while the restoration activities have predominantly occurred in the last 15 years. If river process is to be returned to stretches of river such as the MRG, it may take a similar amount of time to reverse changes in process as new priorities and techniques are pursued. Recent river restoration strategies which aid in flood control of engineered systems, such as levee setback initiatives and levee breaching strategies, which often connect substantially larger floodplain areas are more likely to impact flood wave shape [*Jaffe and Sanders*, 2001; *Sanders et al.*, 2006; *Jacobson et al.*, 2015]. Most often, the goal of modern river restoration strategies is not for flood wave attenuation purposes [*Bernhardt et al.*, 2005]. However, flood wave attenuation does depend on channel-floodplain connectivity and floodplain processes that are key to heterogeneous floodplain ecology [*Woltemade and Potter*, 1994; *Opperman et al.*, 2010]. Therefore, because these features are not of large enough extent to produce attenuation, the features are also likely not of great enough area to create long-term ecological integrity on the floodplain or promote the ecosystem services that are prevalent in floodplain systems. As river science continues to grow in terms of analytical analysis and description of river processes and as management of rivers begins to include less intrusive, natural process driven methods, complementary restoration initiatives should be pursued.

This study sought to model flood wave attenuation processes using high resolution 2D models with results displaying the benefits of 2D modeling approaches in river science. Returning to the analysis of Figure 2.4B and Figure 2.5, the incorporation of 2D calculations and microtopography are important in the description of delayed floodplain flow and thus a high rate of attenuation within this length of river. While there are 1D modeling techniques to limit floodplain flow until bankfull discharge is attained, the sourcing of the flow on the right floodplain in Figure 2.5 is from an upstream connection and channel-floodplain connections are limited for nearly a kilometer. One-dimensional models based upon cross-sectional information are likely to miss the intricacies of this type of connectivity and the process in which the flood wave is

attenuated, wherein a certain volume of water on the floodplain is delayed compared to the more direct channel flow. This is an example of complex channel-floodplain connectivity and the impact bank levees may have on hydrodynamic processes. With continuing increases in computational power and parallel computing techniques, high resolution two-dimensional meshes can provide further information about connectivity processes which influence flood wave attenuation in various river systems.

Uncertainty is always important to consider in modeling studies and likely increases from several sources in this study. First, while the study is limited to the availability of data, uncertainty within likely results from combination of data from different years for all the meshes created. Thus, no model therefore represents a specific point in time. Sand bed rivers are inherently dynamic with highly mobile beds [*Leopold et al.*, 1964], which produce uncertainty even with the field measurement of discharge and stage [*Isaacson and Coonrod*, 2011]. Therefore, even with optimal data sources at one point in time, hydrodynamic conditions are likely to change often. Another source of uncertainty arises from differences in data quality between historical and contemporary models, more specifically the inclusion of microtopography in LiDAR models. Here, microtopography is described as undulations in terrain within the two-meter contours. The uncertainty due to microtopography was minimized by creating a smooth contemporary floodplain model (CC conditions) for comparison with the historical conditions. However, because contemporary conditions were confined to areas within bounding levees and topography while historical conditions included a much larger lateral floodplain, influences created by the lack of microtopography are likely to be larger for historical conditions. While uncertainties no doubt arise in the comparison of LiDAR and contour attenuation results [*Dottori et al.*, 2013], the differing patterns in contemporary contour (CC) and LiDAR (PL, CL) model runs suggest that microtopography creates more attenuation at least during short duration events when the highest water surface elevations are limited. This is likely due to more dynamic mass and momentum exchange at the channel-floodplain interface and on the floodplain [*Knight and Shiono*, 1990; *Helmiö*, 2004; *Vermaas et al.*, 2011]. Therefore, historical rates of attenuation may be conservative in nature, although further research is necessary to investigate this point. With these uncertainties in mind, it

is believed that the methods used here produce reasonable representations of certain time periods and time periods worthy of comparison in the study of flood wave attenuation.

2.6. Conclusions

The impact of historical and contemporary anthropogenic river alterations on flood wave attenuation processes was described using advanced, high-resolution two-dimensional hydrodynamic modeling techniques. Results suggest the importance of heterogeneous floodplain topography and dynamic channel-floodplain connectivity in driving differences between historical and contemporary flood wave attenuation. Further, dynamic flow processes are illustrated through two-dimensional modeling methods that may not be captured in one-dimensional applications. Normalized metrics used in this study can be applied to other river systems to extend understanding of similarities and differences in attenuation rates between river systems with different hydrology, geomorphology, and ecology. Future management of rivers must include more comprehensive knowledge of how river systems function and the integrative nature of small to large-scale processes. While engineered infrastructure will always be necessary in the management in rivers, it is also likely that there exists great opportunity to improve complementary ecosystem services along these corridors.

Chapter 3

Sensitivity of flood wave attenuation to contemporary and altered channel-floodplain characteristics

3.1. Introduction

As a flood wave passes through a river reach it can be a threat to human infrastructure when viewed through the lens of flood protection as well as a critically important process for river geomorphology and ecology. The process of flood wave attenuation due to the hydrodynamic processes associated with channel-floodplain interaction is classified as an ecosystem service along river corridors [*Brauman et al.*, 2007]. In terms of flood control, flood wave attenuation is beneficial to downstream communities that can be subjected to reduced discharge and river stage during flood events [*Shankman and Samson*, 1991; *Acreman et al.*, 2003]. Further, inundation of floodplains during high flow events is fundamental to geomorphic and ecological processes [*Poff et al.*, 1997]. Modern river management strategies now include integrated floodplain management approaches that focus both on infrastructure and hydrodynamic processes to work in tandem to promote attenuation, decrease economic losses, and restore floodplain ecology [*Dierauer et al.*, 2012; *Guida et al.*, 2015; *Hudson and Middelkoop*, 2015; *Jacobson et al.*, 2015; *Guida et al.*, 2016]. However, restoration projects within severely altered river systems are often small due to the constraints of societal interests [*Stanford et al.*, 1996; *Bernhardt et al.*, 2005]. Therefore, it is important to understand current conditions defined by existing infrastructure and how changes within the bounds of infrastructure impact the attenuation process both for flood control and ecological interests. Integrated floodplain management should strive to limit flood risks at some locations while improving connectivity and ecological interests at others.

Flood wave attenuation as a physical process is dependent on the hydrodynamics associated with mass and momentum transfer. A river floodplain surface plays a substantial role in the degree of attenuation within a reach [*Wolff and Burges*, 1994; *Woltemade and Potter*, 1994]. With classic river engineering strategies often creating

52

channelized and leveed conditions, flood wave attenuation is often reduced [*Di Baldassarre et al.*, 2009; *Castellarin et al.*, 2011]. Mass and momentum transfer to the floodplain are dependent on the complex topographic and roughness characteristics which are defined by river channel and floodplain geomorphology and ecology. Previous work has shown that the channel-floodplain interface, often where distinct changes in topography and roughness occur, is of critical importance to mass and momentum fluxes [*Shiono and Knight*, 1991; *Helmiö*, 2004; *Vermaas et al.*, 2011]. The channel-floodplain interface is also an area that will be subjected to both channel and floodplain changes, whether those are the result of anthropogenic alterations or more natural dynamics. While the channel-floodplain interface is key to connectivity characteristics of mass and momentum exchange, the extent to which this specific area influences flood wave attenuation is not known specifically. Because river banks are often the sight of restoration or infrastructure activities [*Tunstall et al.*, 2000; *Pedroli et al.*, 2002; *Bernhardt et al.*, 2005; *Florsheim et al.*, 2008], the relative degree of influence on attenuation should be considered. While changes to banks are small in area compared to entire floodplain systems, bank changes may have disproportionate influence. Understanding the relative influence of floodplain and bank restoration strategies on flood wave attenuation can help inform river management strategies for flood protection and restoration.

Measurement of flood wave attenuation along rivers is extremely difficult due to the complex nature of unconfined, three-dimensional hydrologic systems. Therefore, computational modeling is often conducted to isolate the process along a river reach. Previous studies have sought to explain attenuation influences in the context of theoretical modeling efforts [*Wolff and Burges*, 1994; *Anderson et al.*, 2006], simplified systems without bounding levees [*Woltemade and Potter*, 1994; *Turner-Gillespie et al.*, 2003], or restoration influences on attenuation [*Acreman et al.*, 2003; *Liu et al.*, 2004; *Ghavasieh et al.*, 2006; *Sholtes and Doyle*, 2010; *Jacobson et al.*, 2015]. Although both one-dimensional and two-dimensional models have been used in the study of attenuation, previous studies suggest high-resolution, two-dimensional modeling may more appropriately capture important attenuation processes [*Wolff and Burges*, 1994; *Ghavasieh et al.*, 2006]. Predominantly, attenuation within past studies has been

documented in the context of downstream hydrographs and comparison of hypothetical alterations to a baseline condition. Hypothetical modeling practices are beneficial in understanding changes to the system, but analysis of attenuation sensitivity to existing conditions has not been a focus. With the advancement of computing techniques, this type of analysis is now more feasible. Detailed analysis of attenuation within heavily altered systems should be a focus as most rivers have been altered to a great degree. Further, with the availability of high-resolution topographic and spatially distributed roughness data, correlation with channel-floodplain conditions can now be extracted from more detailed modeling environments.

As river and floodplain management continues to integrate natural processes in heavily engineered river systems, it is important to understand how changing channel-floodplain characteristics can alter flood wave dynamics. While previous research has sought to quantify attenuation in simplified channel-floodplain conditions [*Wolff and Burges*, 1994; *Woltemade and Potter*, 1994; *Ghavasieh et al.*, 2006], in comparison to restored conditions [*Acreman et al.*, 2003; *Sholtes and Doyle*, 2010; *Jacobson et al.*, 2015], or as a watershed process [*Liu et al.*, 2004], statistical correlation of existing attenuation sensitivities to river conditions along a heavily-modified reach is a novel approach. Therefore, the first objective of this study was to investigate the sensitivity of flood wave attenuation to existing channel and floodplain characteristics. This was accomplished by applying a high-resolution, two-dimensional hydrodynamic model to a study reach and investigating which characteristics correlate with attenuation rates. The second objective of this study was to assess how channel and floodplain alterations affect flood wave attenuation. This objective was accomplished by altering the floodplain and channel conditions within the hydrodynamic model to isolate impacts of flood wave attenuation processes.

3.2. Site Description

The Middle Rio Grande (MRG) is defined here as the portion of the Rio Grande between Cochiti Dam and Elephant Butte Reservoir in New Mexico, USA. This study focused on the 27-kilometer reach that runs through the city of Albuquerque, NM (Fig. 3.1). The MRG has been subjected to substantial hydrological, geomorphological, and ecological

changes throughout the past century. Hydrologic changes to the MRG have been substantial in the form of flood control and water withdrawals. Water is diverted out of the main channel upstream of Albuquerque for deliveries, while long duration flood peaks on the main stem of the MRG are now largely controlled by Cochiti Dam, an upstream flood control dam. Although long-duration flood peaks (~weeks to months) are controlled, moderate and major short duration (~hours to days) flood events may still reach the MRG through localized storm events in unimpounded tributary basins with an estimated 1 percent probability event having a magnitude of approximately 350 m^3s^{-1}.

Geomorphic alterations have been prominent in the name of flood control and water conveyance. Levees were constructed to confine overbank flows and protect the city of Albuquerque from periodic inundation [*Phillips et al.*, 2011]. River training and straightening was also conducted along much of the MRG with Kellner jetty jacks, which strengthened and created heavily vegetated river banks [*Woodson et al.*, 1965]. Sediment loads were significantly reduced immediately downstream of Cochiti Dam, an intended consequence of the construction of the dam [*Lagasse*, 1980; *Richard and Julien*, 2003]. With sediment inputs from the main stem and other tributaries reduced and channel banks fortified, the aggradation of the main channel in the Albuquerque Reach was reversed to induce channel degradation and further reduce flooding concerns [*Happ*, 1948; *Lagasse*, 1980].

In approximately the past twenty years, the Rio Grande has been subjected to river restoration strategies to promote native ecosystems primarily in the name of the Endangered Species Act [*Tetra Tech EM Inc.*, 2004]. These strategies have included clearing and planting of vegetation on islands and floodplains, removal of jetty jacks and bank lowering along the main channel, and the creation of side channels, backwaters, and scalloped terraces on floodplains [*Tetra Tech EM Inc.*, 2004]. These methods influence both the hydrodynamics of the river system as well as the channel and floodplain ecology. However, the influence such changes have on flood wave dynamics has not been quantified. As other river systems in the southwestern United States are subject to similar historical and contemporary alterations, analysis of the current influences and potential alteration of flood wave attenuation is of broad interest.
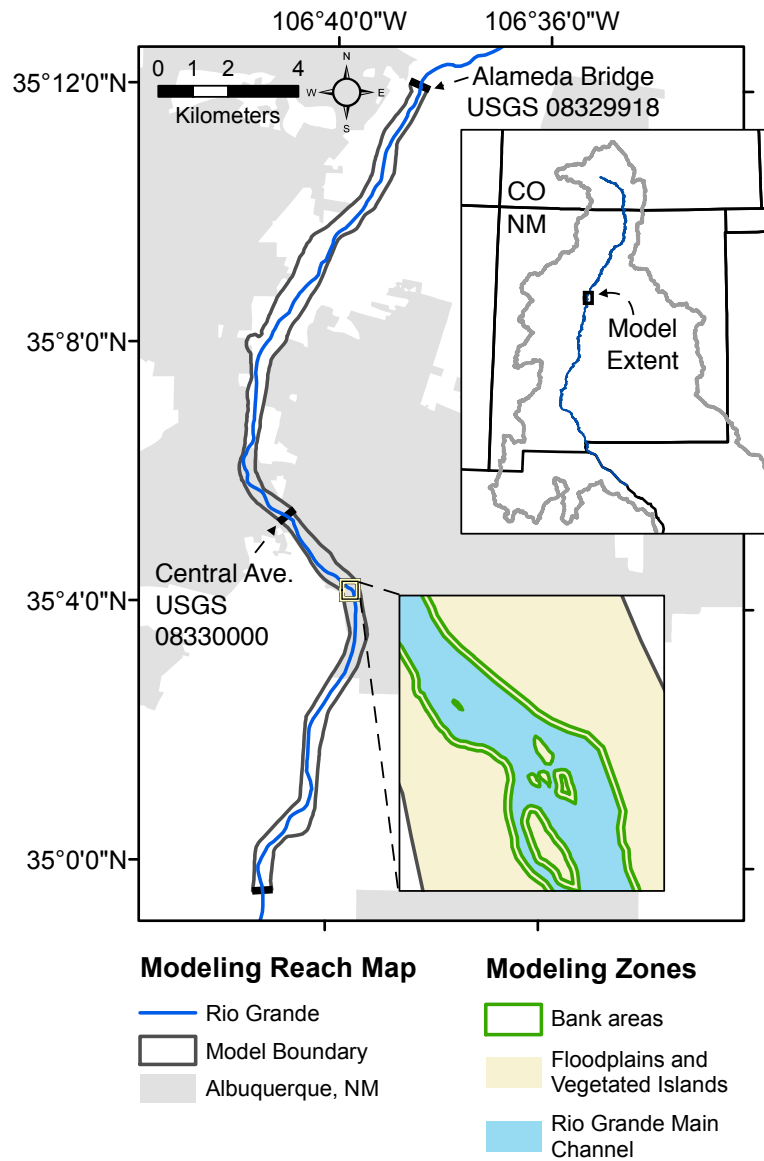
Figure 3.1. Location of modeled reach within the Middle Rio Grande and representation of zones which were altered within the study.

3.3. Methodology

3.3.1.   Modeling Environment and Mesh Development

Two-dimensional (2D) hydrodynamic modeling was conducted using Deltares' D-Flow Flexible Mesh (D-Flow FM) [*Deltares*, 2015]. All modeling scenarios used the same 2D

mesh with the main channel predominantly composed of curvilinear elements while more complex floodplain topography was described with triangular elements. Mesh elements averaged approximately 25 m^2 in area. The mesh was developed based upon the 2010 channel alignment of the MRG with vegetated islands also described with triangular elements while unvegetated bars remained curvilinear. The mesh covered 32 km of the MRG near and through Albuquerque, NM. The upstream and downstream boundaries of the model coincide with United States Geological Survey (USGS) stream gages 08329918 (Alameda Bridge) and 08330875 (Isleta Lakes), respectively. The upstream boundary was defined by discharge while the downstream boundary was assigned a water surface elevation. Because the Isleta Lakes gage only has a 15-year period of record, no gage data existed for high flows. Therefore, instead of a stage-discharge boundary, a water surface elevation boundary was applied and the bottom 5 km of the model were removed to avoid boundary effects, resulting in a 27-km study reach. Channel and floodplain width was defined by topography along the reach including anthropogenic and natural embankments. Modeling was conducted under the assumption that all constructed levees and berms would not fail under the flooding scenarios.

All modeled scenarios were subjected to the same hydrology. All models were run for steady conditions at 30 and 150 m^{3}s^{-1}, the initial conditions for the moderate and major flood events, respectively. The 30 and 150 m^{3}s^{-1} steady conditions are representative of a wet main channel and approximate bankfull discharge, respectively. Flood peaks for all events were 150 m^{3}s^{-1} above the respective initial condition and duration of the flood pulse was either 1, 1.5, or 3 days. Examples of the 1 day events are depicted in Figure 3.7. In addition, steady flows were also run at 180 and 300 m^{3}s^{-1}, the peak flows for moderate and major flood events, respectively. The moderate and major flood events are representative of 5-year and 50-year flood magnitude events. Two types of modeling were conducted for this study: (1) modeling of a contemporary condition with distributed roughness values and (2) alternative scenario modeling which involved adjustments to channel and floodplain topography and roughness.

3.3.2. Contemporary Model

The contemporary model was created to analyze how channel and floodplain geomorphology impacts attenuation rates and to what degree high-resolution, 2D models can lend insights into the underlying physical processes. For this purpose, the topographic and roughness data was interpolated to the mesh. Floodplain topography was defined by a digital elevation model (DEM) created from 2010 Light Detection and Ranging (LiDAR) data. Because the LiDAR data did not accurately represent channel bathymetry below the water surface at the time of acquisition, U.S. Bureau of Reclamation cross-section data were used to interpolate a channel bottom which was then combined with the floodplain topography [*Adair*, 2016]. Manning's roughness values were assigned based upon MRG vegetation mapping and previously documented techniques of equating the vegetation type to roughness values [*Hink and Ohmart*, 1984; *Mussetter Engineering*, 2002; *Callahan and White*, 2004; *Adair*, 2016]. Channel roughness was lumped at 0.025 for the entire reach. Any further discussion of roughness relates to Manning's roughness which was the chosen roughness attribute for D-Flow FM.

3.3.3. Channel and Floodplain Characteristics Extraction

Channel and floodplain characteristics were quantified using spatial analysis techniques within a geographic information system (GIS). ESRI's ArcMap 10.1 was used to extract and summarize data pertaining to total area, floodplain area, channel area, inset floodplain area, island area, floodplain roughness, bank roughness, average channel depth in comparison to floodplain and bank elevations, channel and floodplain width, and channel slope. Data were then summarized for each kilometer of the reach. The main channel was defined by unvegetated sand bars and inundated areas at the time of the 2010 LiDAR acquisition. Floodplain surfaces were defined as any vegetated area outside of the main channel as well as vegetated islands within the reach. Island surfaces were also analyzed separately. Finally, inset floodplain surfaces were described as surfaces below the historical floodplain that are often created by the process of vegetated islands attaching to the bank as a result of decreased streamflows [*Meyer and Hepler*, 2007; *Swanson et al.*, 2011].

The areas for each of the channel and floodplain surfaces were calculated between cross-sections located 1 km apart and for the full lateral extent of the model. Bank areas were defined as 10 meter buffers on the floodplain side of the channel boundary. Roughness values for each 1 km segment were recorded as spatially averaged means based upon distributed mapping. Average channel depth was calculated by subtracting the mean channel elevation from the mean bank and mean floodplain elevations for each segment. Slope was calculated via the difference in mean elevations between the segment's upstream and downstream bounding cross-sections. Finally, two flood wave dependent metrics were applied to investigate correlations between flood wave attenuation and channel and floodplain characteristics. First, the peak water surface elevation recorded at each cross-section was compared to both bank and floodplain elevations. Second, for each 1-km segment, the ratios of total area inundated at initial conditions to total area were calculated. In total, 15 characteristics were summarized for each flow event as possible predictors of attenuation (Table 3.1).

Table 3.1. Summary of predictor characteristics used in simple and multiple linear regression analyses.

Characteristic Groups	Single Characteristics	Calculation Method
Feature Dimensions	Total Area (TA) Channel Area (CA) Floodplain Area (FA) Island Area (ISA) Inset Floodplain Area (IFA)	Areas defined by digitized bounding polygons
	Channel Width (CW) Floodplain Width (FW)	Widths measured every 50 m and averaged for each kilometer section
Roughness	Bank Roughness (BR) Floodplain Roughness (FR)	Mean of all roughness cells within defining digitized boundary polygon
Static Elevation	Bank - Channel Elevation (BCE)	Difference between mean streambank elevation and mean channel elevation for each kilometer segment
	Floodplain - Channel Elevation (FCE)	Difference between mean floodplain elevation and mean channel elevation for each kilometer segment
	Slope (S)	Change in minimum elevation between upstream and downstream cross-sections
Flow Dependent Elevation	Peak water surface elevation - bank elevation (WSE-BE)	Difference between peak water surface elevation recorded during flood event and mean bank elevation
	Peak water surface elevation - floodplain elevation (WSE-FE)	Difference between peak water surface elevation recorded during flood event and mean floodplain elevation
Flow Dependent Area	Ratio of inundated area at initial condition to total area (RIATA)	Summation of total area inundated at initial flow conditions within the kilometer segment divided by the total area of the kilometer segment

3.3.4. Statistical Analysis of Characteristics and Attenuation

All calculated predictors were compared to the change in discharge attenuation ratio (ΔQAR; Eqn. 1) in each kilometer segment which represents the possibly correlated response, or dependent variable. Discharge attenuation ratio (QAR; Eqn. 2) was calculated at each 1-km segment providing an upstream and downstream value of total attenuation.

$$\Delta QAR = QAR_{i-1} - QAR_i \qquad\qquad (1)$$

$$QAR = Q_{p,i}/Q_{p,upstream\ boundary} \qquad\qquad (2)$$

Here i represents the downstream cross-section number and Q_p is peak discharge recorded at i and at the upstream boundary. Only 1-day duration models were used for this portion of the statistical analysis. Linear and multiple linear regression methods were utilized to assess the relationships between the channel and floodplain characteristics and ΔQAR as well as transformation of both predictor and response data. All correlations are reported in adjusted coefficients of determination (R^2).

3.3.5. Altered Model Scenarios

A series of hypothetical model alternatives were developed to investigate the impacts of specific channel and floodplain modifications on flood wave attenuation. The alterations were designed to represent, while magnifying, characteristic changes that have been observed and implemented within the MRG. The alterations included bank, channel, and floodplain modifications to both topography and bed roughness. Table 3.2 describes the modeled conditions as well as the real-world associated process. While the alterations to topography and roughness were uniformly applied to the entire reach for modeling purposes, real-world changes to the river environment are not likely to be as drastic. The alterations represented realistic changes while magnifying attenuation results due to the alterations being applied along the entire reach. This approach allowed us to isolate the influence of each altered condition.

Specifically, each alteration was produced by modifying the associated topographic or roughness value from the conditions in the baseline model. Channel roughness values held constant at a value of 0.025. Floodplain roughness values were assigned a constant value of 0.060 for the baseline model and altered from there. This is in contrast to the statistical portion of the study which used distributed roughness values. The purpose of this alteration in the baseline data was to remove complications associated with distributed vegetation mapping and associated roughness values.

Table 3.2. Conditions for topographic and roughness scenario alteration model runs with the corresponding processes represented.

		Alteration Type & Abbreviation		Elevation		Roughness n-value		Processes Represented
				Channel	Bank	Floodplain	Bank	
Topographic	Channel	Aggradation and Incision	CU	+0.3	Baseline	0.06	0.06	Channel aggradation/degradation
			CD	-0.3				
	Streambank	Increase or Decrease in Streambank Elevation	BU	Baseline	Sloped +0.3m	0.06	0.06	Sedimentation along stabilized banks; restorative bank lowering for improved connectivity
			BD		Sloped -0.3m			
Roughness	Floodplain	Increase or Decrease in Floodplain Roughness	F04	Baseline	Baseline	0.04	0.04	Invasive vegetation; Floodplain clearing to deter wildfire
			Baseline			0.06	0.06	
			F08			0.08	0.08	
			F10			0.10	0.10	
	Streambank	Increase or Decrease in Streambank Roughness	B04	Baseline	Baseline	0.06	0.04	Historical bank stabilization; restorative bank clearing
			Baseline				0.06	
			B08				0.08	
			B10				0.10	

3.3.6. Topographic Alteration

Channel topography was modified to represent channel incision or aggradation. River engineering in the MRG was conducted with the purpose of incising the Albuquerque Reach to prevent flooding [*Lagasse*, 1980]. However, the Rio Grande and other southwestern rivers have been subject to continual channel aggradation and degradation processes throughout historical time [*Scurlock*, 1998; *Friedman et al.*, 2015]. In addition, many tributaries to the MRG remain unimpounded, thus the river can be subjected to pulses of sediment at tributary confluences [*Vivoni et al.*, 2006].

Both bank and channel topography were altered in this study. Incision was represented by lowering channel elevations by 0.3 m using raster calculations and reinterpolated to the previously created mesh. Aggradation was represented by raising channel elevations by 0.3 m and again interpolated to the existing mesh. Bank elevations were lowered to represent bank lowering restoration techniques while elevations were raised to represent further sedimentation that has occurred along the heavily engineered and vegetated banklines in the MRG [*Woodson et al.*, 1965; *Tetra Tech EM Inc.*, 2004]. Bank alterations were made on both floodplains within a 10-meter buffer along the main channel. Bank elevation rasters were created with an increase or decrease of 0.3 m at the bank channel-interface and sloped to existing topography at 10 m from the channel.

3.3.7. Roughness Alteration

Roughness alterations were applied to bank areas or the entire floodplain. Reduced floodplain and bank roughness values represented the clearing of invasive riparian species to support restoration strategies and reduce wildfire risks [*Tetra Tech EM Inc.*, 2004; *Najmi et al.*, 2005]. Increased roughness represented invasive species colonization, which often occurs in the form of dense monocultures, and thickening vegetation associated with bank stabilization [*Woodson et al.*, 1965; *Howe and Knopf*, 1991; *Shafroth et al.*, 2005]. Floodplain roughness was adjusted for all floodplain and vegetated island surfaces. Bank roughness was applied to a 10-m buffer created on both sides of the main channel and on the 10-m buffer of vegetated islands within the reach. Floodplain roughness values were then updated with these bank roughness values.

3.3.8. Quantification of Alteration Scenario Impacts on Flood Wave Attenuation

Both unsteady and steady flows were used in the assessment of how hypothetical alterations influence flood waves. Unsteady results are presented as QARs (Eqn. 2) and stage attenuation ratios (SAR). Stage attenuation ratios were taken as the ratio of relative peak stage measured under unsteady conditions to the relative peak stage measured under steady peak flow conditions (Eqn. 3). Within Equation 3, $h_{p,i}$ is the water surface elevation of the flood wave at a defined downstream cross-section, i, $h_{S,i}$ is the water surface elevation under steady peak flow conditions at a defined downstream cross-section, and $z_{min,i}$ is the local minimum channel elevation at the cross-section.

$$SAR = \left(h_{p,i} - z_{min,i}\right)/\left(h_{S,i} - z_{min,i}\right) \tag{3}$$

Further analysis of hydrodynamics specific to channel and floodplain flow under the various conditions was conducted using steady flow analysis. Steady analysis was applied to conditions that produced the most substantial attenuation throughout the reach. A steady flow approach was used to describe fundamental processes of each condition in order to quantify uniform changes in water surface elevation and velocity to prevent these hydrodynamics from being impacted by attenuation lower in the reach.

3.4. Results

3.4.1. Influence of Channel and Floodplain Characteristics on Flood Wave Attenuation

Characterization of channel and floodplain metrics was conducted for each kilometer segment (Fig. 3.2). The moderate flood wave was attenuated to a greater total proportion as represented by QAR. In contrast, ΔQAR reached a peak under the major flood wave conditions. Total area was predominantly composed of the in-levee floodplain, however, channel area, represented by the difference between TA and FA averaged 21.9% of total flow area. The high proportion of channel area is indicative of the leveed nature of the contemporary MRG. Roughness of banks compared to the entire floodplain were similar (FR vs BR), however, bank elevations were consistently less than those recorded for the

entire floodplain (BCE vs FCE). This is representative of many inset floodplain surfaces along the channel-floodplain interface. Water surface elevations were predominantly greater than bank elevations under moderate flows while the majority of mean floodplain surfaces were greater than peak water surface elevation under the same flow conditions (WSE-BE, WSE-FE). Under the major flood scenarios, both WSE-BE and WSE-FE were primarily greater than zero, indicating active inundation of both surfaces. Finally, the RIATA was greater under major flood conditions as expected, however, the ratio did not increase substantially in the areas of greatest ΔQAR. This indicates that at flood wave onset, that segment of floodplain still had substantial water storage potential.

The statistical analysis revealed correlations between channel and floodplain characteristics and the process of flood wave attenuation (Fig. 3.3). Correlations were stronger for the major flood event, which resulted in a high degree of floodplain connectivity as compared to the moderate flood event. The greatest coefficients of determination (R^2) describing the natural logarithm ΔQAR for the major flood scenarios were found in a positive correlation with TA, which was the summation of floodplain area and channel area, and a negative correlation with RIATA, or the ratio of area inundated at 150 m^3s^{-1} to total area, represented by RIATA (Fig. 3.3A & 3.3B). A multiple linear regression analysis was then conducted by combining indicators that were determined to belong to different classification groups described in Table 3.1 to remove correlated individual characteristics. All terms were related to the natural logarithm of ΔQAR. The correlation was highest for a model combining TA, BCE, and RIATA (Fig. 3.3C). It was determined that TA and RIATA displayed a degree of collinearity (R^2 = 0.459). Therefore, the greatest multiple linear correlation with only one of these two metrics was calculated. The linear model including the BCE, WSE-BE, and RIATA was found to have the greatest correlation (Fig. 3.3D).
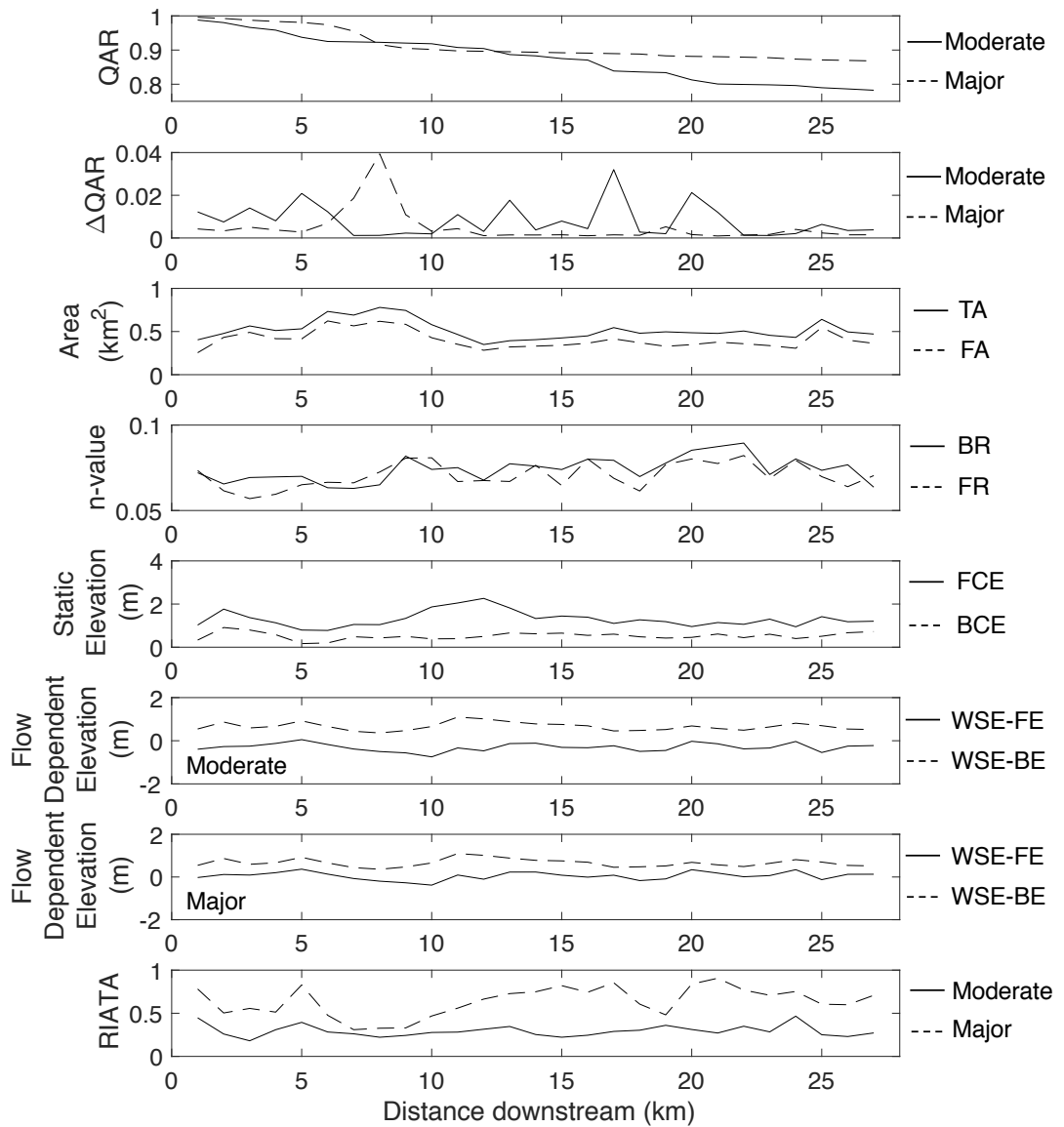
Figure 3.2. Attenuation ratios of 1-day moderate and major flood waves along the contemporary Rio Grande, kilometer-length change in QAR, and selected longitudinal channel-floodplain characteristics used in linear and multiple linear regression models.

67
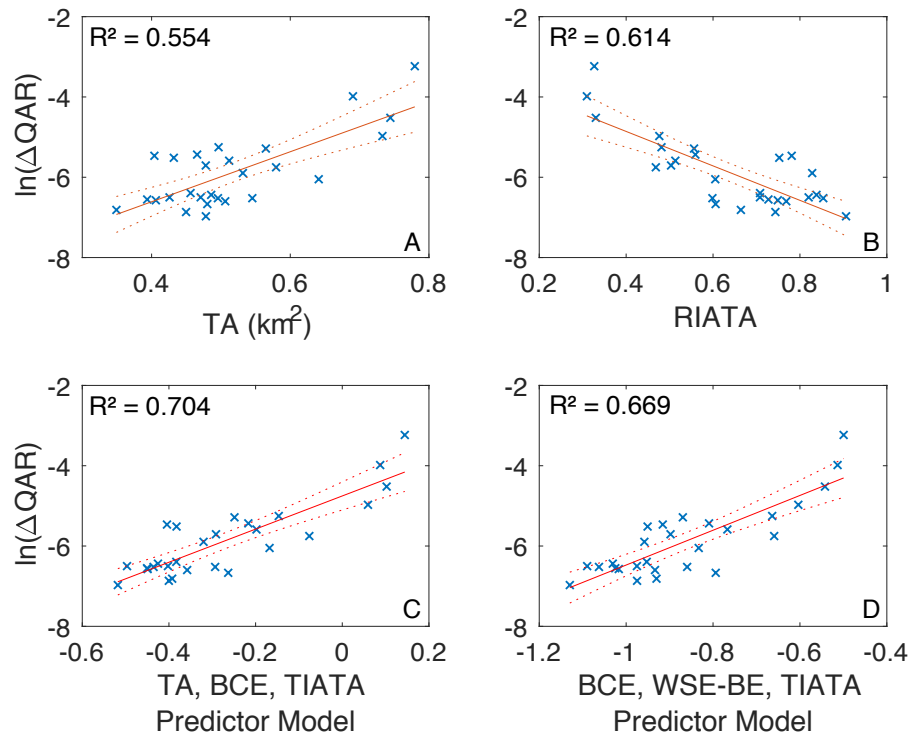
Figure 3.3. Linear (A & B) and multiple linear (C & D) regression models between flood wave attenuation ratios and channel-floodplain characteristics.

The moderate, short duration flood event did not show the same levels of correlation between channel floodplain characteristics and attenuation. The greatest correlation for a single characteristic was a negative relationship between the natural logarithm of degree of attenuation and the difference between modeled peak water surface elevation and mean floodplain elevation ($R^2 = 0.264$). Again, a multiple linear regression of all combinations of predictors was conducted for the moderate, short duration flood. The greatest correlation was found in the linear model with bank roughness and the difference between modeled peak water surface elevation and mean floodplain elevation, however, the R^2 value did not rise substantially with the addition of the bank roughness characteristic ($R^2 = 0.290$).

3.4.2. Hypothetical Alteration Scenarios

Results from hypothetical modeling of alteration scenarios indicate that bank alterations have a relatively small impact on flood wave attenuation within the reach compared to changes to the entire floodplain (Figs. 3.4 & 3.5). Percent difference from total baseline attenuation (i.e. lumped floodplain n = 0.060) at km-27 under bank alteration scenarios ranged from -6.0 to 4.0% for topographic bank alterations and –12.4 to 9.0% for roughness bank alterations. Complete alterations to the floodplain had much larger impacts on flood wave attenuation with percent differences from baseline conditions ranging from -129.6 to 46.4% for topographic alterations and -28.5 to 22.9% for roughness alterations.

Topographic alterations had a non-uniform effect on flood wave QARs where abrupt changes in attenuation ratios were observed in channel segments that experienced extensive overbanking (Fig. 3.4). The stepped decreases are often located along the same length of river for floods of the same magnitude but different duration. For example, a high rate of attenuation occurs between km-5 and km-10 for the moderate flood, raised channel conditions (Figs. 3.4 A, C, & E). This indicates the same floodplain areas are impacting attenuation. However, the step is observably smaller in Figure 3.4E than Figure 3.4C. This indicates, a limited amount of storage capacity. Increasing the volume associated with a flood (i.e. increased duration) will also decrease the influence of connected floodplains. While topographic bank alterations influence connectivity in a similar manner to channel aggradation and degradation, the influence is not of the same magnitude, thus the changes in connectivity do not alter attenuation to a similar degree. Channel aggradation resulted in increased attenuation for the moderate flood event because this condition resulted in additional floodplain inundation (Fig. 3.4). In contrast, greater attenuation was observed under the incised channel scenario for the major flood event because the floodplain remains connected even under the incised conditions.

Roughness alterations across the entire floodplain display greater attenuation under increasing roughness scenarios with as much as two times the degree of attenuation in the system with the highest floodplain roughness compared with the lowest roughness scenario (Fig. 3.5). While floodplain alterations lead to consistent results with increased roughness leading to increased attenuation, bank alteration scenarios are not consistent.

In the bank scenarios, the roughness alteration can impact the degree of connectivity at downstream locations, thus leading to changes in attenuation. For example, in the moderate, 1.5-day duration event (Fig. 3.5F), decreasing bank roughness to 0.040 creates less attenuation in the upstream portion of the reach (km-0 to km-22). However, because there is less attenuation, downstream locations are subject to greater discharges, higher water surface elevations, and greater lateral connectivity. This connectivity to the floodplain provides attenuation at approximately km-22, leading to a stepped decrease in attenuation. In this scenario, decreases in bank roughness ultimately lead to greater attenuation rates at downstream locations compared with increased bank roughness. Therefore, while bank alterations no doubt influence attenuation rates, the alteration can influence floodplain connectivity, mass storage, and further momentum dissipation in other stretches.

Figure 3.4. Channel (CD and CU) and streambank (BD and BU) topographic alteration influences on baseline QAR values for (A) 1-day, moderate, (B) 1-day, major, (C) 1.5-day, moderate, (D) 1.5-day, major, (E) 3-day, moderate, and (F) 3-day, major flood events.
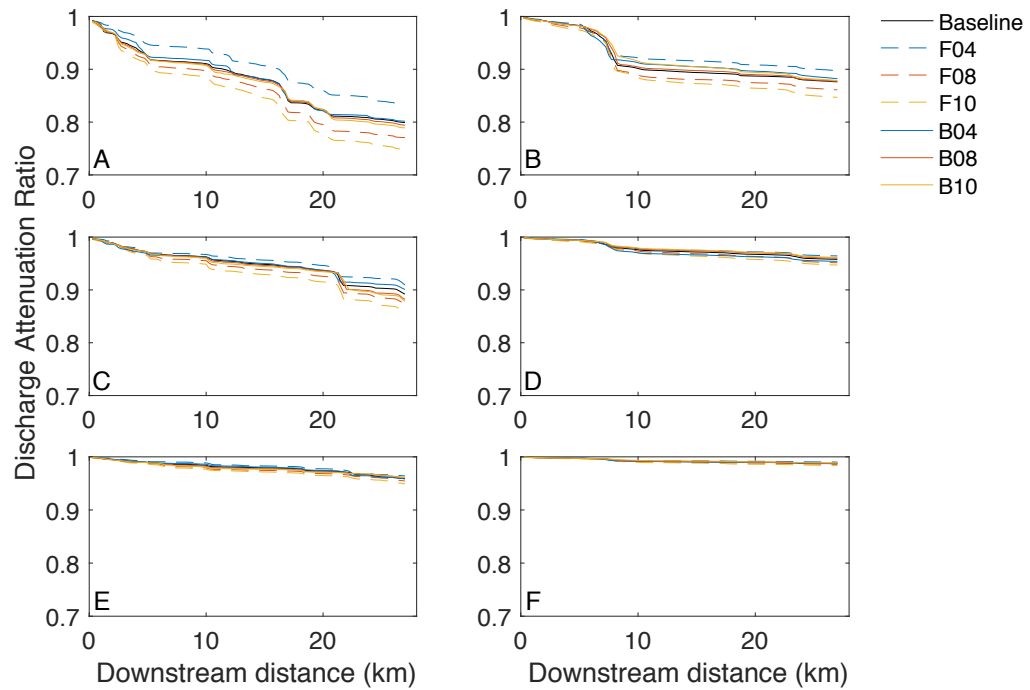
Figure 3.5. Floodplain (F04, F08, and F10) and streambank (B04, B08, and B10) roughness alteration influences on baseline QAR values for (A) 1-day, moderate, (B) 1-day, major, (C) 1.5-day, moderate, (D) 1.5-day, major, (E) 3-day, moderate, and (F) 3-day, major flood events.

Stage attenuation ratios predominantly follow the same patterns as discharge attenuation ratios for channel and floodplain alterations (Figs. 3.6 & 3.7), however, stage attenuation ratios are much more dependent on local channel geometry. Therefore, water surface elevations can be altered differently. Topographic alterations to the entire channel led to differences in stage attenuation of -186.1 to 47.0% as compared to baseline scenarios. Bank aggradation and lowering resulted in stage attenuation values that represent a range of -6.1 to 9.6% change from baseline. As demonstrated in the discharge attenuation ratios, aggradation of the channel can drive increased connectivity for the moderate flood events. This drives a notable decrease in water surface elevation near km-10 in the moderate events (Figs 3.6A, C, & E). However, downstream water surface elevations often rebound to near baseline levels as increased connectivity leads to less storage in downstream regions for moderate flood conditions. For major flood conditions, stage attenuation ratios under topographic alterations are most substantially altered from

baseline conditions during the long duration event in conjunction with discharge attenuation ratios (Fig. 3.6E).

Roughness alterations revealed more consistent results in conjunction with baseline stage attenuation ratios as compared to topographic adjustments (Fig. 3.7). Differences in stage attenuation ratios varied between -46.0% and 30.7% for complete floodplain alteration and -14.6% and 9.4% for bank alterations. Stage attenuation ratios were predominantly lowest under the floodplain conditions with the greatest roughness. While short duration, moderate flood wave results (Fig. 3.7A) display a moderately consistent downward trend, the other modeled flood scenarios displayed dependency on areas of localized attenuation to markedly decrease the stage attenuation ratio (Figs. 3.7C & E; Figs. 3.7B, D, & F). The influence of local topography presumably drives these stepped decreases in water surface elevation in combination with decreases in flood wave discharge in the most influential of downstream locations.
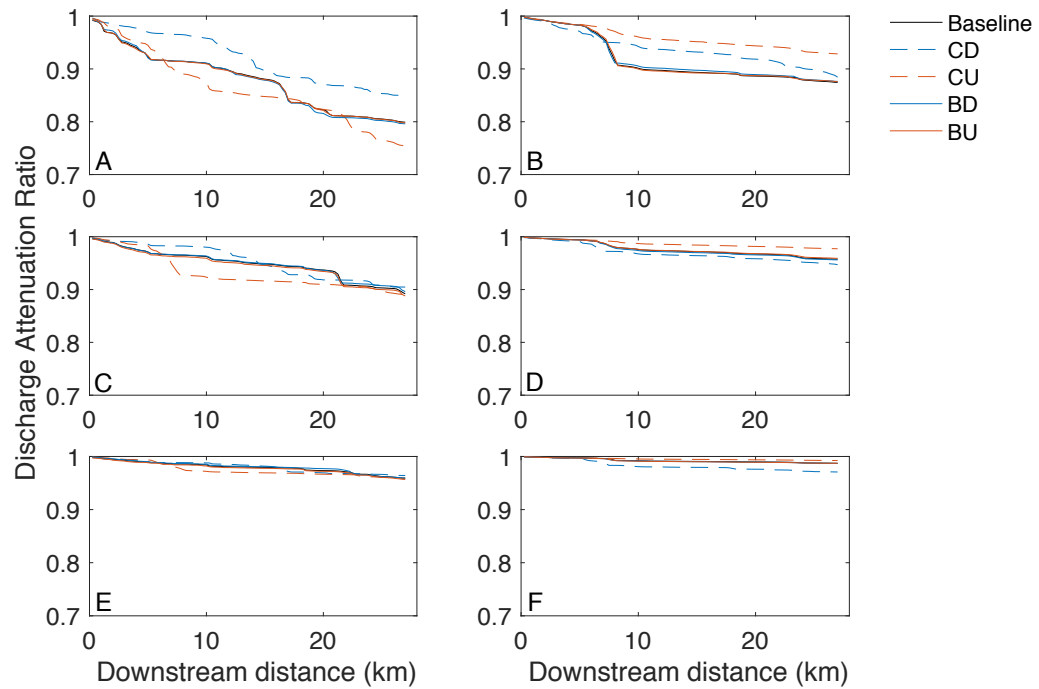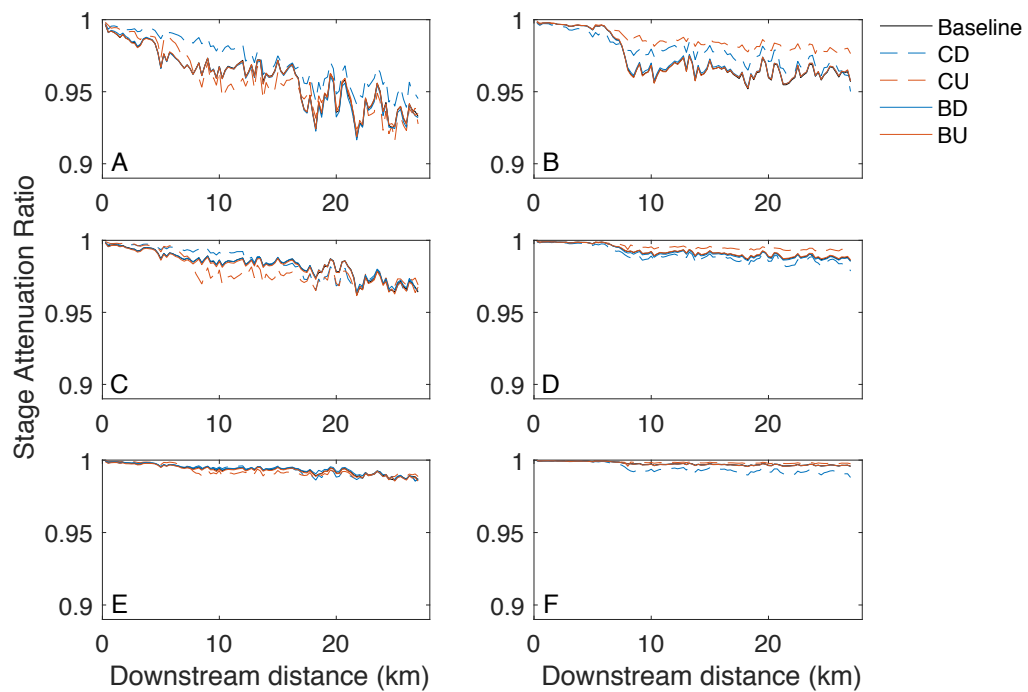

Figure 3.6. Channel (CU and CD) and streambank (BU and BD) topographic alteration influences on baseline SAR values for (A) 1-day, moderate, (B) 1-day, major, (C) 1.5-day, moderate, (D) 1.5-day, major, (E) 3-day, moderate, and (F) 3-day, major flood events.
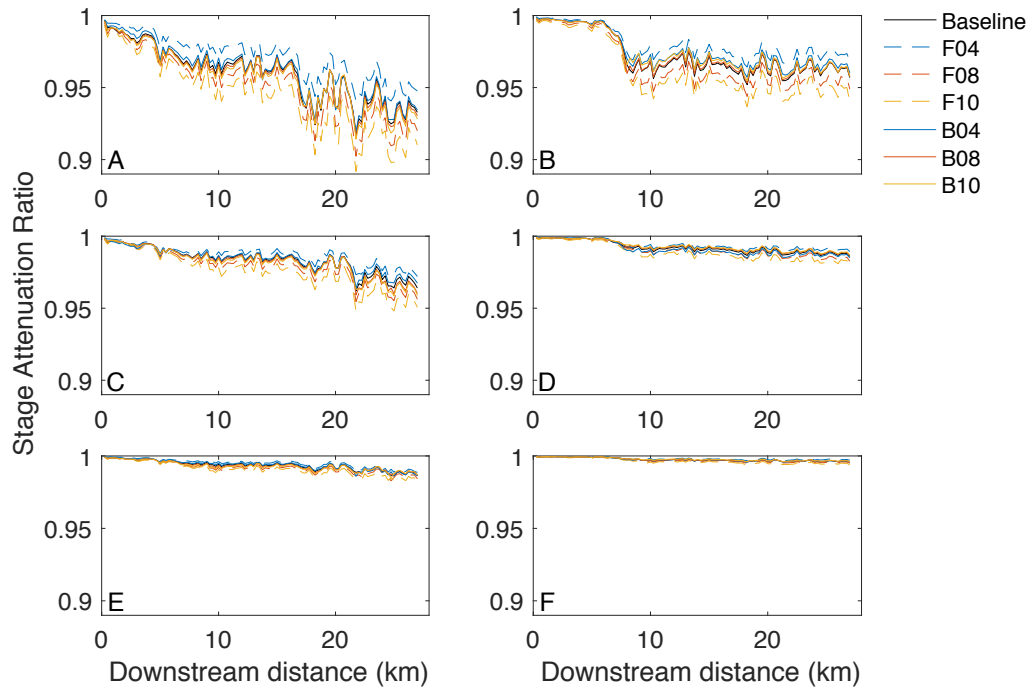
Figure 3.7. Floodplain (F04, F08, and F10) and streambank (B04, B08, and B10) roughness alteration influences on baseline SAR values for (A) 1-day, moderate, (B) 1-day, major, (C) 1.5-day, moderate, (D) 1.5-day, major, (E) 3-day, moderate, and (F) 3-day, major flood events.

Complementary analysis of both discharge and water surface elevation attenuation ratios exhibits the dynamics of channel-floodplain connectivity critical to the process of attenuation. Changes over short distances can greatly impact the rate of attenuation over the entire reach. This is expressed in the comparison of major flood events for models in which the channel topography was lowered (Figs. 3.4B, D, and F & 3.6B, D, and F). In the 1-day duration event (Figs. 3.4A & 3.6A), discharge and stage are attenuated within the first five kilometers to a degree in which floodplain connectivity is lost for several 1-km segments (~ km-6 to km-8) which creates high rates of attenuation in the baseline model. While attenuation rates began to approach baseline levels by km-27, the dynamics between attenuation and connectivity at upstream locations effectively increased flood peaks for most of the reach. As flood volume increases with 1.5 and 3-day events, flood peaks in the first 5 kilometers are not reduced to the same degree as the

1-day event. For these events, connectivity is again restored to km-6 through km-8 and attenuation rates are substantially greater when compared with baseline conditions.

A second example of the impacts of channel-floodplain connectivity exists for the baseline conditions under major flood conditions (Fig. 3.4) and raised channel topography under moderate flood conditions (Fig. 3.6A, C, & E). In this example, the process of attenuation is essentially translated from the baseline condition under major flood scenarios to the raised channel for moderate flood wave scenarios. The process being captured in the similar attenuation patterns is the connection of the same elevated surface between river km-6 and km-8. The attenuation rate is greater for the raised channel topography because flood peak is lower during moderate flood waves than major flood waves. Therefore, the floodplain can detain a larger fraction of flow.

Attenuation of flood waves is both a physical and temporal process, therefore, flood hydrographs at km-27 are presented to show differences in timing under topographic and roughness alteration scenarios (Fig. 3.8). Downstream flood waves again display the different degree in attenuation between topographic alteration scenarios (Figs. 3.8A & C) as compared to roughness alteration scenarios (Figs. 3.8B & D). In terms of process, the results indicate that channel-floodplain connectivity drives large changes in the timing of the flood wave when flows are lower (Fig. 3.8A). That is, an incised channel will deliver water to a downstream location more quickly as lateral connections are decreased. This indicates that mass transfer is a dominant temporal attenuation process when the potential storage volume is a greater proportion of the flood wave. Under major flood wave conditions, roughness drove greater differences in flood wave timing and topographic changes created similar flood wave timing but substantially different degrees of discharge attenuation (Fig. 3.8C). This indicates that individual connections between the river and floodplain become less important for the aggraded channel condition and critical to attenuation in the degraded channel condition producing similar timing. The greater roughness conditions drive momentum dissipation and decreased channel velocities, supported by the following steady flow analysis.
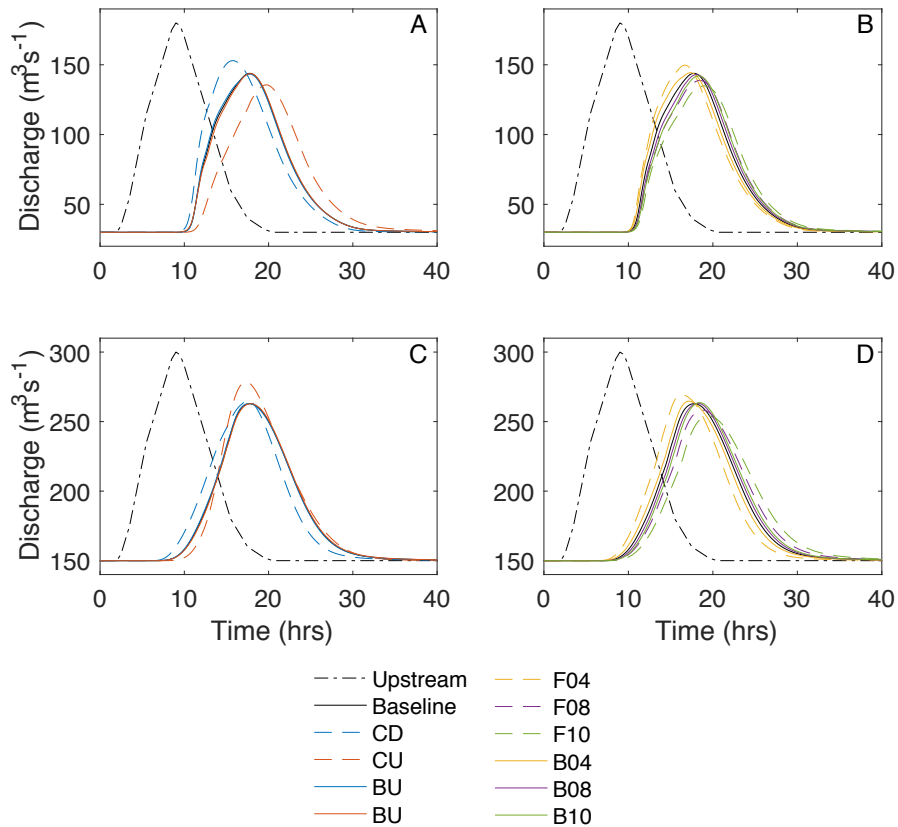
Figure 3.8. Modeled hydrographs of 1-day scenarios at river km-27 under (A) modified channel topography; (B) modified streambank topography; (C) modified floodplain roughness, and (D) modified streambank roughness. Note the differences in scales.

Steady flow analysis presents the implications that changes in topography and roughness have on main channel water surface elevations and velocity without the influences of attenuation (Fig. 3.9). Intuitively, mean in-channel water surface elevations are the greatest for raised channel topography (CU) and the least for lowered channel topography (CD) (Fig 3.9A). Roughness increases of the entire floodplain (e.g. F10) also drive mean in-channel water surface elevations to greater levels. Alteration of only bank roughness (e.g. B10) has the same impact on water surface elevation, albeit to a lesser degree. Differences in mean water surface elevation under the more connected 300 m^3s^{-1} are greater than those for 180 m^3s^{-1} (Figs. 3.9A & B). Main channel mean water surface elevation is as much as 0.21 m different between high (F10) and low (F04) floodplain roughness scenarios at 300 m^3s^{-1}. Mean water surface elevation as compared to baseline

75

conditions under the F10 condition, 0.12 m, approaches those recorded in CU, 0.15 m. Main channel mean velocities are most greatly impacted by floodplain roughness alterations albeit in an opposite relationship to mean channel water surface elevation (Figs. 3.9C & D). Velocities between F04 and F10 scenarios differ between 0.12 ms^{-1} and 0.16 ms^{-1} for 180 and 300 m^{3}s^{-1} flow events, respectively.

Proportion of longitudinal floodplain flow to total flow was also analyzed under steady flow conditions (Figs. 3.9E & F). Of course, raising and lowering the channel changed the fraction of floodplain flow to the greatest degree. However, more interesting are the differences in proportion of floodplain flow associated with changes in floodplain and bank roughness. Increasing floodplain roughness is inversely related to the amount of discharge on the floodplain with F04 having on average 1.3% more flow than F10 at 300 m^{3}s^{-1}. In contrast, increases in bank roughness also lead to increases in the fraction of flow on the floodplain with low roughness banks (B04) having on average 2.8% less flow than high roughness banks (B10) at 300 m^{3}s^{-1}. Furthermore, with increases in water surface elevation under high roughness conditions, increases in connectivity and floodplain flow would be expected. However, this analysis shows that the increases in roughness actually prevent increased floodplain flow even with greater water surface elevations.
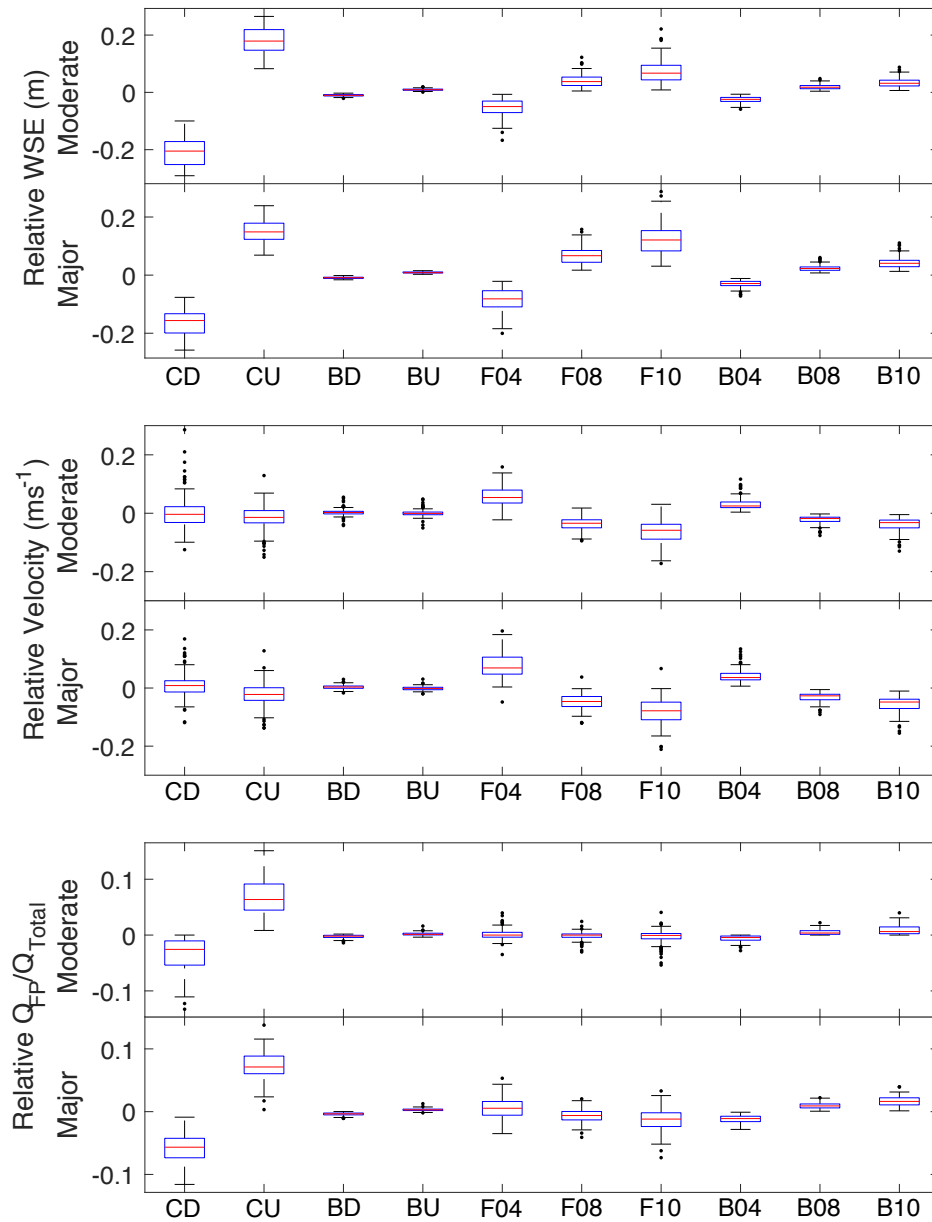
Figure 3.9. Mean channel water surface elevation (WSE) (A & B), mean channel velocity (C & D), and proportion of floodplain discharge (E & F) under all topography and roughness alterations moderate and major peak discharge.

3.5. Discussion

Because flood wave attenuation is considered an ecosystem service in terms of flood control and channel-floodplain dynamics during flood waves are critical to ecologically functioning floodplains [*Junk et al.*, 1989; *Brauman et al.*, 2007; *Opperman et al.*, 2010], understanding of channel-floodplain processes is needed for the improvement of integrated floodplain management. Additionally, flood wave attenuation science has focused on a number of theoretical modeling strategies to investigate the fundamental process of attenuation and effects of river engineering and restoration [*Wolff and Burges*, 1994; *Woltemade and Potter*, 1994; *Acreman et al.*, 2003; *Anderson et al.*, 2006; *Ghavasieh et al.*, 2006; *Sholtes and Doyle*, 2010], however modeling strategies have not studied the questions concerning attenuation with the use of high-resolution, two-dimensional hydrodynamic models. These models are capable of capturing local feature and reach length processes fundamental to flood wave attenuation. It was within this context that sensitivities of attenuation to contemporary river conditions were statistically analyzed and hypothetical alteration scenario modeling was conducted.

The statistical results within this study have important implications for the river management in heavily modified systems. Correlations were found between attenuation and both the TA and RIATA single characteristics. The correlation between total channel-floodplain area complements the findings of previous research which has found floodplain width in unconfined systems is also important for large flood waves [*Woltemade and Potter*, 1994]. Because the modeling conducted here was done in a fairly uniform, leveed system, the results strengthen the case for levee setback strategies and the sensitivity that flood waves have to accessible floodplain area. However, this study also displays the importance of understanding flood magnitudes and the influence of storage capacity on the process of attenuation. While levee setback strategies are likely to increase attenuation in areas already inundated by a design flood, the correlation with attenuation was stronger with surfaces that have the capacity for additional inundation during flood events. Homogeneity of channel-floodplain connectivity is likely to attenuate one magnitude of flood to a great extent but impact other events to a relatively small degree. A system with floodplain surfaces which include various elevations in which water surface elevations eclipse an inundation threshold will provide more

dynamic attenuation patterns. River reaches which provide the greatest levels of flood wave attenuation are likely to be those in which heterogeneous connectivity patterns exist, conditions which should also be considered in levee setback situations.

While statistical analysis for moderate flood waves did not show high levels of correlation, there are two points worth discussing. First, the correlation with the greatest R^2, a value substantially higher than all other predictors, was found between peak water surface elevation and floodplain elevation. The potential relationship implies that areas in which the peak water surface elevation is at or near the floodplain elevation have a stronger correlation to greater rates of attenuation than do areas in which the water surface elevation is either well above or below floodplain elevation. This result complements the idea that during moderate flood events, channel-floodplain connectivity is critical to the attenuation of flood waves. More simply, areas in which water surface elevation eclipses a threshold of floodplain elevation likely provide rapid storage of water and in turn attenuation of the flood wave. The second point involves the fact that correlations under moderate flood events were very low. This likely arises from the fact that influences on attenuation are considerably more localized than the kilometer scale. Whereas major flood events inundate much of the floodplain surface and kilometer-scale influences can be recognized, more localized connections likely drive moderate flood wave attenuation. Specific study of flood waves near bankfull level can likely be of more significance in explaining local influences.

Improved understanding of how flood wave dynamics have changed within the confined MRG can be inferred from results presented here. In complement with previous studies, results here suggest moderate floods are attenuated to a greater degree. However, the hypothetical alterations to the channel-floodplain system indicate the impacts of channel incision, bank stabilization, and vegetation changes to banks and floodplains. Channel incision will increase the discharge at which overbank flows eclipse the historical floodplain surface. Therefore, channel incision brought upon by the control of sediment inputs with the construction of Cochiti and other dams is likely to have disconnected the floodplain to an extent that large magnitude flood waves are more greatly attenuated within these reaches compared with an aggraded, connected, yet still levee-confined channel. Increases in only bank roughness, characteristic of dense,

invasive vegetation on the channel banks, appear to promote a greater fraction of water flowing on the floodplain. In contrast, roughness increases to the entire floodplain, indicative of dense, invasive floodplain monocultures, lower the fraction of discharge on the floodplain. These results are likely to apply to many southwestern rivers subjected to similar alterations and ecological change. Description of processes associated with changes in channel topography and floodplain roughness exhibit important implications both for the reach scale process of attenuation, but also for river management and river ecology.

Topographic and roughness alterations revealed impacts on attenuation to relatively the same magnitude, however differences in the patterns of attenuation inform attenuation processes. Roughness alterations displayed more uniform impacts on flood wave attenuation when compared with topographic changes. That is, roughness alterations retain the form of baseline attenuation patterns. This suggests that attenuation due to roughness is an accruing process in which local influences are small but reach length influences are large. In comparison, topographic alterations modify attenuation rates differently, exemplified by attenuation ratios that can differ drastically from baseline conditions along the river. This indicates that attenuation due to topographic alterations also accrues but is dependent on the accumulation of attributed by local features. It should be noted that topographic and roughness alterations in a real-world setting are unlikely to occur independently of one another if the alterations occur due to natural processes. However, the timescales at which characteristic changes occur are likely to differ and the interdependency will drive feedbacks in the context of river morphology and ecology [*Merritt and Cooper*, 2000; *Poff et al.*, 2007; *Tal and Paola*, 2010]. Anthropogenic alterations may be more prone to individual topographic or ecological changes. For example, clearing of floodplain vegetation is a strategy used for invasive species control and fire risk reduction, but likely has little impact on topography along the Rio Grande [*Najmi et al.*, 2005]. Because short duration flood waves along the Rio Grande are part of the natural flow regime due to the southwestern climate, any anthropogenic vegetation alteration of the entirety floodplain is likely to influence these types of flood pulses. In all river systems, alterations to flood wave dynamics should be considered when implementing channel-floodplain alterations.

Due to the complex nature of river management, the results of this study can be interpreted differently depending on perspective. Often, societal perspectives display rivers as a hazard or a resource [*Knighton*, 1998]. In terms of flood control in the MRG, it is evident that both engineered channel incision and increases in roughness through the spread of salt-cedar monocultures are likely to attenuate major flood waves to a greater degree. For protection of infrastructure, this is reassuring, especially in the MRG where short duration major flood waves still occur. However, from an ecological point of view, these changes to the Rio Grande and its floodplain have already proven detrimental to biogeochemical processes, fish populations, and floodplain heterogeneity [*Howe and Knopf*, 1991; *Platania*, 1991; *Shafroth et al.*, 2005; *Valett et al.*, 2005; *Dudley and Platania*, 2007]. Model scenarios representing restoration of floodplain systems are at odds with flood protection strategies in that attenuation of major flood events is decreased as floodplain topography and roughness are lowered. Further, as flood waves are a natural process within river systems, the greater attenuation of a flood wave in engineered or monoculture systems means that less river distance will be subjected to elevated flood stages and the dynamic processes associated with these events. While alterations associated with restoration for the entire floodplain are not in line with flood protection interests, smaller scale changes such as bank restoration do not greatly influence flood wave attenuation as similar attenuation rates have been documented here. Therefore, in terms of reach scale flood protection, these types of projects should be continued to be pursued if ecological gains can be created. If floodplain-scale ecological restoration works are a goal it is likely that infrastructure along many rivers will need to be adjusted to continue to attenuate flood waves in the same manner with heterogeneity of floodplain elevations crucial to attenuation of floods of various magnitude. Further flood wave attenuation research should focus on possible impacts of levee setbacks within heavily modified systems with a focus on ensuring both ecological and attenuation processes. The realities of river management also suggest that there may also need to be a focus on certain stretches of river being infrastructure based for flood protection while other reaches provide ecological integrity due to the realities of existing river alteration.

3.6. Conclusions

This study had two main objectives: (1) to investigate the sensitivity of flood wave attenuation to existing channel and floodplain characteristics, and (2) to assess how historical and contemporary channel and floodplain alterations affect flood wave attenuation. Statistical results showed flood wave attenuation is impacted by total area accessible to flow and the potential for water storage even within a fairly uniform, confined system. Implications of this finding suggest that contemporary anthropogenic attenuation strategies, such as levee setbacks, are likely to have substantial impact on flood peaks, however, care must be taken to understand the heterogeneous nature of attenuation in terms of floodplain elevation. Results of alteration scenario modeling displayed the large local influence that topographic features have on attenuation while attenuation was an accruing process under roughness alterations. Finally, while bank alterations did not impact flood wave attenuation to a great degree, bank and floodplain roughness alterations did display differences in process under steady floodplain flow conditions. While every river system is different, many rivers in the southwestern United States have been subjected to similar alterations in the name of flood control and water use. The hypothetical results can therefore directly inform river management along many of the rivers in this region as well as other rivers with similar geomorphology and climate. As flood wave attenuation is important to those concerned with flood protection as well as ecological interests, the dual, and often contrasting, impacts to attenuation must be considered in floodplain management.

Chapter 4

Unsteady hydrodynamic processes at the channel-floodplain interface as indicators of lateral floodplain connectivity

4.1. Introduction

Floodplain connectivity to river channels is of critical importance to spatial and temporal floodplain heterogeneity [*Ward et al.*, 2001; *Wohl et al.*, 2015]. While connectivity is no doubt three-dimensional in nature, lateral channel to floodplain surface connections can transfer large quantities of water and associated biogeochemical material and processes within well connected systems. Integral elements of connectivity, river hydrology and hydrodynamics, develop complex relationships with river form and biota. These spatial and temporal relationships are interdependent on one another and critical for the existence of natural processes in river and floodplain systems [*Junk et al.*, 1989; *Ward*, 1989; *Amoros and Bornette*, 2002]. The interdependence of hydrodynamics, geomorphology, and ecology means that understanding how one field impacts another is not trivial [*Thoms*, 2003]. In addition, reach-scale conceptualizations of river connectivity provide qualitative understanding of river process and form, but quantification of connectivity and exchange processes proves difficult. Past studies have strived to attain this unification between process and form [*Lane and Richards*, 1997; *Richards et al.*, 2002; *Croke et al.*, 2013], connectivity and biota [*Barko et al.*, 2006; *Morrison and Stone*, 2014; *Blettler et al.*, 2016], and connectivity and biogeochemical processes [*Tockner et al.*, 1999; *Scott et al.*, 2014; *Jones et al.*, 2015]. These studies provide critical knowledge in the combination of hydrologic processes with river geomorphology and ecology but often are of small spatial scale or limited by the inherent nature of empirical study in highly dynamic and heterogeneous river systems.

River systems throughout the developed world have been subjected to substantial modifications, typically in the name of water use, energy production, or flood protection. These modifications have led to altered hydrologic and geomorphic processes and drastic changes in floodplain connectivity. More recently, anthropogenic alterations have been in

the form of river restoration, including rehabilitation projects [*Wohl et al.*, 2005]. While a great number of river restoration projects have been conducted in the name of water quality, species habitat, or riparian management, a more limited number have focused on restoring floodplain connectivity [*Bernhardt et al.*, 2005]. More thorough understanding of river dynamics has led to a push for river restoration that restores dynamic processes and the need for process metrics [*Palmer et al.*, 2005, 2014; *Kondolf et al.*, 2006; *Beechie et al.*, 2010; *Harvey and Gooseff*, 2015; *Wohl et al.*, 2015; *Covino*, 2017]. Increased hydrodynamic processes allow a river to shape a more natural landscapes and create functional ecosystems [*Stanford et al.*, 1996; *Ward et al.*, 2002]. Measuring or estimating hydrodynamic processes over large spatial and temporal scales proves difficult but is needed in multiple fields of study. For example, if nutrient exchange between the channel and floodplain is of interest, flow volumes are likely of importance as well as residence times associated with floodplain flow. In comparison, if sediment transport or river geomorphic dynamics are the focus of investigation, the description of both the water volume and the forces associated with the movement of water are necessary. The importance of reestablishing river processes when restoring altered river systems is clear, but the question remains as to how to quantify hydrodynamic processes in a way that can be applied to our understanding of river science and river restoration strategies.

River and floodplain hydrodynamics are important at various scales throughout a river system [*Hughes et al.*, 2001]. At bedform scales ($\sim 10^{-1} - 10^{1}$ m) turbulence, either stemming from the movement of water across bedforms and vegetation or from viscous effects within the flow of water, is important to processes such as sediment transport [*Bennett and Best*, 1995; *Nelson et al.*, 1995; *Nepf and Vivoni*, 2000], nutrient exchange [*Schulz et al.*, 2003; *Murphy et al.*, 2007], and vegetation community structuring [*Nilsson et al.*, 2002]. At a planform feature scale ($\sim 10^{1} - 10^{3}$ m), turbulent eddies and differences in mass and momentum transfer exist due to channel-floodplain topography found in complex channels and changes in roughness associated with bed material or vegetation [*Shiono and Knight*, 1991; *Nepf*, 1999; *Helmiö*, 2004; *Vermaas et al.*, 2011]. Accumulation of these processes at reach scales ($\sim 10^{3} - 10^{5}$ m) leads to floodplain landscape dynamics [*Thorp et al.*, 2006; *Winemiller et al.*, 2010], river planform [*Knighton*, 1998], and large-scale ecosystem services such as flood wave attenuation

84

[*Woltemade and Potter*, 1994; *Wyzga*, 1996; *Brauman et al.*, 2007]. Within the context of floodplain connectivity, the transfer of water to the floodplain is of the utmost importance due to the known influence of associated hydrodynamic processes. Therefore, quantification of key physical attributes of water exchanges between the main channel and the floodplain can advance our understanding of these processes. The exchange of water occurs at the channel-floodplain interface which exists across these scales of geomorphic and ecological interest.

Lateral floodplain connectivity, and more specifically floodplain geomorphology and ecology, ultimately depend on the transfer of a quantity of water, here presented as mass flux, from the main river channel to the floodplain. A mass flux of water will also transport dissolved and suspended biogeochemical elements. Studies have displayed the importance of mass flux in relationship to these biogeochemical processes [*Hughes*, 1997; *Jones et al.*, 2015]. For example, spatial and temporal dynamics of nutrient exchange have been shown to be important to the quality of nutrients supplied to the main channel [*Atkinson et al.*, 2009]. In addition, large scale sedimentation rates are likely to be related to retention times of water on the floodplain [*Middelkoop and Van Der Perk*, 1998]. Due to the importance of water and elements it carries, continued development of new methods to quantify the flux of water in a channel-floodplain system needs to be pursued.

The mass of water transferred to the floodplain is associated with a water velocity and consequently imparts momentum exchange to the floodplain as well. While momentum flux, or the time rate of change in momentum, can be a product of both turbulence and mass transfer, in non-prismatic channels and thus natural channels, momentum flux to the floodplain is most highly associated with mass transfer [*Proust et al.*, 2009]. Momentum flux, presented here as a time rate of change in momentum at the channel-floodplain interface, can provide insights regarding ecological and geomorphic processes beyond those provided from the study of mass flux. Differences in momentum at key interfaces, such as changes in roughness, topography, and vegetation, have been shown to enhance turbulent mixing [*Shiono and Knight*, 1991; *Helmiö*, 2004; *Vermaas et al.*, 2011], therefore quantifying and identifying areas where momentum flux is high may correlate with areas where turbulent mixing processes are important to floodplain ecology

such as phytoplankton life cycles [*Sommer et al.*, 2004], sedimentation [*Asselman and Middelkoop*, 1995; *Poulsen et al.*, 2014], and perirheic zones [*Jones et al.*, 2014]. Expanding hydrodynamic mapping to geomorphic and ecological questions over large spatial and temporal scales provides a myriad of possibilities.

While knowledge of lateral flow processes is important, these processes ultimately occur within some temporal context of a longitudinal flow regime [*Poff et al.*, 1997]. Broad understanding of the timing of connectivity during a flood wave is at the foundation of modern river science [*Junk et al.*, 1989; *Ward*, 1989], and more recent temporal conceptualizations have been developed to understand the exchange of sediments, organic matter, and nutrients [*Tockner et al.*, 1999; *Steiger et al.*, 2005; *Harvey and Gooseff*, 2015; *Covino*, 2017]. Measurement of river discharge has focused on river stage and downstream flow volumes as those metrics are logical in the studies of basin hydrology or flood potential. However, if channel-floodplain connectivity or ecological floodplain science are of interest, integration of lateral and longitudinal discharge needs to be investigated [*Covino*, 2017]. Because discharge is the most relatable metric between systems throughout the world, understanding lateral discharge as a function of heavily measured downstream discharge is likely to be of interest in a multitude of applications.

The objective of this research was to quantify hydrodynamic processes of lateral surface connectivity at the channel-floodplain interface during unsteady flow events. Within a heavily manipulated river system, the quantification of such lateral processes can identify key spatial and temporal elements of floodplain connectivity and the relative impact of river restoration efforts in a context of river process. Results from the study are presented as mass and momentum fluxes associated with the transfer of water from the main channel to the floodplain. Geomorphic classification of the channel-floodplain interface is analyzed to further the conclusions about floodplain connectivity. A secondary objective of this study was to assess the relationship between lateral connectivity and longitudinal magnitude and timing of discharge. The objectives of this study were achieved using two-dimensional hydrodynamic modeling and post-processing scripting techniques to analyze hydrodynamic model results. The goal of this research is to further the understanding of channel-floodplain hydrodynamic processes with a focus

on surface connectivity, to display new strategies of computational modeling, and ultimately to inform multidisciplinary river management strategies.

4.2. Site Description

This study focuses on a 27-kilometer stretch of the Rio Grande adjacent to the city of Albuquerque, NM known as the Albuquerque Reach of the Middle Rio Grande (MRG) between USGS 08329918 (Alameda Bridge Gage) and USGS 08330875 (Isleta Lakes Gage; Fig. 4.1). The MRG has been heavily engineered for water use in a semi-arid climate and flood protection for agricultural and urban use of the floodplain. The combination of large-scale river and floodplain engineering projects with changing land use and climate has had significant geomorphic impacts on the river over the past century [*Scurlock*, 1998; *Richard and Julien*, 2003; *Meyer and Hepler*, 2007; *Schmidt and Wilcock*, 2008; *Swanson et al.*, 2011]. The result of these changes is a channelized river, predominantly confined between bounding levees and jetty jacks, and with diminished ecological integrity of native ecosystems.

Three distinct floodplain feature types exist within the study reach: (1) inset, (2) historical, and (3) restored. Inset floodplains remain connected to the river under moderate flows and include channel-islands and bank-attached islands and bars which have stabilized with vegetation under extended drought conditions over the past two decades and flow regulation [*Meyer and Hepler*, 2007; *Swanson et al.*, 2011]. The second feature type, or the historical floodplain, retains some connectivity as this surface is within the bounding levees or defining topography. However, due to channel incision and reinforced banks, the inundation frequency of this surface varies from relatively often to never [*Stone et al.*, 2017]. Implications of this disconnected floodplain in the MRG include impacts to native ecology including fish populations [*Pease et al.*, 2006], biogeochemical and metabolic responses [*Valett et al.*, 2005], and changing vegetation patterns [*Howe and Knopf*, 1991; *Taylor et al.*, 1999]. The third category of floodplain feature type is composed of restored floodplain features. These occur within the historical floodplain where vegetation and topography have been mechanically manipulated to improve ecological conditions prior to 2012. New connections to the river have been created primarily for the endangered Rio Grande silvery minnow (*Hybognathus amarus*),

which has been subject to substantial loss of habitat and habitat fragmentation in the MRG [*Bestgen and Platania*, 1991; *Alò and Turner*, 2005].

The dominant hydrology of the MRG is defined by a late spring, early summer snowmelt pulse and late summer, short-duration flood pulses produced by convective, monsoonal storm events. Historically, these flow conditions were already highly variable, both in terms of yearly snowmelt peak flows and the development of monsoonal moisture [*Scurlock*, 1998]. However, with upstream flood control and diversion dams, the natural flow regime is now greatly altered for flood protection and water use [*Stone et al.*, 2017].
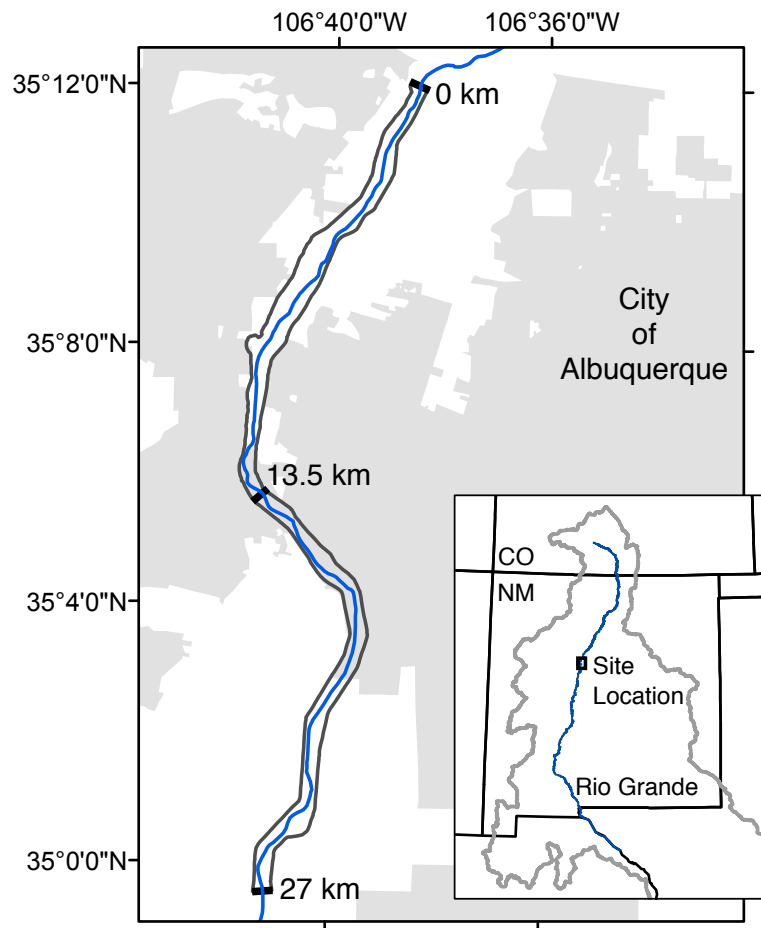
Figure 4.1. Location of modeled study reach near Albuquerque, NM.

4.3. Methodology

4.3.1. Hydrodynamic Model Setup

A two-dimensional mesh was developed using Deltares' D-Flow Flexible Mesh (D-Flow FM) software [*Deltares*, 2015]. The mesh covered approximately 32 km of channel and predominantly leveed floodplain in the most heavily urbanized reach of the MRG. Mesh elements averaged 26 m^2. Elevations of each floodplain mesh element were interpolated from a two-meter digital elevation model (DEM) created using 2010 Light Detection and Ranging (LiDAR) data and supplemented by 2012 LiDAR data at specific river restoration locations. In the main channel of the Rio Grande where water prevented LiDAR of the river bed from being acquired, United States Bureau of Reclamation cross-section surveys from 2014 were used to interpolate channel bathymetry between cross-sections [*Adair*, 2016].

4.3.2. Boundary and Roughness Conditions

Upstream conditions were defined by an unsteady discharge boundary. Because hydrodynamic processes will occur at different rates depending on various characteristics of a flood wave, six distinct flood waves were routed through the hydrodynamic model, all of relatively short duration (several days). While the hydrology of the MRG is defined by long-duration snowmelt events in the spring and early summer, these events are likely to be less dynamic along the channel-floodplain interface (i.e. changes in hydrodynamics will be more gradual). Therefore, shorter duration events were the focus of this paper. The downstream boundary was set to a water surface elevation based on the upstream flow hydrograph. Gage data at the downstream boundary did not have records of high flow events due to the relatively recent (2002) installation of the gage. In addition, it has been documented that gage information in sand-bed rivers is susceptible to considerable amounts of error [*Isaacson and Coonrod*, 2011]. To minimize uncertainty associated with the lower boundary condition, the most downstream 5 km of data were removed, resulting in the 27-km reach presented in Figure 4.1. Manning's roughness coefficients were held constant for the two models and were defined by vegetation mapping

conducted from previous ground and aerial surveys [*Hink and Ohmart*, 1984; *Callahan and White*, 2004].

4.3.3. Modeled Hydrology

Because this research focused on the theoretical implications of flood waves and flood processes on the dynamics of floodplain connectivity, hypothetical flood waves were used at the upstream model boundary as opposed to historical events. Moderate and major floods, 180 and 300 m^3s^{-1} flood peaks, respectively, were modeled for three durations: 1, 1.5, and 3 days (Fig. 4.2). The moderate and major flood magnitudes are roughly equivalent to the 5-year and 50-year return periods under the present flow regime. Moderate flood events are representative of flows exceeding historical bankfull discharge (~2-year flood discharge, 135 m^3s^{-1}) only near flood peak. Major flood events are representative of a flood occurring when flows are already exceeding historical bankfull discharge to a small degree. Therefore, initial conditions for moderate and major flood events were 30 and 150 m^3s^{-1}, respectively. For the Albuquerque Reach of the Rio Grande, these types of flood events would be most common during monsoonal storm events in late-summer (moderate flood) or in the form of storm events occurring during snowmelt (e.g. rain on snow) in late-spring and early summer (major flood).
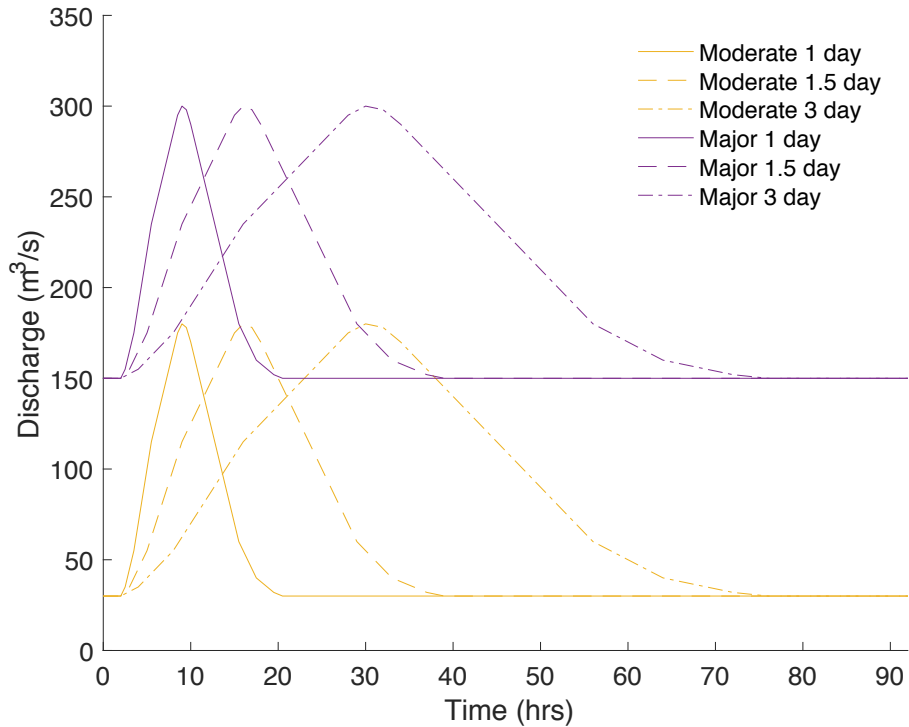
Figure 4.2. Hydrographs at the upstream boundary under six different flood wave conditions.

4.3.4. Model Pre-Processing

To study mass and momentum fluxes across the channel-floodplain interface, those control surfaces needed to be defined along the entire river corridor. ESRI's ArcMap 10.1 [*ESRI*, 2012] was used to digitize the approximate interface with the use of 2010 orthophotography. The interface was digitized at the boundary between the main channel and areas of established floodplain vegetation. Vegetation was used as a key indicator of the channel-floodplain interface because the Rio Grande is a sand-bed river and orthophotography was taken during a period of low flow. Sandbars within the river are likely to be considerably more mobile than areas with established vegetation [*Mussetter Engineering, Inc.*, 2006], and thus likely to become part of the main channel during bankfull discharge. The model elements along the channel-floodplain interface were identified using a Matlab 2016a [*MathWorks, Inc.*, 2016] script resulting in time series of

depth and velocity results at 10 minute intervals for a total of 8622 and 8405 elements for the left and right floodplains, respectively.

4.3.5. Post-Processing Analysis

Mass and momentum fluxes were calculated using post-processing scripting techniques. The process of calculating fluxes is based upon the idea that the channel-floodplain interface is a control surface. Consequently, at any surface along the interface, the mass flow rate (mass flux) or time rate of change of momentum (momentum flux), is defined by the quantity of water flowing normal to the interface surface. Any water flowing parallel to the interface is moving in the downstream direction and not being transferred from the channel to the floodplain. The normal unit vector was computed for each interface surface in the channel to floodplain direction. Therefore, mass or momentum fluxes from the main channel to the floodplain were defined as positive.

Mass flux was defined as the exchange of mass per unit time between the main channel and the floodplain. Mass flux (M_f, kg s^{-1}) was calculated using average depth (d, m), normal velocity (V, m s^{-1}), connection length (l, m), and fluid density (ρ, kg m^{-3}) for every element along both left and right floodplain interfaces (Eqn. 1).

$$M_f = \rho * d * l * V \qquad\qquad (1)$$

Momentum flux was defined as the time rate of change of momentum across the channel-floodplain boundary. Therefore, the momentum flux (P_f, N) is the product of mass flux and the absolute value of the normal velocity and was calculated for each boundary element (Eqn. 2).

$$P_f = M_f * |V| = \rho * d * l * V * |V| \qquad (2)$$

With mass and momentum flux calculated at every model time step, further analysis was conducted to investigate flood wave process and better understand floodplain connectivity during the simulated floods. Spatial, temporal, and frequency analyses were investigated for these floodplain types to elucidate the differences in river process under

different geomorphic conditions. Temporal mass and momentum flux were calculated above initial conditions to isolate the influence of the flood wave at the two initial condition discharges.

Because discharge is often an integral metric to river science, lateral and longitudinal discharge were quantified in terms of time and magnitude. The ratio of lateral to longitudinal discharge was calculated for each flood wave for each kilometer of the reach. Timing of maximum discharge was computed using individual elements with maximum or minimum discharges greater than or less than $0.01 \text{ m}^3\text{s}^{-1}$, respectively, to remove elements that fluctuated near zero. The timing of each element's maximum or minimum flux was subtracted from a linearly interpolated line of longitudinal peak discharges produced at 250 meter cross-sections. Positive time of arrival represents peak lateral discharge which occurs after the longitudinal flood peak while negative time of arrival represents lateral peak discharge which occurs before the longitudinal flood peak.

4.4. Results

Large-scale patterns of floodplain connectivity were described by investigating the dynamic nature of mass transfer as a function of time. Net mass flux across the left and right channel-floodplain interfaces were calculated as a function of time for each of the six flood scenarios (Fig. 4.3). To allow for direct comparison, positive and negative total mass fluxes were also determined for each floodplain feature type. The period for which the flood peak was located within the reach of interest is also indicated by the shaded gray region.

Positive and negative total mass fluxes remained on the same order of magnitude for the entire flood wave, pointing to consistent exchange at the interface rather than channel-to-floodplain or floodplain-to-channel processes dominating on the rising or falling limb of the flood wave. However, small changes in positive and negative total fluxes create the patterns of net mass flux. Net mass flux totals are approximately one to two orders of magnitude smaller than total mass flux. While net mass flux totals are therefore small in relation to total mass flux, the totals do give a good indication of dominating inundation or recession flood wave processes and the nature of connectivity in the reach. In addition, these flux relationships here are in the context of a heavily

manipulated and constrained river-floodplain system. This pattern may change at more local scales of interest or under less altered conditions.

4.4.1. Flood Duration and Magnitude Influences on Mass Flux

The net mass flux plots display the variability in the transfer of water to the floodplain as it relates to flood duration and initial flow volumes. The peak magnitude of net mass flux to the floodplain decreased as the flood duration was increased (comparison of results in each column of Fig. 4.3). With increased flood duration, peak mass flux is dampened by the rate of change of the hydrograph and, in tandem, the rate of change of total mass flux. Differences in the rate of change of total mass flux are evident (e.g. Fig. 4.3C, G, and K). In perhaps a more intuitive description, it is a slower increase in water surface elevation in connected portions of the floodplain during long duration events compared to flashier, short duration events which drives the more gradual and lower maximum net mass fluxes. Maximum net mass flux increased with increases in initial conditions from 30 to 150 m^3s^{-1} (comparison of results in a respective row), although to a lesser degree during long duration events. Events at greater initial flows will have greater total mass flux due to the increased volume of water passing through the reach. However, these results show that even when initial flow rates are removed from the calculated flux, as was the comparison in this research, the same flood wave still transfers more mass to the floodplain under high initial conditions (Fig. 4.3C vs D, G vs H, and K vs L). This is attributed to both an increased number of connections providing pathways for water to flow onto the floodplain and many of those connections remaining connected for the entirety of the flood event.
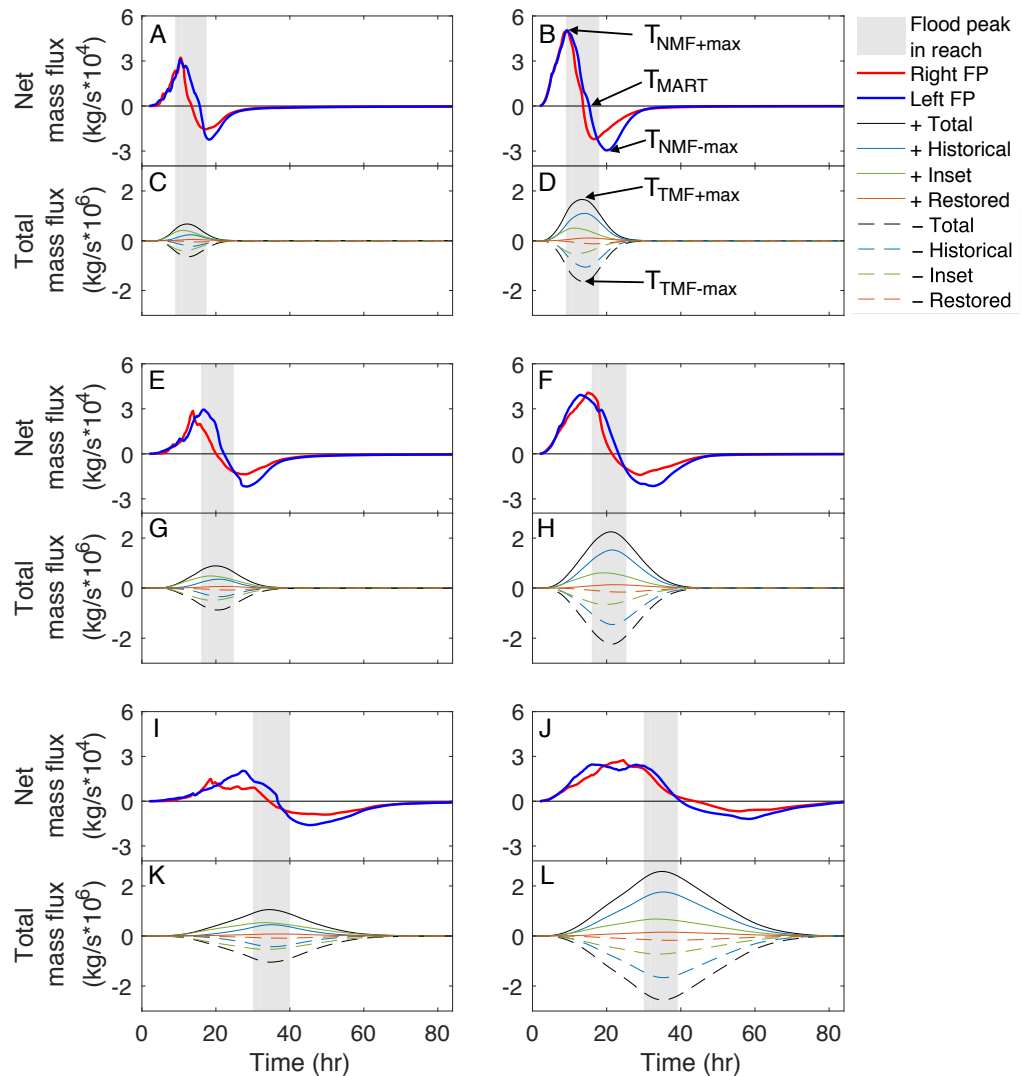
Figure 4.3. Net mass flux (left and right floodplain) and total mass flux (by floodplain class) as a function of time for (A,C) 1-day, moderate, (B,D) 1-day, major, (E,G) 1.5-day, moderate, (F,H) 1.5-day, major, (I,K) 3-day, moderate, and (J,L) 3-day, major flood events. The gray region in each plot indicates the period over which the flood peak was present in the simulated reach. Key timings described in Table 4.1 are labeled in for net mass flux of the left floodplain in Figure 4.3B and total mass flux in Figure 4.3D.

4.4.2. Channel-Floodplain Connectivity Influences on Mass Flux

Temporal net mass flux characteristics imply heterogeneity of reach-scale connectivity patterns within the modeled reach. Temporal changes in net mass flux across left and right interfaces display differences between left and right floodplain connectivity,

95

especially in moderate flood events and between moderate and major long duration events. For example, as flood duration increases for moderate flood events, (Fig. 4.3A, E, and I), the right floodplain reaches maximum net mass flux at an earlier time relative to the left floodplain for events of increasing duration. The left floodplain net mass flux is also at greater rates for longer periods of time. This indicates that the right floodplain has greater connectivity in the upstream portion of the reach, and in comparison, the left floodplain is more greatly connected in the downstream portion of the reach. An increase of initial flow conditions between moderate and major, 3-day flood events (Fig. 4.3I and J), indicates further characteristics of floodplain connectivity. The 3-day, major flood event shows evidence of dual maximum net mass fluxes on the left floodplain (Fig. 4.3J). Perhaps the most evident result of temporal net mass flux quantification is that the heterogeneous floodplain connectivity is highly dependent on the characteristics of the flood wave passing through a reach of interest.

The net mass flux curves also display distinct characteristics of feature scale connectivity in terms of magnitude and duration. Moderate flood net mass fluxes tend to be less smooth than the flux curves associated with major flood events. This indicates that moderate flood flux quantities are more susceptible to influences of local topography, evident in the sub-peaks and more jagged form compared to the major flood curves. The sharp increases in flux rates and sub-peaks indicate activation of local connections, while the general trend of the curve shows the connectivity relative to the entire floodplain as the flood wave moves through the system. The smoothness of the major flood curves suggests that the main connections are already inundated at initial conditions and therefore mass transfer increases more uniformly. Elongation of the fluxes is no doubt due to the elongation of the flood wave; however, the real-world implication of this process is that peak mass flux magnitudes are reduced as inundation becomes more gradual at lateral connection points.

4.4.3. Temporal Characteristics of Mass Flux

The mass flux plots include several key points in time important for describing flood wave processes and are summarized in Table 4.1 and labeled in Figure 4.3. Time of maximum net mass flux ($T_{NMF+max}$) tends to occur shortly after the flood peak enters the

reach for short duration events and arrives earlier in regard to the flood peak for longer duration events. In comparison with total mass flux, it is apparent that the greatest rate of channel-to-floodplain mass transfer does not necessarily coincide with the time of maximum total mass flux ($T_{TMF+max}$). The $T_{TMF+max}$ occurs at nearly the same time as the maximum negative mass flux ($T_{TMF-max}$) for all flood events and always while the flood peak is within the reach of interest. This is a logical result as water surface elevations at flood peak are likely highest leading to maximum total connectivity. Maximum negative net mass fluxes ($T_{NMF-max}$) predominantly occur after the flood wave has left the reach of interest with the exception of the right floodplain during short duration flood events. The timing and magnitude of this high rate of return flow is ultimately defined by the combination of many return flow paths still highly connected and a large amount of mass remaining on the floodplain. The final temporal point of interest is that in which net mass flux shifts from positive to negative, or here labeled the time of mass activation-recession transition (T_{MART}). This point is defined by the time in which more water is now returning to the main channel from the floodplain than previously when channel-to-floodplain fluxes were dominant. The T_{MART} is nearly always before the flood peak leaves the reach, apart from Figure 4.3F. This merely quantifies the fact that as flood peak and durations increase, the floodplain is hydrologically connected for a longer period. More importantly, during long duration events, mass can still accrue on the floodplain after the flood peak has moved beyond a reach. In summary, the quantification of net mass fluxes presents three distinct time periods: a time of increasing mass flux in which floodplain connections activate, a time of peak connectivity in which mass flux shifts from positive to negative, and a time of negative mass flux in which flood wave recession processes dominate.

Table 4.1. Timing (hr) of lateral processes including mass flux, momentum flux, and discharge.

			Moderate Floods			Major Floods		
			1-day	1.5-day	3-day	1-day	1.5-day	3-day
Mass	$T_{NMF+max}$	Left	10.3	16.7	27.3	9.3	13.0	16.0
		Right	10.5	13.8	18.5	9.5	15.0	24.5
	T_{MART}	Left	15.7	22.3	36.8	15.3	23.3	40.0
		Right	13.5	20.2	34.5	13.7	21.5	43.8
	$T_{NMF-max}$	Left	18.2	28.3	45.5	20.0	32.3	58.5
		Right	17.0	27.8	49.0	16.5	29.0	56.0
	$T_{TMF+max}$		12.3	19.8	34.5	13.3	21.2	35.0
	$T_{TMF-max}$		12.7	20.3	34.8	14.0	21.3	35.2
Momentum	$T_{NPF+max}$	Left	11.7	17.7	27.8	12.2	20.0	34.0
		Right	10.3	13.8	30.3	9.7	17.3	32.0
	T_{PART}	Left	16.3	26.8	50.7	19.7	34.3	72.0
		Right	14.0	22.3	39.7	17.2	31.3	63.7
	$T_{NPF-max}$	Left	18.3	30.5	56.5	22.2	39.5	78.2
		Right	17.7	28.0	49.3	21.3	37.3	72.7
	$T_{TPF+max}$		11.5	19.3	34.0	12.5	20.7	34.7
	$T_{TPF-max}$		11.7	19.5	34.2	12.8	20.8	34.7
Discharge	$T_{QpLat} - T_{QpLong}$		-0.7	-1.5	-2.7	-0.8	-1.6	-3.0
	$T_{-QpLat} - T_{QpLong}$		0.7	0.7	0.7	0.6	0.9	1.4

4.4.4. Momentum Flux Characteristics in Relation to Mass Flux Patterns

Net momentum flux (N) at the left and right channel-floodplain interfaces and total positive and negative momentum fluxes for each floodplain type were calculated as a function of time and flood type (Fig. 4.4). There are two notable differences in quantification patterns between net mass and momentum flux. First, the relative magnitudes of net momentum flux across the left and right floodplain interfaces follow different patterns of change between moderate (Figs. 4.4A, E, and I) and major flood events (Figs. 4.4B, F, and J). During moderate flow events, the left floodplain has a greater maximum net momentum flux and contributes more total momentum to the floodplain than the right floodplain, represented by the area below the curves. However, when initial flow volume increases, the right floodplain experiences the greatest momentum flux and total momentum transfer. The second major difference between the

mass and momentum plots is evident in the negative net fluxes at the tail end of a flood event. In the measure of net mass flux, a large proportion of the mass transferred to the floodplain is returned to the main channel because the majority of mass transferred to the floodplain returns to the main channel while only a small proportion ponds on the floodplain. In contrast, the quantification of net momentum flux shows that while momentum is returned to the channel, the quantity returned does not approach the total transferred from channel to floodplain. This is because momentum is being dissipated on the floodplain surface. Maximum net momentum flux and total momentum transferred to the floodplain increase with increasing duration and initial flow discharge, while maximum negative net fluxes from the floodplain to the channel decrease under the same flood wave manipulation, meaning channel-to-floodplain momentum transfer dominates longer duration events.

Temporal patterns of net momentum flux also differ from net mass flux. While maximum positive and negative total momentum fluxes, $T_{TPF+max}$ and $T_{TPF-max}$, respectively, occurred at similar times in comparison with total mass flux, net momentum flux times display different patterns compared with net mass flux times. In comparison with maximum net mass flux which occurs prior to the flood peak entering the reach with increasing flood duration, the time of maximum net momentum flux ($T_{NPF+max}$) occurs when the flood peak is within the reach boundaries for all flood waves apart from the right floodplain during the moderate, 1.5-day event. However, even in this exception, momentum flux reaches a secondary peak while the flood peak passes through the reach. Net momentum fluxes are therefore highly dependent on the flood peak, whereas net mass fluxes are both dependent on the flood regime and floodplain storage availability, meaning there is a lag in return of mass during the rising limb of the flood wave. Due to the relationship between flood peak and net momentum flux, the time of the momentum activation-recession transition (T_{PART}) and the maximum negative net momentum flux ($T_{TPF-max}$) are delayed with increasing flood duration. This is in comparison to the net mass flux transition timings which typically occur as the flood peak leaves the reach and the maximum negative net mass flux timings which are not delayed to the same extent as maximum negative net momentum fluxes. These results show that while mass and

99

momentum fluxes are related, net flux timing characteristics differ substantially during a flood event.

4.4.5. Temporal Fluxes Resulting from Floodplain Feature Type

The partitioning of positive and negative total mass and momentum fluxes into floodplain type, based upon geomorphic characteristics, presents several interesting results. Results discussed here are presented for the medium duration events (Fig 4.3G and H), however, patterns of total mass flux along various floodplain types are similar between flood durations with the exception of the previously discussed elongation in flux. Connected inset floodplain elements, while smaller in number than historical floodplain elements, 1800 elements compared to 8730 elements, respectively, contribute a greater amount of mass during moderate flood events than do historical floodplain elements (Fig. 4.3G). Under major flood conditions, the historical channel-floodplain interface is more connected than under lower flood magnitude (12668 elements), contributing to the majority of total mass flux (Fig. 4.3H). However, momentum fluxes follow a different pattern. Inset floodplains are subject to a large percentage of the momentum transferred to the entire floodplain under moderate flood conditions and remain a substantial fraction of total momentum flux during major flood events (Fig. 4.4G and H). This suggests that while the historical floodplain is more greatly connected during major flood events, floodplain connections likely remain at low depths and velocities. Restoration sites activate during moderate and major flood events but at a much smaller level when compared to the historical and inset floodplain features, limiting the impact such features have on flux totals.
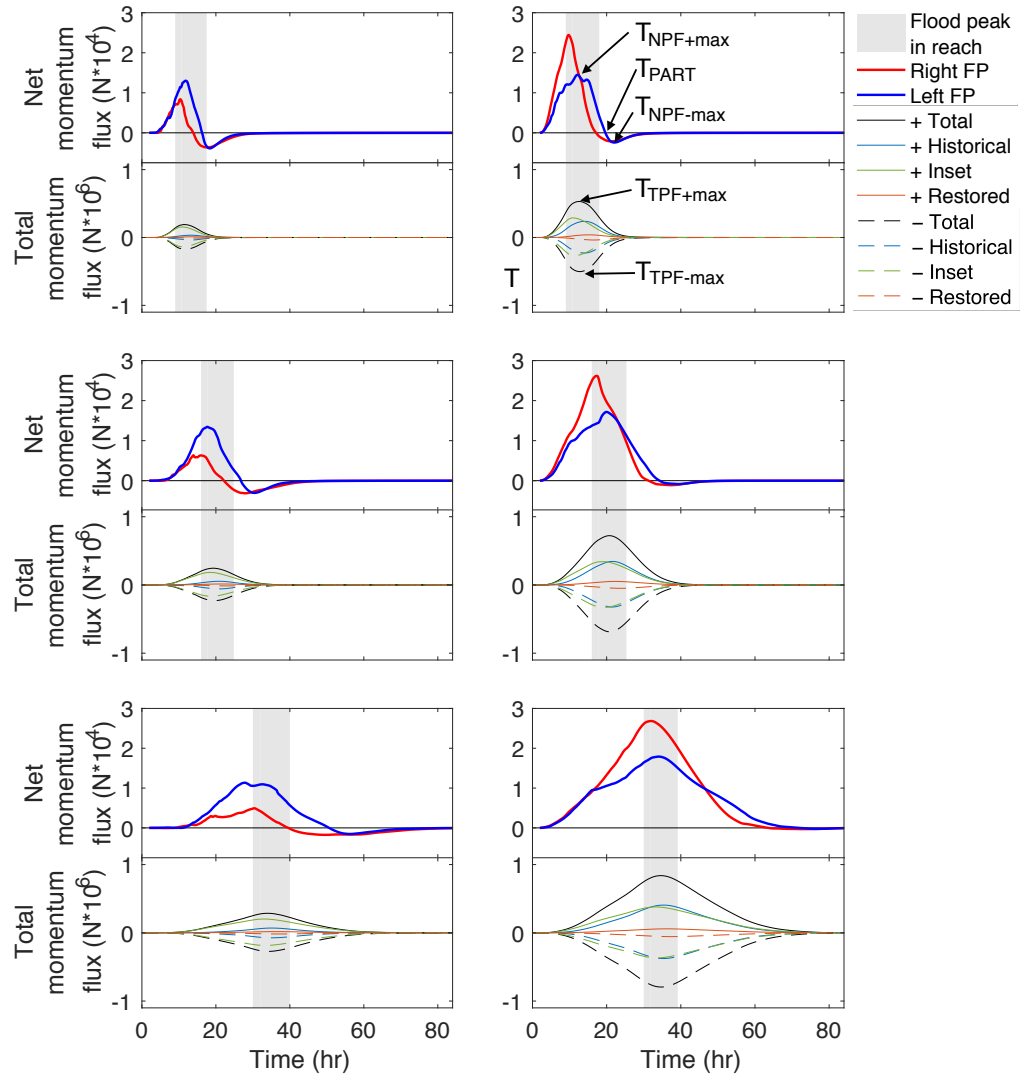
Figure 4.4. Net momentum flux (left and right floodplain) and total momentum flux (by floodplain class) as a function of time for (A,C) 1-day, moderate, (B,D) 1-day, major, (E,G) 1.5-day, moderate, (F,H) 1.5-day, major, (I,K) 3-day, moderate, and (J,L) 3-day, major flood events. The gray region in each plot indicates the period over which the flood peak was present in the simulated reach. Key timings described in Table 4.1 are labeled in for net momentum flux of the left floodplain in Figure 4.4B and total momentum flux in Figure 4.4D.

4.4.6. Maximum Interface Flux

Maximum mass and momentum fluxes at the interface, normalized for element length, were measured for the entire flood duration and are plotted for both the 27-km reach (Fig.

4.5) and at a feature scale (Fig. 4.6). Reach length mapping of flux values indicates portions of the reach have differing processes based upon large scale channel-floodplain geomorphology and local floodplain feature type. In terms of large-scale channel-floodplain geomorphology, there are lengths of the river that have a more connected floodplain, evident in the greater density of interface connections, while other areas are less connected. Connectivity based upon floodplain type can be seen in the upper portion of the reach where inset floodplain features are dominant. This result is further complemented by the timing of mass flux at inset floodplain boundaries (Fig. 4.3G and H), which activate earlier than other floodplain types. Inset features not only inundate during the moderate flood events, but some inset features also achieve similar maximum fluxes independent of the initial discharge. The historical floodplain throughout the reach is relatively disconnected during moderate flood events. During major flood events, the number of elements inundated increases dramatically, thus contributing to greater mass and momentum flux. In the middle of the reach, these connections achieve magnitudes similar to the inset floodplains, compared to the upper and lower third of the reach, where mass flux magnitudes remain relatively low. Restoration sites are apparent during moderate and major floods but cover minimal lengths of the channel-floodplain interface.

Spatial fluxes at historical, inset, and restoration feature types are displayed at a kilometer scale in Figure 4.6. The differences in magnitude of connections between inset and historical floodplains is again evident in consecutive channel meanders. Channel to floodplain exchange is evident at outside bend meander locations at inset elevations, but is lacking at elevations of the historical floodplain. Topographic manipulation at restoration sites does produce greater flux quantities, especially at the southern-most restoration site. However, while the inset floodplain experiences high flux magnitudes across nearly the entire upstream interface of the feature, the restoration site provides a more confined connection. Historical floodplain magnitudes at this location remain relatively small even with increases in discharge.
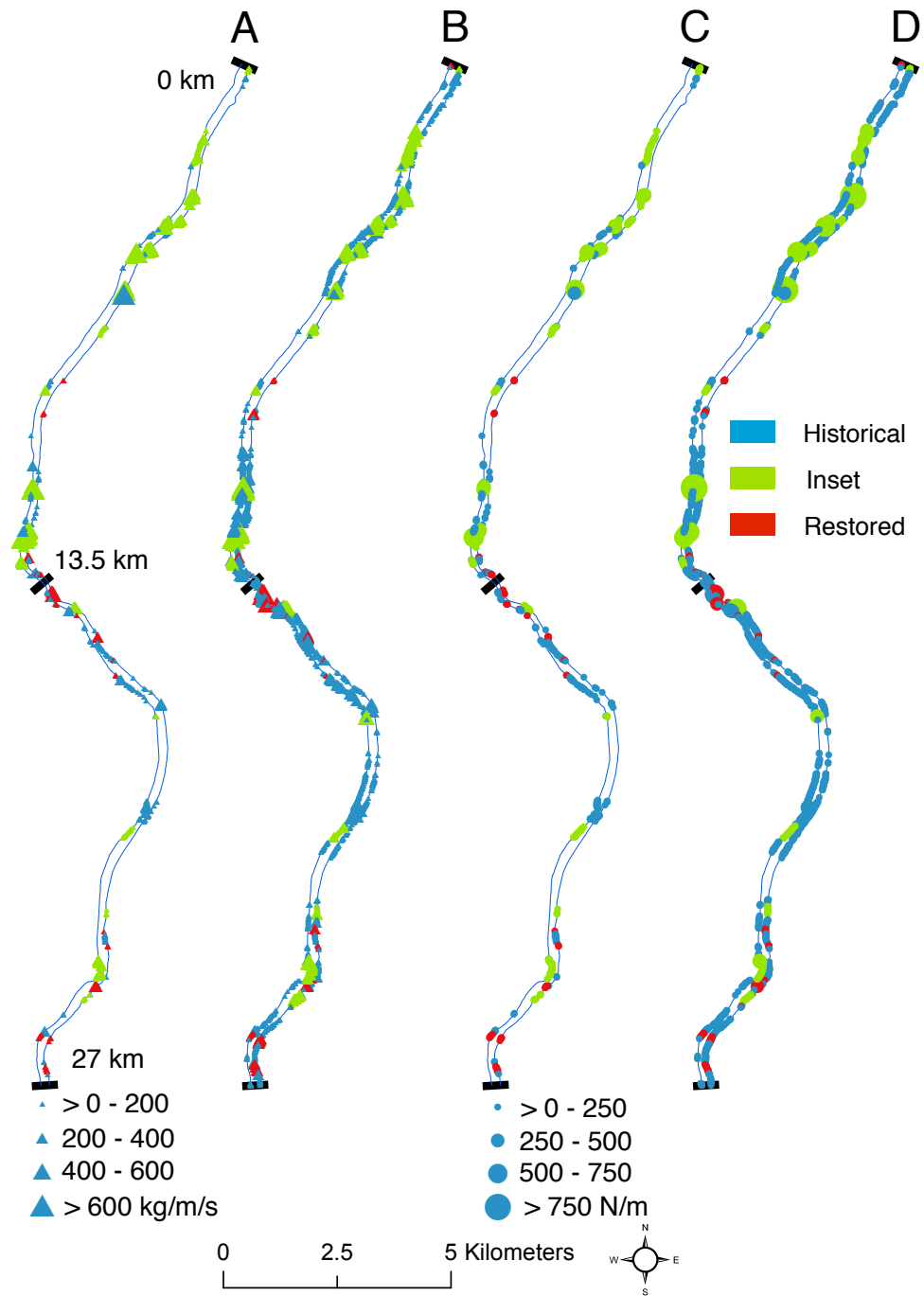
Figure 4.5. Maximum mass and momentum flux per unit length for connected channel-floodplain interface elements for the 1.5-day, moderate flood (A and C) and major flood (B and D) for the full study reach (27 km). The black line at 13.5 km represents the location represented in greater detail in Figure 4.6.
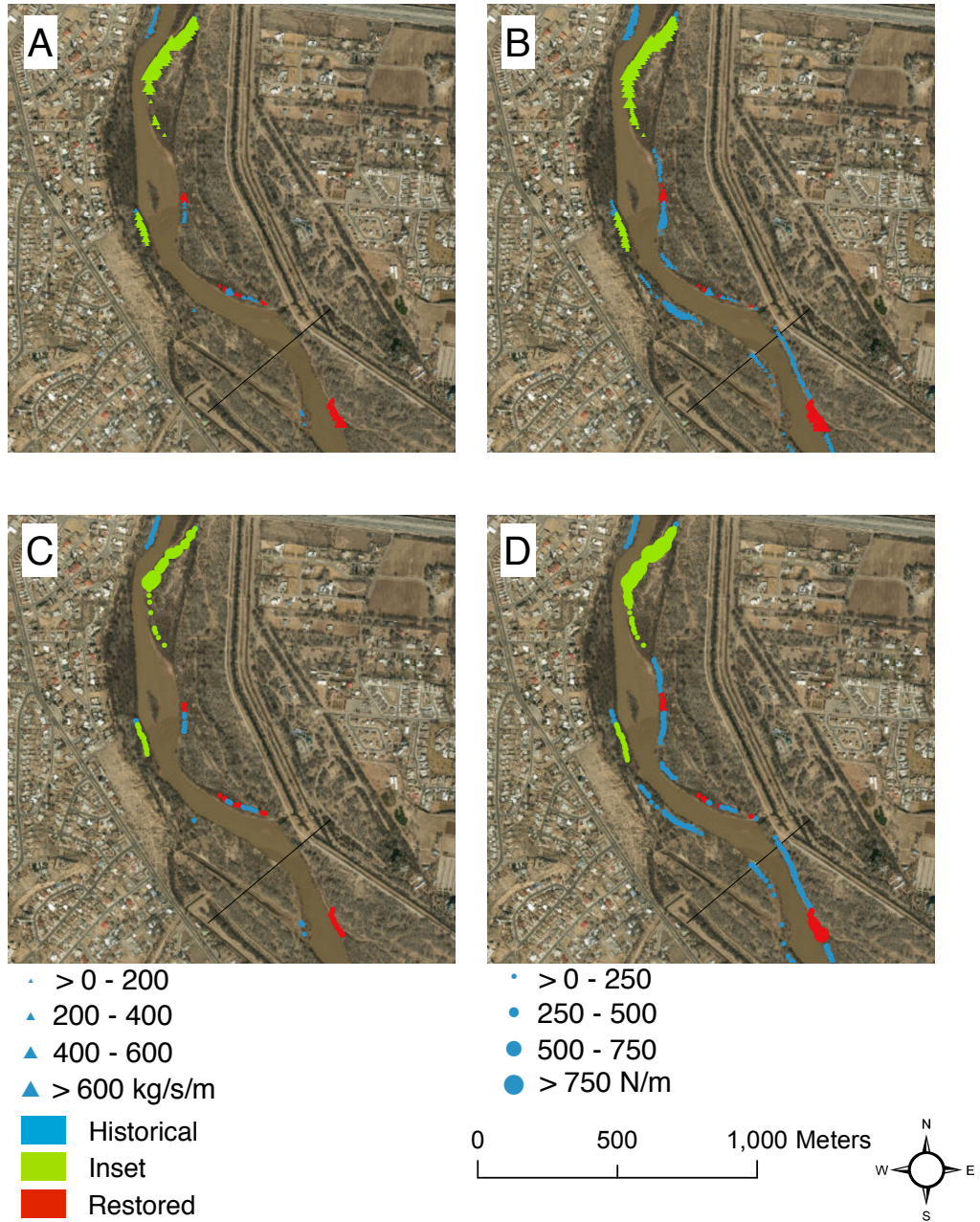
Figure 4.6. Maximum mass and momentum flux per unit length for connected channel-floodplain interface elements for the 1.5-day, moderate (A and C) and major flood (B and D) for a 1 km section between 13 km and 14 km.

While spatial assessments of maximum mass and momentum flux indicate areas of connectivity and differences in magnitude of flux, a numerical summary of all maximum values for the entire interface can provide insights into the distribution of process across each floodplain feature type. Figure 4.7 displays the relative frequency of modeled maximum mass and momentum fluxes at the channel-floodplain interface for each type of feature type as well as the mean maximum flux value for each type. Figures 4.7A and 4.7B display maximum mass fluxes during the 1.5-day events. All plots display high probabilities near zero. This is expected as some points along the floodplain never inundate and others are primarily areas where flow is returning from the floodplain to the main channel. For the moderate flood event, Fig. 4.7A, mass flux at inset and restored feature types is predominantly higher for mass flux values greater than 50 kg s^{-1}m^{-1}. This result complements those found in both the temporal and spatial plots and suggests that inset and restored features activate during moderate flood events. During the major flood event, Fig. 4.7B, there is a higher likelihood of connectivity on the historical surface, but mass fluxes greater than 100 kg s^{-1}m^{-1} along historical interfaces remain less common than inset and restored floodplains. These patterns are even more pronounced for momentum in Figures 4.7C and 4.7D. Mean mass and momentum flux were always greatest at inset locations and least for historical floodplain surfaces.
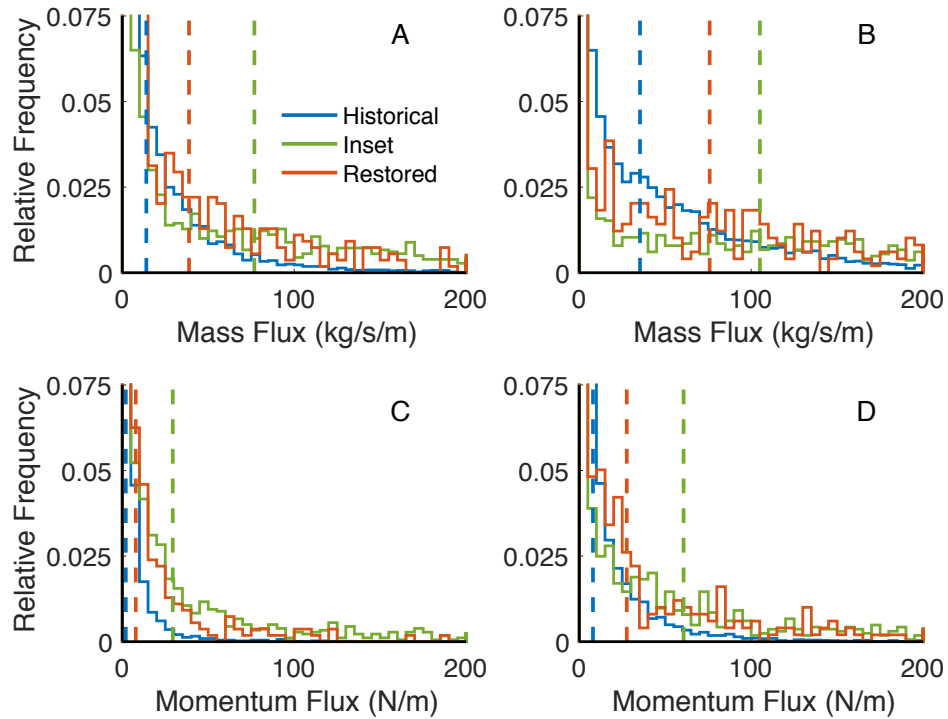
Figure 4.7. Relative frequency of maximum modeled mass and momentum fluxes for the 1.5-day, moderate (A and C) and major flood (B and D). Dashed lines represent mean maximum values for each geomorphic classification. Note that portions of the distribution above a 0.075 fraction and above 200 kg s^{-1}m^{-1} and 200 N m^{-1} are not plotted to focus on changes at lower mass and momentum fluxes.

4.4.7. Lateral and Longitudinal Discharge Relationships

Of interest in the study of river connectivity is the relationship between lateral and longitudinal movement of surface water. Therefore, modeled discharges at the channel-interface boundary and longitudinal cross-sections were quantified to understand how lateral and longitudinal volumes relate to one another. Figure 4.8 shows ratios of lateral to longitudinal discharge at specified stations. As expected, during moderate flood events ratios remain at zero before and after the flood wave passes each reach, while under major flood conditions, ratios begin at and end at fractions characteristic of the 150 m^{3}s^{-1} initial condition. For example, at 11 km a positive ratio is recorded, meaning more water is being transferred to the floodplain during when the flood wave enters the reach, and at 12 km a negative ratio is recorded, meaning water is being returned to the main channel.

For all model simulations, a maximum ratio of 0.33 was recorded (not shown), however this occurred at a location in which severe channel narrowing creates an almost perpendicular channel-floodplain interface 20 km downstream. Lateral discharge predominantly remained below 10% of longitudinal discharge (89%). Increases in the ratio occur when the floodplain in the region of interest becomes connected to the main channel. This can occur under moderate or major flood events. When a kilometer of the reach activates to a high degree during moderate flood events, ratios can increase greatly. The impact of connectivity during major flood events results in a more dampened increase or decrease in the ratio.
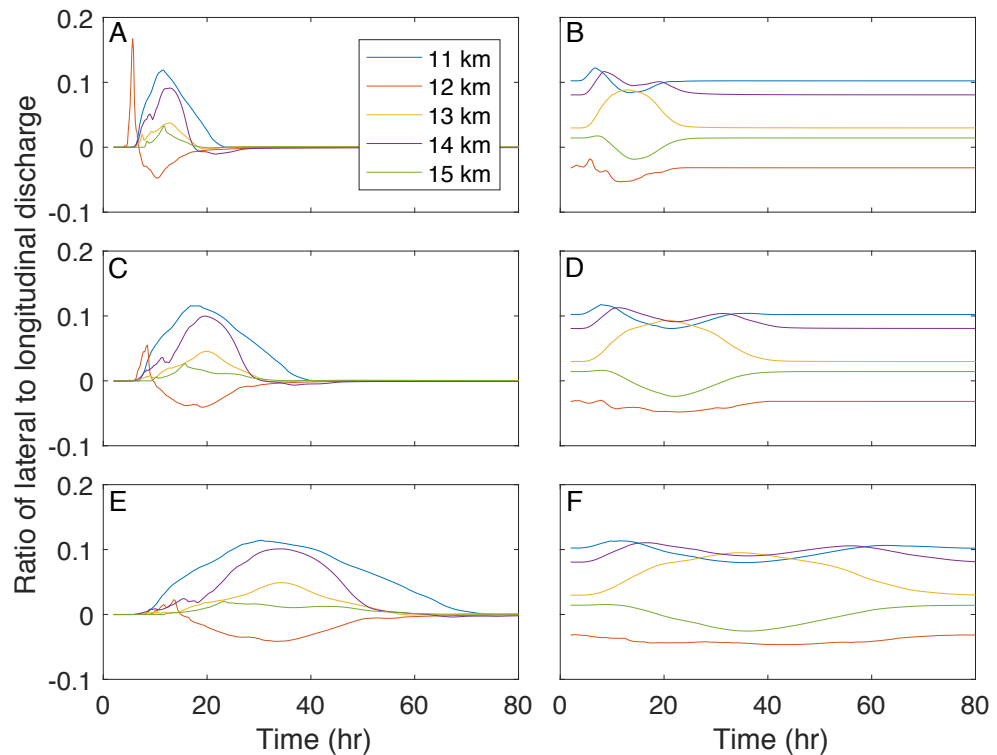
Figure 4.8. Ratio of lateral to longitudinal discharge at 5 km length sections of channel-floodplain interface for (A) 1-day, moderate, (B) 1-day, major, (C) 1.5-day, moderate, (D) 1.5-day, major, (E) 3-day, moderate, and (F) 3-day, major flood events.

A final analysis of flood wave processes aimed to understand how temporal lateral connectivity relates to downstream peak discharge. Maximum positive lateral discharge

107

occurred before peak longitudinal discharge. For increasing duration events, the early arrival increased approximately in proportion with the increase in duration. Maximum negative lateral discharges did not follow the same pattern. For moderate flood events, timing of maximum negative lateral discharges (i.e. time when the greatest discharge is returning to the channel) is relatively uniform. In comparison, for major flood events, time to maximum negative discharge occurs at later times, although not delayed to the same extent to which maximum lateral discharge arrives early. The delayed return is likely indicative of elevated water surface elevations in the main channel preventing a floodplain to channel flow gradient from developing until substantially later. During moderate flood events, the water surface elevation is not high enough to inundate the majority of interface connections, thus water can flow back to the main channel immediately after the flood peak has passed.

4.5. Discussion

The quantification of mass and momentum fluxes provide key insights for understanding river processes. While leading ideas in river science have stressed the importance of lateral surface connectivity for biogeochemical processes and ecological heterogeneity of the floodplain [*Junk et al.*, 1989; *Ward*, 1989; *Ward and Stanford*, 1995; *Hughes*, 1997], the literature remains limited in regard to methods that quantify physical processes of mass and momentum flux in natural settings beyond discrete sampling points [*Babaeyan-Koopaei et al.*, 2002]. The methodology presented here provides the ability to quantify flux totals subjected to the floodplain at various spatial scales and at high temporal resolution. Impacts of hydrologic and geomorphic alteration on long-term mass flux have been documented [*Stone et al.*, 2017]. This work expands upon the implications of geomorphic alteration on mass flux and includes analysis of momentum flux and lateral flow quantities and timing during discrete flow events. Results suggest that reach-scale floodplain connectivity drives net mass and momentum fluxes and lower magnitude, short duration events have a greater impact on feature scale connections. While it has been known for some time that different flow events will likely alter the geomorphology and ecology of different features based upon flow event characteristics, quantification of flux totals will lead to greater understanding of these phenomena. Applications for the

quantification of mass and momentum transfer abound. There has been a call for the description of disturbance forces in application to ecosystem dynamics [*Lake*, 2000; *Formann et al.*, 2013]. This type of work is also optimal for the study of biogeochemical hotspots and hot moments at key interfaces [*McClain et al.*, 2003].

Differences in the characteristics of mass and momentum flux display the importance of expanding hydrologic metrics beyond inundation depths and volumes. Within the MRG, variations in connectivity of the left and right floodplains leads to considerable differences in total momentum transferred to the floodplain surface and the amount of momentum dissipation during moderate and major flood events. Therefore, it is likely that processes relating to momentum flux and dissipation on these surfaces will be subject to the same patterns. In addition, momentum flux is by definition a force, such that lengths of the channel-floodplain interface with greater momentum flux will have more force acting on both the biological and geomorphic processes associated with that location, at least in terms of advective movement of water.

Results indicate that inset floodplains within the previously trained channel are key locations for mass and momentum transfer and display greater heterogeneity than historical floodplain surfaces. Under moderate flood scenarios the inset and restored floodplain features have higher connectivity than the historical floodplain surfaces. It is likely that many of these surfaces are relatively new due to the formation of vegetated islands and consequently bank attached islands [*Meyer and Hepler*, 2007], but the establishment of vegetation indicates that these surfaces are stable and active floodplain elements due to extended drought and river engineering practices [*Mussetter Engineering, Inc.*, 2006]. Therefore, these surfaces do activate as expected during moderate flood events which exceed the estimated bankfull flow volume [*Swanson et al.*, 2011]. With the existence of a large number of vegetated islands within the reach [*Meyer and Hepler*, 2007], these surfaces likely are subject to similar fluxes as inset floodplains. In contrast, the historical floodplain minimally inundates under moderate flood events and as documented above, the activation is best described by low mass and momentum flux.

While geomorphic observations on the reach have described the incision of the channel below its former floodplain [*Richard and Julien*, 2003; *Swanson et al.*, 2011],

this research describes the impact that channel incision has on physical processes. Even at major flood discharges, which are likely greater than the reach will be subject to due to flood control operations [*Llewellyn and Vaddey*, 2013], the characteristics of the connectivity on the historical floodplain are altered from heterogeneous to more homogeneous mass and momentum connections. Momentum flux remains low even when mass flux increases. The lack of high momentum flux locations along the historical floodplain is likely beneficial to the protection of levees and other engineered structures but detrimental for supporting heterogeneous floodplain ecosystems. Further, a lack of high momentum flux locations suggests that these historical floodplain features are likely dominated by overtopping connections and lack more concentrated, high velocity connections (e.g. high flow side channels or down valley flow at outside meander bends). Other altered systems like the MRG, which have been cut off from channel and floodplain adjusting flows, will also likely be subject to more homogeneous flux patterns. One implication is that the use of flood pulses or environmental flows may not drive heterogeneous hydrodynamic processes to the degree that is presumed. Instead, the defining geomorphology of a system may impact hydrodynamics to the extent in which disproportionally high flows are needed to achieve similar flux magnitudes.

Understanding spatial heterogeneity at the river channel and floodplain interface is critical to improved understanding of process based restoration. Analysis of restoration site boundaries indicates that while the sites do provide improved mass and momentum transfer within the river reach, the restored connections provide limited exchange of mass and momentum in comparison with inset and historical surfaces. The inset floodplain features which have formed from the river's adjustment to changing upstream inputs (i.e. climate, sediment load) and local controls (channelization and invasive vegetation) therefore remain as the dominant features for floodplain processes to occur. Although many restoration projects within the Albuquerque Reach of the Rio Grande have been implemented, this research quantifies the fact that mechanical restoration can only achieve so much in terms of restoring floodplain connectivity and river process. It is unlikely that the physical reconnection of floodplains through mechanical means will ever produce the magnitudes of river process needed to establish fully functioning native systems. However, it must be noted that the historical floodplain within much of the

110

MRG is relatively disconnected due to channel incision. Therefore, reconnecting historical floodplain in the reach involves excavation. In other systems, reconnection of floodplains that are still at appropriate topographic levels is likely to be more influential in accruing channel to floodplain processes through levee setback or environmental flow strategies. Further, restoration features in the MRG were not constructed to restore river process but predominantly for the creation of Rio Grande silvery minnow habitat. Thus, other restoration strategies may promote greater returns of river process.

Although mechanical restoration of floodplain features is unlikely to produce the levels of river process to achieve functional native systems, this research does display the importance of river hydrology in the magnitude of process to which a floodplain is subjected. It may be that managed flood pulses, or environmental flows, can be mapped to specific areas of interest using the methods displayed here [*Thoms and Parsons*, 2003]. As is shown in Figures 4.5 and 4.6, key locations of connectivity activate at certain discharges and are substantially less engaged at other discharges. Therefore, the rejuvenation of certain areas within a landscape or the desire to ensure quantities of nutrients reach a specific area could potentially be addressed by fine-tuning environmental flows to spatial and temporal dynamics of floodplain connectivity. Further, climate change will impart changes to the flow regime [*Llewellyn and Vaddey*, 2013], and the ecological integrity of various surfaces is likely to change due to differences in process and transport at altered flow levels.

Lateral and longitudinal discharge relationships were analyzed and show relationships to changes in flood magnitude and duration. The early arrival of lateral flood peaks provides greater insights into the occurrence of previously described connectivity patterns. For example, timing of high flow volumes and velocities are also likely to be important in the description of geomorphic and ecological changes across the floodplain [*Tockner et al.*, 1999; *Lake*, 2000]. In terms of lateral to longitudinal flow ratios, moderate flood events created sharp increases in the ratio. During major flood events, the ratio does not increase to the same degree. This suggests that topography dominates channel-floodplain exchanges when connections activate, while roughness characteristics likely limit exchange during high magnitude and long duration events through the dissipation of momentum. Ratios predominantly remained below ten percent

of longitudinal flow, a substantially lower number than was estimated along the highly connected, larger, low-gradient, and low-floodplain relief Atchafalaya River [*Scott et al.*, 2014]. Main factors in this lower ratio are likely the lack of floodplain area due to levee construction for the storage of water, channel incision limiting the time of connectivity, and decreased flood magnitude relative to the size of each river.

This research no doubt suffers from limitations but also presents improved metrics in the quantification of river processes important to river geomorphology and ecology. Limitations include the assumptions built into hydrodynamic models, description of interpolated channel topography, and restricting hydrologic processes to those occurring on the surface. Of course, modeling studies alone are not optimal in the study of rivers due to the previously discussed uncertainties and empirical data can provide critical information about discrete occurrences along a river. However, new methods in river modeling can provide important complementary insights to previous field and flume studies and provide context for future data collection [*Covino*, 2017]. With the continual improvement of hydrodynamic models and computational power, numerical modeling is a tool to be utilized. While this research does not seek to address specific ecological challenges, the metrics displayed in the paper do have implications for ecological issues and the methods can be shifted to better understand direct impacts on an ecological question of interest. Linking hydrodynamics with specific ecological or geomorphic processes, measuring temporal connectivity over various time scales, and comparing quantified hydrodynamics in other types of river systems should be the next steps in application of such methods. This research focused on a 27-km reach of the MRG, but the methods are applicable for any stretch of river given the availability of appropriate model requirements and sufficient computational time. Ultimately, field collection of data presented here would be nearly impossible based upon the spatial scale and dynamics of flood waves, however values could be verified by future field studies. The spatial and temporal possibilities with numerical modeling approaches should continue to be pursued and expanded in conjunction with physical modeling and field data.

4.6. Conclusions

The goal of this study was to analyze spatial and temporal lateral hydrodynamics along the channel-floodplain interface during unsteady flow events. More specifically, the objectives were to improve understanding of floodplain connectivity through the quantification of mass and momentum fluxes, and analyze how lateral discharge relates to longitudinal flow characteristics. These objectives were achieved through the two-dimensional, hydrodynamic modeling of the Rio Grande near Albuquerque, New Mexico and subsequent scripting techniques to analyze model outputs. Results indicate that inset floodplains are subjected to greater and more heterogeneous mass and momentum transfer. In addition, flood magnitude and lateral connectivity drive differences in dynamic mass and momentum flux which ultimately yield implications for the nature of process along rivers. Finally, lateral and longitudinal flow ratios and timings are of distinctly different nature under changing flood magnitudes. With the call within river science for quantification of driving forces and processes, quantification of lateral fluxes presented here provides a measure of context for a heavily manipulated, dryland river. Further studies are needed to provide these relationships for other types of rivers, however, results presented display the ability to investigate and quantify floodplain connectivity using modeling techniques. Spatial and temporal investigations into mass and momentum flux as well as the relationship between lateral and longitudinal discharge are necessary for many specific ecological research topics and to unify conceptual river science with more thorough process-based approaches.

Chapter 5

Conclusions

An understanding of hydrodynamic flood wave processes is critical to river management, whether the management goals are based on flood control, water use, or river restoration strategies. In addition, improved description of these processes over larger spatial and temporal scales will continue to inform future hydrologic, geomorphic, and ecologic science. With river systems in the United States and developed world heavily impacted by anthropogenic alterations, it is also important to understand the scope to which processes have changed through time.

The research presented in Chapters 2 through 4 addresses the needs for quantification of hydrodynamic processes both in the context of historical changes and altered contemporary geomorphology and ecology. The research implements novel approaches in high-resolution, two-dimensional hydrodynamic modeling of historical and contemporary systems (Chapters 2 and 3) and novel metrics with which hydrodynamics can be assessed both longitudinally (Chapter 2) and laterally (Chapter 4).

5.1. Objective Summaries

This dissertation addressed the following three objectives:

1. Evaluate how the ecosystem service of flood wave attenuation has changed with the implementation of river engineering practices in the name of flood protection and water use as well as contemporary river restoration efforts
2. Describe the sensitivities of flood wave attenuation to contemporary and altered conditions representative of historical river manipulation
3. Characterize channel-floodplain connectivity through lateral connectivity metrics important in the consideration of biogeochemical processes

These objectives were more specifically addressed in Chapters 2, 3, and 4, respectively, and summarized below.

5.1.1. Chapter 2

The main objective of this chapter was to assess how humans have impacted the ecosystem service of flood wave attenuation within the Middle Rio Grande. The anthropogenic changes to the Middle Rio Grande are most notable in historical river engineering practices for the purpose of flood control and water use. These changes have drastically limited the lateral extent of connected floodplain surfaces and, in combination with extended drought conditions, created a narrower, deeper channel near the city of Albuquerque. More recently, river restoration strategies have sought to improve channel-floodplain connections through mechanical lowering of floodplain surfaces in the name of habitat creation for the endangered Rio Grande silvery minnow (*Hybognathus amarus*). While these features are not designed for flood wave attenuation, the influence of these features on river process was of interest. The objective was achieved through the modeling of three representative time periods in the Albuquerque Reach of the Middle Rio Grande. The first time-period, 80 – 100 years before present, was representative of the time immediately prior to the construction of levees and implementation of channelization techniques within the reach. The second time-period, 15 – 20 years before present, was representative of the river before restoration strategies began. The last time-period was representative of contemporary conditions. This methodology provided novel approaches to quantification of flood wave attenuation through modern times and the presentation of normalized metrics which may be used for comparison of rivers or river reaches. In addition, hydrograph skewness was investigated as a function of channel-floodplain connectivity and heterogeneity of floodplain surfaces

Results indicate that historical conditions do lead to the greatest levels of attenuation in both flood magnitude and timing along the reach. Water surface elevations under historical conditions are attenuated to a lesser degree at historical discharge most likely due to less sensitivity of water surface elevation to increases in discharge. Moderate flood wave shape under historical conditions is of considerably different form than those under pre-restoration and contemporary conditions. This change in flood wave shape is attributed to the considerably larger floodplain area available for inundation and the heterogeneity of elevation on that surface to connect at various discharge levels. The availability of floodplain surfaces for inundation is displayed in inundated area

attenuation ratios, with historical floodplain surfaces continuing to display water storage availability even at major flood discharges. Finally, characteristics described by theoretical flood modeling are also observed in the simulation of a historical flood along the MRG. The research presented in this chapter displays the ability of two-dimensional, hydrodynamic modeling to capture processes associated with channel-floodplain connectivity important to flood wave attenuation. In addition, metrics used are applicable to other systems to better understand how differences in river system hydrology and geomorphology lead to differences in the attenuation process in terms of surface water processes.

5.1.2. Chapter 3

Chapter 3 investigates the sensitivity of attenuation to channel and floodplain characteristics. The alterations both planned and unplanned along rivers is evident, thus understanding how alterations impact downstream attenuation is important in the context of both flood control and ecological function. Channel and floodplain characteristics (e.g. floodplain roughness, channel depth, island area, etc.) were spatially quantified along 1000 meter segments of the Rio Grande to determine the influence of each on the rate of flood wave attenuation using statistical approaches. In addition, theoretical changes in roughness and topography were also investigated to investigate how uniform changes to these important river characteristics influence attenuation as well. All modeling was conducted on the contemporary channel of the Albuquerque Reach of the Middle Rio Grande. The research can be applied to the understanding of attenuation as a process and more specifically to the processes occurring in dryland rivers of the southwestern United States which have been subjected to similar ecological and anthropogenic changes over the last century.

      Simple and multiple linear regression analysis found contemporary flood wave attenuation within the heavily manipulated MRG to be correlated to available area for flow and inversely correlated to the proportion of total area inundated at flood wave onset. Theoretical alteration of channel and floodplain characteristics suggest reach length topographic and roughness alterations can have similar magnitude impacts on the degree of attenuation. However, attenuation is altered differently by changes in

topography and roughness. The processes associated with channel incision and aggradation are influenced to a great magnitude on a local feature, while those processes associated with roughness are influenced locally to a small magnitude but accrue to similar reach length magnitudes. Finally, in terms of physical flow conditions, changes to topography and roughness drive differences in water surface elevation, flow velocity, and proportion of downstream flow on the floodplain. While the physical conditions and qualitative river processes of many river systems are known, this chapter quantifies how changes to channel-floodplain conditions drive changes in the dynamic process of flood wave attenuation.

5.1.3. Chapter 4

Reach length hydrodynamic processes such as flood wave attenuation and ecological floodplain heterogeneity are ultimately dependent on the transfer of mass and momentum from the main channel to the floodplain. Chapter 4 sought to expand new techniques in the quantification of mass and momentum flux at local and feature scales and to quantify differences in lateral connectivity within the Middle Rio Grande due to defining channel-floodplain morphology. All modeling for this chapter was conducted on the contemporary Albuquerque Reach of the Middle Rio Grande. The data needed to address these objectives was extracted from model outputs along the channel-floodplain interface and integrated through time. The implications of variable geomorphology and the influence of channelization were a focus of investigation. Three floodplain feature types were analyzed: inset, historical, and restored floodplains. Additionally, temporal, lateral discharge was compared to longitudinal flow to understand the extent of lateral transfer and the timing with which connectivity occurs.

Mass and momentum flux display similarities in temporal fluxes, however, differences in these fluxes indicate interesting findings about the nature of connectivity in the reach. Inset floodplains were found to have the greatest magnitude in flux values and the largest amount of heterogeneity in flux. Historical floodplain mass flux increased in total flux under major flood events due to the connection of a larger length of channel-floodplain interface, but the nature of that connection is limited in that it remains less heterogeneous and momentum flux magnitudes remained low. Lateral and longitudinal

flow timings indicate that maximum lateral discharge occurs before longitudinal peak. Lateral-longitudinal exchange ratios are driven by instantaneous topographic connectivity at moderate flows and controlled by mass and momentum flux processes under major flows. The results indicate a number of implications for altered river systems and strategies for restoration, such as environmental flows, in that river process is not always restored to heterogeneous levels even when flows are of large magnitude. The quantification of fluxes is a technique that can be applied to other stretches of river for comparison of channel-floodplain hydrodynamics or in modeling biogeochemical processes.

5.2. Future Research

River science includes topics such as hydrodynamic process, three-dimensional temporal connectivity, and environmental flows. The research presented within this dissertation sought to describe process and connectivity in the context of unsteady flows and altered river conditions. There are a number of potential pathways for future research including applications of the modeling methodologies, expansion of the hydrodynamic metrics, and verification and implementation of the flux dynamics into approaches focusing on geomorphic and ecologic processes. Further research relating to flood wave attenuation and lateral, hydrodynamic fluxes can help inform knowledge about ecosystem services along rivers and associated floodplains.

5.2.1. Application of Modeling Methodologies

The modeling methodologies presented within this research displayed the inherent benefit to high-resolution two-dimensional modeling for studies in which channel-floodplain connectivity is considered important. Chapter 2 displayed the impacts of heterogeneous floodplain surfaces and the impact instantaneous floodplain storage can have on flood wave attenuation. Chapter 3 statistical results suggested that two-dimensional modeling is able to capture channel-floodplain characteristics important to flood wave attenuation. Chapter 4 displayed the ability of two-dimensional models to estimate fluxes at key locations along the channel-floodplain interface. With the importance of high-resolution data inherent to all three chapters, the methodologies presented should be used in other

systems. The ability to partition each model and run in reasonable computational times provides a host of applications for this approach. Computational modeling of hydrodynamic systems should continue to be pursued as a complementary tool to field-based science in understanding process based river science [*Covino*, 2017].

5.2.2. Expansion of Hydrodynamic Metrics

Results presented here focus predominantly on attenuation ratios, discharge ratios, and mass and momentum fluxes. Chapter 2 introduced flood wave attenuation ratios and characterized changes in flood wave shape. Chapter 3 expanded upon those metrics developed in Chapter 2. Chapter 4 introduced feature and reach flux quantification in addition to lateral-longitudinal flow characteristics. Possibly the most accessible future research is in the combination of Chapter 3 and Chapter 4 methodologies. The results of Chapter 3 indicated differences in process associated with floodplain alteration in comparison to only bank alteration. It would be of interest to better understand how mass and momentum fluxes are impacted by changes in floodplain and bank roughness. Using methods of Chapter 4, elemental flux magnitudes are likely to inform these differences to a great degree. Relatively recent research has helped to describe this process in a simplified environment [*Vermaas et al.*, 2011], however, the application within high-resolution, two-dimensional hydrodynamic modeling can inform larger scales and bank versus floodplain alteration scenarios.

In addition to the combination of chapter methodologies, attenuation ratios, lateral-longitudinal discharge patterns, and mass and momentum fluxes should be quantified for other river systems. The work conducted here was implemented on a sand-bed, dryland river. While results may be similar for rivers with similar geomorphologic and anthropogenic inputs, results in other rivers may be drastically different. Because many of the metrics presented are novel approaches, little can be said of other environments at this point.

5.2.3. Implementation in Geomorphic and Ecologic Approaches

Chapter 4 presented novel metrics in an attempt to quantify temporal and spatial channel-floodplain connectivity. These metrics go beyond the typical hydrodynamic modeling

metrics reported in previous literature such as depth, velocity, and shear stress. Expansion of local hydrodynamic metrics should continue and be verified by field studies. Chapter 4 quantifies connectivity in terms of mass and momentum flux and lateral and longitudinal discharge. These metrics can and should be implemented in studies involving biogeochemical processes important to floodplain geomorphology and ecology [*Harvey and Gooseff*, 2015]. Studies involving the connectivity and hydrodynamic exchange metrics used here can inform a plethora of geomorphic and ecologic interests with the improved spatial and temporal resolution the metrics provide.

References

Acreman, M. C., R. Riddington, and D. J. Booker (2003), Hydrological impacts of floodplain restoration: a case study of the River Cherwell, UK, *Hydrology and Earth System Sciences Discussions*, *7*(1), 75–85.

Adair, J. (2016), Reconstructing the historical Albuquerque reach of the Middle Rio Grande to evaluate the influence of river engineering on floodplain inundation, Master's Thesis, University of New Mexico.

Åkesson, A., A. Wörman, and A. Bottacin-Busolin (2015), Hydraulic response in flooded stream networks, *Water Resources Research*, *51*(1), 213–240, doi:10.1002/2014WR016279.

Alò, D., and T. F. Turner (2005), Effects of Habitat Fragmentation on Effective Population Size in the Endangered Rio Grande Silvery Minnow: *Genetic Effects of River Fragmentation*, *Conservation Biology*, *19*(4), 1138–1148, doi:10.1111/j.1523-1739.2005.00081.x.

Amoros, C., and G. Bornette (2002), Connectivity and biocomplexity in waterbodies of riverine floodplains, *Freshwater Biology*, *47*(4), 761–776, doi:10.1046/j.1365-2427.2002.00905.x.

Anderson, B. G., I. D. Rutherfurd, and A. W. Western (2006), An analysis of the influence of riparian vegetation on the propagation of flood waves, *Environmental Modelling & Software*, *21*(9), 1290–1296.

Archer, D. R. (1989), Flood Wave Attenuation due to Channel and Floodplain Storage and Effects on Flood Frequency, in *Floods: hydrological, sedimentological, and geomorphological implications*, edited by K. J. Beven, P. Carling, British Geomorphological Research Group, and British Hydrological Society, J. Wiley, Chichester [England]; New York.

Asselman, N. E. M., and H. Middelkoop (1995), Floodplain sedimentation: Quantities, patterns and processes, *Earth Surf. Process. Landforms*, *20*(6), 481–499, doi:10.1002/esp.3290200602.

Atkinson, C. L., S. W. Golladay, S. P. Opsahl, and A. P. Covich (2009), Stream discharge and floodplain connections affect seston quality and stable isotopic signatures in a coastal plain stream, *Journal of the North American Benthological Society*, *28*(2), 360–370, doi:10.1899/08-102.1.

Babaeyan-Koopaei, K., D. A. Ervine, P. A. Carling, and Z. Cao (2002), Velocity and turbulence measurements for two overbank flow events in River Severn, *Journal of Hydraulic Engineering*, *128*(10), 891–900.

Balcombe, S. R., and A. H. Arthington (2009), Temporal changes in fish abundance in response to hydrological variability in a dryland floodplain river, *Marine and Freshwater Research*, *60*(2), 146–159.

Barko, V. A., D. P. Herzog, and M. T. O'Connell (2006), Response of fishes to floodplain connectivity during and following a 500-year flood event in the unimpounded upper Mississippi River, *Wetlands*, *26*(1), 244–257, doi:10.1672/0277-5212(2006)26[244:ROFTFC]2.0.CO;2.

Baxter, R. M. (1977), Environmental effects of dams and impoundments, *Annual Review of Ecology and Systematics*, *8*(1), 255–283.

Beechie, T. J., D. A. Sear, J. D. Olden, G. R. Pess, J. M. Buffington, H. Moir, P. Roni, and M. M. Pollock (2010), Process-Based Principles for Restoring River Ecosystems, *BioScience*, *60*(3), 209–222, doi:10.1525/bio.2010.60.3.7.

Beesley, L., A. J. King, F. Amtstaetter, J. D. Koehn, B. Gawne, A. Price, D. L. Nielsen, L. Vilizzi, and S. N. Meredith (2012), Does flooding affect spatiotemporal variation of fish assemblages in temperate floodplain wetlands?, *Freshwater Biology*, *57*(11), 2230–2246, doi:10.1111/j.1365-2427.2012.02865.x.

Bennett, S. j., and J. l. Best (1995), Mean flow and turbulence structure over fixed, two-dimensional dunes: implications for sediment transport and bedorm stability, *Sedimentology*, *42*(3), 491.

Bernhardt, E. S. et al. (2005), Synthesizing U.S. River Restoration Efforts, *Science*, *308*(5722), 636–637.

Bestgen, K. R., and S. P. Platania (1991), Status and Conservation of the Rio Grande Silvery Minnow, Hybognathus amarus, *The Southwestern Naturalist*, *36*(2), 225, doi:10.2307/3671925.

Birkland, T. A., R. J. Burby, D. Conrad, H. Cortner, and W. K. Michener (2003), River ecology and flood hazard mitigation, *Natural Hazards Review*, *4*(1), 46–54.

Blettler, M. C. M. et al. (2016), Linking hydro-morphology with invertebrate ecology in diverse morphological units of a large river-floodplain system, *Water Resour. Res.*, *52*, n/a-n/a, doi:10.1002/2016WR019454.

Bloodgood, D. W. (1930), ground water of the Middle Rio Grande Valley and its relation to drainage,

Bousmar, D., and Y. Zech (1999), Momentum transfer for practical flow computation in compound channels, *Journal of hydraulic engineering*, *125*(7), 696–706.

Brauman, K. A., G. C. Daily, T. K. Duarte, and H. A. Mooney (2007), The Nature and Value of Ecosystem Services: An Overview Highlighting Hydrologic Services,

Annual Review of Environment and Resources, *32*(1), 67–98, doi:10.1146/annurev.energy.32.031306.102758.

Callahan, D., and L. White (2004), Vegetation Mapping of the Rio Grande Floodplain 2002-2004,

Cao, Z., J. Meng, G. Pender, and S. Wallis (2006), Flow resistance and momentum flux in compound open channels, *Journal of hydraulic engineering*, *132*(12), 1272–1282.

Carnie, R., D. Tonina, J. A. McKean, and D. Isaak (2016), Habitat connectivity as a metric for aquatic microhabitat quality: application to Chinook salmon spawning habitat, *Ecohydrol.*, *9*(6), 982–994, doi:10.1002/eco.1696.

Castellarin, A., G. Di Baldassarre, and A. Brath (2011), Floodplain management strategies for flood attenuation in the river Po, *River Research and Applications*, *27*(8), 1037–1047.

Chaudhry, M. H. (2007), *Open-channel flow*, Springer Science & Business Media.

Chow, V. T. (1959), *Open channel hydraulics*, McGraw-Hill Book Company, Inc; New York.

Corenblit, D., E. Tabacchi, J. Steiger, and A. M. Gurnell (2007), Reciprocal interactions and adjustments between fluvial landforms and vegetation dynamics in river corridors: A review of complementary approaches, *Earth-Science Reviews*, *84*(1–2), 56–86, doi:10.1016/j.earscirev.2007.05.004.

Costabile, P., and F. Macchione (2012), Analysis of One-Dimensional Modelling for Flood Routing in Compound Channels, *Water Resources Management*, *26*(5), 1065–1087, doi:10.1007/s11269-011-9947-2.

Costanza, R. et al. (1997), The value of the world's ecosystem services and natural capital, *Nature*, *387*(6630), 253–260.

Costanza, R. et al. (1998), The value of ecosystem services: putting the issues in perspective, *Ecological economics*, *25*(1), 67–72.

Costanza, R., R. de Groot, P. Sutton, S. van der Ploeg, S. J. Anderson, I. Kubiszewski, S. Farber, and R. K. Turner (2014), Changes in the global value of ecosystem services, *Global Environmental Change*, *26*, 152–158, doi:10.1016/j.gloenvcha.2014.04.002.

Covino, T. (2017), Hydrologic connectivity as a framework for understanding biogeochemical flux through watersheds and along fluvial networks, *Geomorphology*, *277*, 133–144, doi:10.1016/j.geomorph.2016.09.030.

Croke, J., K. Fryirs, and C. Thompson (2013), Channel–floodplain connectivity during an extreme flood event: implications for sediment erosion, deposition, and delivery, *Earth Surf. Process. Landforms*, *38*(12), 1444–1456, doi:10.1002/esp.3430.

Crowder, D. W., and P. Diplas (2000), Using two-dimensional hydrodynamic models at scales of ecological importance, *Journal of hydrology*, *230*(3), 172–191.

Crowder, D. W., and P. Diplas (2006), Applying spatial hydraulic principles to quantify stream habitat, *River Research and Applications*, *22*(1), 79–89, doi:10.1002/rra.893.

Daily, G. (1997), *Nature's services: societal dependence on natural ecosystems*, Island Press.

Daraio, J. A., L. J. Weber, T. J. Newton, and J. M. Nestler (2010), A methodological framework for integrating computational fluid dynamics and ecological models applied to juvenile freshwater mussel dispersal in the Upper Mississippi River, *Ecological Modelling*, *221*(2), 201–214, doi:10.1016/j.ecolmodel.2009.10.008.

Deltares (2015), *D-Flow Flexible Mesh User Manual*, Deltares, Delft, The Netherlands.

Di Baldassarre, G., A. Castellarin, and A. Brath (2009), Analysis of the effects of levee heightening on flood propagation: example of the River Po, Italy, *Hydrological sciences journal*, *54*(6), 1007–1017.

Dierauer, J., N. Pinter, and J. W. Remo (2012), Evaluation of levee setbacks for flood-loss reduction, Middle Mississippi River, USA, *Journal of Hydrology*, *450*, 1–8.

Dottori, F., G. Di Baldassarre, and E. Todini (2013), Detailed data is welcome, but with a pinch of salt: Accuracy, precision, and uncertainty in flood inundation modeling, *Water Resour. Res.*, *49*(9), 6079–6085, doi:10.1002/wrcr.20406.

Dudley, R. K., and S. P. Platania (2007), Flow regulation and fragmentation imperil pelagic-spawning riverine fishes, *Ecological Applications*, *17*(7), 2074–2086.

Dynesius, M., and C. Nilsson (1994), Fragmentation and Flow Regulation of River Systems in, *Science*, *266*, 4.

ESRI (2012), *ArcGIS Desktop*, Environmental Systems Research Institute, Redlands, CA.

Fleischmann, A. S., R. C. D. Paiva, W. Collischonn, M. V. Sorribas, and P. R. M. Pontes (2016), On river-floodplain interaction and hydrograph skewness: FLOODPLAINS AND HYDROGRAPH SKEWNESS, *Water Resources Research*, *52*(10), 7615–7630, doi:10.1002/2016WR019233.

Florsheim, J. L., J. F. Mount, and A. Chin (2008), Bank Erosion as a Desirable Attribute of Rivers, *BioScience*, *58*(6), 519–529, doi:10.1641/B580608.

Fong, C. S., S. M. Yarnell, and J. H. Viers (2016), Pulsed Flow Wave Attenuation on a Regulated Montane River, *River Res. Applic.*, *32*(5), 1047–1058, doi:10.1002/rra.2925.

Formann, E., G. Egger, C. Hauer, and H. Habersack (2013), Dynamic disturbance regime approach in river restoration: concept development and application, *Landscape Ecol Eng*, *10*(2), 323–337, doi:10.1007/s11355-013-0228-5.

Friedman, J. M., K. R. Vincent, E. R. Griffin, M. L. Scott, P. B. Shafroth, and G. T. Auble (2015), Processes of arroyo filling in northern New Mexico, USA, *Geological Society of America Bulletin*, *127*(3–4), 621–640.

Garbrecht, J., and G. Brunner (1991), Hydrologic Channel-Flow Routing for Compound Sections, *Journal of Hydraulic Engineering*, *117*(5), 629–642, doi:10.1061/(ASCE)0733-9429(1991)117:5(629).

Ghavasieh, A.-R., C. Poulard, and A. Paquier (2006), Effect of roughened strips on flood propagation: Assessment on representative virtual cases and validation, *Journal of Hydrology*, *318*(1–4), 121–137, doi:10.1016/j.jhydrol.2005.06.009.

Graaf, G. (2003), The flood pulse and growth of floodplain fish in Bangladesh, *Fisheries Management & Ecology*, *10*(4), 241–247, doi:10.1046/j.1365-2400.2003.00341.x.

Graf, W. L. (1999), Dam nation: A geographic census of American dams and their large-scale hydrologic impacts, *Water resources research*, *35*(4), 1305–1311.

Graf, W. L. (2006), Downstream hydrologic and geomorphic effects of large dams on American rivers, *Geomorphology*, *79*(3–4), 336–360, doi:10.1016/j.geomorph.2006.06.022.

Guida, R. J., T. L. Swanson, J. W. Remo, and T. Kiss (2015), Strategic floodplain reconnection for the Lower Tisza River, Hungary: Opportunities for flood-height reduction and floodplain-wetland reconnection, *Journal of Hydrology*, *521*, 274–285.

Guida, R. J., J. W. F. Remo, and S. Secchi (2016), Tradeoffs of strategically reconnecting rivers to their floodplains: The case of the Lower Illinois River (USA), *Science of The Total Environment*, *572*, 43–55, doi:10.1016/j.scitotenv.2016.07.190.

Happ, S. C. (1948), Sedimentation in the Middle Rio Grande Valley, New Mexico, *Geological Society of America Bulletin*, *59*(12), 1191–1216.

Harvey, J., and M. Gooseff (2015), River corridor science: Hydrologic exchange and ecological consequences from bedforms to basins, *Water Resour. Res.*, *51*(9), 6893–6922, doi:10.1002/2015WR017617.

Helmiö, T. (2004), Flow resistance due to lateral momentum transfer in partially vegetated rivers, *Water Resources Research*, *40*(5), doi:10.1029/2004WR003058.

Hink, V. C., and Ohmart (1984), *Middle Rio Grande Biological Survey*, U.S. Army Corps of Engineers.

Howe, W. H., and F. L. Knopf (1991), On the Imminent Decline of Rio Grande Cottonwoods in Central New Mexico, *The Southwestern Naturalist*, *36*(2), 218, doi:10.2307/3671924.

Hudson, P. F., and H. Middelkoop (2015), Integrated Floodplain Management, Environmental Change, and Geomorphology: Problems and Prospects, in *Geomorphic Approaches to Integrated Floodplain Management of Lowland Fluvial Systems in North America and Europe*, pp. 1–8, Springer.

Hughes, F. M. R. (1997), Floodplain biogeomorphology, *Progress in Physical Geography*, *21*(4), 501–529, doi:10.1177/030913339702100402.

Hughes, F. M. R. et al. (2001), The importance of different scale processes for the restoration of floodplain woodlands, *Regul. Rivers: Res. Mgmt.*, *17*(4–5), 325–345, doi:10.1002/rrr.656.

Isaacson, K., and J. Coonrod (2011), USGS Streamflow Data and Modeling Sand-Bed Rivers, *Journal of Hydraulic Engineering*, *137*(8), 847–851, doi:10.1061/(ASCE)HY.1943-7900.0000362.

Jacobson, R. B., and D. L. Galat (2006), Flow and form in rehabilitation of large-river ecosystems: an example from the Lower Missouri River, *Geomorphology*, *77*(3), 249–269.

Jacobson, R. B., G. Lindner, and C. Bitner (2015), The role of floodplain restoration in mitigating flood risk, Lower Missouri River, USA, in *Geomorphic Approaches to Integrated Floodplain Management of Lowland Fluvial Systems in North America and Europe*, pp. 203–243, Springer.

Jaffe, D. A., and B. F. Sanders (2001), Engineered Levee Breaches for Flood Mitigation, *Journal of Hydraulic Engineering*, *127*(6), 471–479, doi:10.1061/(ASCE)0733-9429(2001)127:6(471).

Jones, C. N., D. T. Scott, B. L. Edwards, and R. F. Keim (2014), Perirheic mixing and biogeochemical processing in flow-through and backwater floodplain wetlands, *Water Resources Research*, *50*(9), 7394–7405, doi:10.1002/2014WR015647.

Jones, C. N., D. T. Scott, C. Guth, E. T. Hester, and W. C. Hession (2015), Seasonal Variation in Floodplain Biogeochemical Processing in a Restored Headwater Stream, *Environmental Science & Technology*, *49*(22), 13190–13198, doi:10.1021/acs.est.5b02426.

Junk, W., P. B. Bayley, and R. E. Sparks (1989), The flood pulse concept in river-floodplain systems, in *International large river symposium*, vol. 106, pp. 110–127, Canadian Special Publication of Fisheries Aquatic Science.

Knight, D. W., and K. Shiono (1990), Turbulence measurements in a shear layer region of a compound channel, *Journal of Hydraulic Research*, *28*(2), 175–196, doi:10.1080/00221689009499085.

Knighton, D. (1998), *Fluvial forms and processes: a new perspective*, Routledge, New York, NY.

Kondolf, G. et al. (2006), Process-Based Ecological River Restoration: Visualizing Three-Dimensional Connectivity and Dynamic Vectors to Recover Lost Linkages, *Ecology and Society*, *11*(2), doi:10.5751/ES-01747-110205.

Lacey, R. W., and R. G. Millar (2004), Reach scale hydraulic assessment of instream salmonid habitat restoration, *Journal of the American Water Resources Association (JAWRA)*, *40*(6), 1631–1644.

Lagasse, P. F. (1980), *An Assessment of the Response of the Rio Grande to Dam Construction: Cochiti to Isleta Reach*.

Lake, P. S. (2000), Disturbance, patchiness, and diversity in streams, *Journal of the north american Benthological society*, *19*(4), 573–592.

Lane, S. N., and K. S. Richards (1997), Linking river channel form and process: time, space and causality revisited, *Earth Surface Processes and Landforms*, *22*(3), 249–260.

Lane, S. N., and K. S. Richards (1998), High resolution, two-dimensional spatial modelling of flow processes in a multi-thread channel, *Hydrol. Process.*, *12*(8), 1279–1298, doi:10.1002/(SICI)1099-1085(19980630)12:8<1279::AID-HYP615>3.0.CO;2-E.

Leopold, L. B., M. G. Wolman, and J. P. Miller (1964), *Fluvial Processes in Geomorphology*, Dover Publications, New York.

Ligon, F. K., W. E. Dietrich, and W. J. Trush (1995), Downstream Ecological Effects of Dams, *BioScience*, *45*(3), 183–192, doi:10.2307/1312557.

Liu, Y. B., S. Gebremeskel, F. de Smedt, L. Hoffmann, and L. Pfister (2004), Simulation of flood reduction by natural river rehabilitation using a distributed hydrological model, *Hydrology and Earth System Sciences*, *8*(6), 1129–1140.

Llewellyn, D., and S. Vaddey (2013), *West-Wide Climate Risk Assessment: Upper Rio Grande Impact Assessment*, U.S. Department of Interior - Bureau of Reclamation.

Marston, R. A., J. D. Mills, D. R. Wrazien, B. Bassett, and D. K. Splinter (2005), Effects of Jackson Lake Dam on the Snake River and its floodplain, Grand Teton National Park, Wyoming, USA, *Geomorphology*, *71*(1–2), 79–98, doi:10.1016/j.geomorph.2005.03.005.

MathWorks, Inc. (2016), *MATLAB and statistics toolbox release*, MathWorks, Inc., Natick, Massachusetts, United States.

McCartney, M. P., and P. S. Naden (1995), A Semi-Empirical Investigation of the Influence of Flood-Plain Storage on Flood Flow, *Water and Environment Journal*, *9*(3), 236–246.

McClain, M. E. et al. (2003), Biogeochemical Hot Spots and Hot Moments at the Interface of Terrestrial and Aquatic Ecosystems, *Ecosystems*, *6*(4), 301–312, doi:10.1007/s10021-003-0161-9.

Merritt, D. M., and D. J. Cooper (2000), Riparian vegetation and channel change in response to river regulation: a comparative study of regulated and unregulated streams in the Green River Basin, USA, *Regul. Rivers: Res. Mgmt.*, *16*(6), 543–564, doi:10.1002/1099-1646(200011/12)16:6<543::AID-RRR590>3.0.CO;2-N.

Meyer, G. A., and C. W. Hepler (2007), Vegetated island formation and change in the Middle Rio Grande near Albuquerque, New Mexico, *University of New Mexico, Albuquerque, NM*.

Middelkoop, H., and M. Van Der Perk (1998), Modelling Spatial Patterns of Overbank Sedimentation on Embanked Floodplains, *Geografiska Annaler: Series A, Physical Geography*, *80*(2), 95–109, doi:10.1111/j.0435-3676.1998.00029.x.

Moriasi, D. N., J. G. Arnold, M. W. Van Liew, R. L. Bingner, R. D. Harmel, and T. L. Veith (2007), Model evaluation guidelines for systematic quantification of accuracy in watershed simulations, *Transactions of the American Society of Agricultural and Biological Engineers*, *50*(3), 885–900, doi:10.13031/2013.23153.

Morrison, R. R., and M. C. Stone (2014), Spatially implemented Bayesian network model to assess environmental impacts of water management, *Water Resources Research*, *50*(10), 8107–8124, doi:10.1002/2014WR015600.

Morvan, H., D. Knight, N. Wright, X. Tang, and A. Crossley (2008), The concept of roughness in fluvial hydraulics and its formulation in 1D, 2D and 3D numerical simulation models, *Journal of Hydraulic Research*, *46*(2), 191–208, doi:10.1080/00221686.2008.9521855.

Murphy, E., M. Ghisalberti, and H. Nepf (2007), Model and laboratory study of dispersion in flows with submerged vegetation, *Water Resour. Res.*, *43*(5), W05438, doi:10.1029/2006WR005229.

Mussetter Engineering, Inc. (2006), *Evaluation of Bar Morphology, Distribution and Dynamics as Indices of Fluvial Processes in the Middle Rio Grande, New Mexico*.

Mussetter Engineering, M. E. (2002), *Hydraulic and Sediment Continuity Modeling of the San Joaquin River from Friant Dam to Mendota Dam, California*, U.S. Bureau of Reclamation, U.S. Bureau of Reclamation.

Myers, W. R. C., J. F. Lyness, and J. Cassells (2001), Influence of boundary roughness on velocity and discharge in compound river channels, *Journal of Hydraulic Research*, *39*(3), 311–319, doi:10.1080/00221680109499834.

Najmi, Y., S. Grogan, and C. Crawford (2005), *Bosque Landscape Alteration Strategy: Objectives, Basic Requirements and Guidelines*, Middle Rio Grande Conservancy District.

Nelson, J. M., R. L. Shreve, S. R. McLean, and T. G. Drake (1995), Role of Near-Bed Turbulence Structure in Bed Load Transport and Bed Form Mechanics, *Water Resour. Res.*, *31*(8), 2071–2086, doi:10.1029/95WR00976.

Nepf, H. M. (1999), Drag, turbulence, and diffusion in flow through emergent vegetation, *Water Resour. Res.*, *35*(2), 479–489, doi:10.1029/1998WR900069.

Nepf, H. M., and E. R. Vivoni (2000), Flow structure in depth-limited, vegetated flow, *J. Geophys. Res.*, *105*(C12), 28547–28557, doi:10.1029/2000JC900145.

Nilsson, C., E. Andersson, D. M. Merritt, and M. E. Johansson (2002), Differences in riparian flora between riverbanks and river lakeshores explained by dispersal traits, *Ecology*, *83*(10), 2878–2887.

Opperman, J. J., R. Luster, B. A. McKenney, M. Roberts, and A. W. Meadows (2010), Ecologically Functional Floodplains: Connectivity, Flow Regime, and Scale, *Journal of the American Water Resources Association (JAWRA)*, *46*(2), 211–226.

Palmer, M. A. et al. (2005), Standards for ecologically successful river restoration: Ecological success in river restoration, *Journal of Applied Ecology*, *42*(2), 208–217, doi:10.1111/j.1365-2664.2005.01004.x.

Palmer, M. A., K. L. Hondula, and B. J. Koch (2014), Ecological Restoration of Streams and Rivers: Shifting Strategies and Shifting Goals, *Annual Review of Ecology, Evolution, and Systematics*, *45*(1), 247–269, doi:10.1146/annurev-ecolsys-120213-091935.

Pease, A. A., J. Justine Davis, M. S. Edwards, and T. F. Turner (2006), Habitat and resource use by larval and juvenile fishes in an arid-land river (Rio Grande, New Mexico), *Freshwater Biology*, *51*(3), 475–486, doi:10.1111/j.1365-2427.2005.01506.x.

Pedroli, B., G. de Blust, K. van Looy, and S. van Rooij (2002), Setting targets in strategies for river restoration, *Landscape Ecology*, *17*(1), 5–18, doi:10.1023/A:1015221425315.

Phillips, F. M., G. E. Hall, and M. E. Black (2011), *Reining in the Rio Grande: people, land, and water*, University of New Mexico Press, Albuquerque.

Phippen, S. J., and E. Wohl (2003), An assessment of land use and other factors affecting sediment loads in the Rio Puerco watershed, New Mexico, *Geomorphology*, *52*(3–4), 269–287, doi:10.1016/S0169-555X(02)00261-1.

Platania, S. P. (1991), Fishes of the Rio Chama and Upper Rio Grande, New Mexico, with Preliminary Comments on Their Longitudinal Distribution, *The Southwestern Naturalist*, *36*(2), 186–193, doi:10.2307/3671919.

Poff, N. L., J. D. Allan, M. B. Bain, J. R. Karr, K. L. Prestegaard, B. D. Richter, R. E. Sparks, and J. C. Stromberg (1997), The natural flow regime, *BioScience*, 769–784.

Poff, N. L., J. D. Olden, D. M. Merritt, and D. M. Pepin (2007), Homogenization of regional river dynamics by dams and global biodiversity implications, *Proceedings of the National Academy of Sciences*, *104*(14), 5732–5737.

Poulsen, J. B., F. Hansen, N. B. Ovesen, S. E. Larsen, and B. Kronvang (2014), Linking floodplain hydraulics and sedimentation patterns along a restored river channel: River Odense, Denmark, *Ecological Engineering*, *66*, 120–128, doi:10.1016/j.ecoleng.2013.05.010.

Proust, S., D. Bousmar, N. Riviere, A. Paquier, and Y. Zech (2009), Nonuniform flow in compound channel: A 1-D method for assessing water level and discharge distribution, *Water Resources Research*, *45*(12), n/a-n/a, doi:10.1029/2009WR008202.

Richard, G., and P. Julien (2003), Dam impacts on and restoration of an alluvial river-Rio Grande, New Mexico, *International Journal of Sediment Research*, *18*(2), 89–96.

Richards, K., J. Brasington, and F. Hughes (2002), Geomorphic dynamics of floodplains: ecological implications and a potential modelling strategy, *Freshwater Biology*, *47*(4), 559–579, doi:10.1046/j.1365-2427.2002.00920.x.

Sanders, B. F., J. C. Pau, and D. A. Jaffe (2006), Passive and active control of diversions to an off-line reservoir for flood stage reduction, *Advances in water resources*, *29*(6), 861–871.

Schmidt, J. C., and P. R. Wilcock (2008), Metrics for assessing the downstream effects of dams: METRICS FOR ASSESSING EFFECTS OF DAMS, *Water Resources Research*, *44*(4), n/a-n/a, doi:10.1029/2006WR005092.

Schulz, M., H.-P. Kozerski, T. Pluntke, and K. Rinke (2003), The influence of macrophytes on sedimentation and nutrient retention in the lower River Spree (Germany), *Water Research*, *37*(3), 569–578, doi:10.1016/S0043-1354(02)00276-2.

Scott, D. T., R. F. Keim, B. L. Edwards, C. N. Jones, and D. E. Kroes (2014), Floodplain biogeochemical processing of floodwaters in the Atchafalaya River Basin during the Mississippi River flood of 2011: Atchafalaya Basin nutrient processing, *Journal of Geophysical Research: Biogeosciences*, *119*(4), 537–546, doi:10.1002/2013JG002477.

Scurlock, D. (1998), *From the Rio to the Sierra: An Environmental History of the Middle Rio Grande Basin. General Technical Report RMRS-GTR-5.*, US Department of Agriculture, Forest Service, Rocky Mountain Research Station, Fort Collins, CO.

Shafroth, P. B., J. R. Cleverly, T. L. Dudley, J. P. Taylor, C. V. Riper, E. P. Weeks, and J. N. Stuart (2005), Control of Tamarix in the Western United States: Implications for Water Salvage, Wildlife Use, and Riparian Restoration, *Environmental Management*, *35*(3), 231–246, doi:10.1007/s00267-004-0099-5.

Shankman, D. (1996), Stream Channelization and Changing Vegetation Patterns in the U. S. Coastal Plain, *Geographical Review*, *86*(2), 216, doi:10.2307/215957.

Shankman, D., and S. A. Samson (1991), Channelization effects on Obion River flooding, western Tennessee, *Journal of American Water Resources Association (JAWRA)*, *27*(2), 247–254.

Shiono, K., and D. W. Knight (1991), Turbulent open-channel flows with variable depth across the channel, *Journal of Fluid Mechanics*, *222*, 617–646.

Sholtes, J. S., and M. W. Doyle (2010), Effect of channel restoration on flood wave attenuation, *Journal of Hydraulic Engineering*, *137*(2), 196–208.

Snell, J., M. Sivapalan, and B. Bates (2004), Nonlinear kinematic dispersion in channel network response and scale effects: application of the meta-channel concept, *Advances in Water Resources*, *27*(2), 141–154, doi:10.1016/j.advwatres.2003.11.003.

Sommer, T. R., W. C. Harrell, A. M. Solger, B. Tom, and W. Kimmerer (2004), Effects of flow variation on channel and floodplain biota and habitats of the Sacramento River, California, USA, *Aquatic Conserv: Mar. Freshw. Ecosyst.*, *14*(3), 247–261, doi:10.1002/aqc.620.

Stanford, J. A., J. V. Ward, W. J. Liss, C. A. Frissell, R. N. Williams, J. A. Lichatowich, and C. C. Coutant (1996), A general protocol for restoration of regulated rivers, *US Department of Energy Publications*, 43.

Steiger, J., E. Tabacchi, S. Dufour, D. Corenblit, and J.-L. Peiry (2005), Hydrogeomorphic processes affecting riparian habitat within alluvial channel-floodplain river systems: a review for the temperate zone, *River Research and Applications*, *21*(7), 719–737, doi:10.1002/rra.879.

Stone, M. C., C. F. Byrne, and R. R. Morrison (2017), Evaluating the impacts of hydrologic and geomorphic alterations on floodplain connectivity, *Ecohydrology*, doi:10.1002/eco.1833.

Swanson, B. J., G. A. Meyer, and J. E. Coonrod (2011), Historical channel narrowing along the Rio Grande near Albuquerque, New Mexico in response to peak discharge reductions and engineering: magnitude and uncertainty of change from air photo measurements, *Earth Surface Processes and Landforms*, *36*(7), 885–900, doi:10.1002/esp.2119.

Syvitski, J. P., C. J. Vörösmarty, A. J. Kettner, and P. Green (2005), Impact of humans on the flux of terrestrial sediment to the global coastal ocean, *Science*, *308*(5720), 376–380.

Tal, M., and C. Paola (2010), Effects of vegetation on channel morphodynamics: results and insights from laboratory experiments, *Earth Surf. Process. Landforms*, *35*(9), 1014–1028, doi:10.1002/esp.1908.

Taylor, J. P., D. B. Wester, and L. M. Smith (1999), Soil disturbance, flood management, and riparian woody plant establishment in the Rio Grande floodplain, *Wetlands*, *19*(2), 372–382.

Tetra Tech EM Inc. (2004), *Habitat Restoration Plan for the Middle Rio Grande*, New Mexico Interstate Stream Commission, Albuquerque, NM, USA.

Thoms, M. C. (2003), Floodplain–river ecosystems: lateral connections and the implications of human interference, *Geomorphology*, *56*(3–4), 335–349, doi:10.1016/S0169-555X(03)00160-0.

Thoms, M. C., and M. Parsons (2003), Identifying spatial and temporal patterns in the hydrological character of the Condamine–Balonne river, Australia, using multivariate statistics, *River Res. Applic.*, *19*(5–6), 443–457, doi:10.1002/rra.737.

Thorp, J. H., M. C. Thoms, and M. D. Delong (2006), The riverine ecosystem synthesis: biocomplexity in river networks across space and time, *River Res. Applic.*, *22*(2), 123–147, doi:10.1002/rra.901.

Tobin, G. A. (1995), The Levee Love Affair: A Stormy Relationship?1, *JAWRA Journal of the American Water Resources Association*, *31*(3), 359–367, doi:10.1111/j.1752-1688.1995.tb04025.x.

Tockner, K., D. Pennetzdorfer, N. Reiner, F. Schiemer, and J. V. Ward (1999), Hydrological connectivity, and the exchange of organic matter and nutrients in a dynamic river–floodplain system (Danube, Austria), *Freshwater Biology*, *41*(3), 521–535, doi:10.1046/j.1365-2427.1999.00399.x.

Tockner, K., F. Malard, J. V. Ward, and others (2000), An extension of the flood pulse concept, *Hydrological processes*, *14*(16–17), 2861–2883.

Tunstall, S. M., E. C. Penning-Rowsell, S. M. Tapsell, and S. E. Eden (2000), River Restoration: Public Attitudes and Expectations, *Water and Environment Journal*, *14*(5), 363–370, doi:10.1111/j.1747-6593.2000.tb00274.x.

Turner-Gillespie, D. F., J. A. Smith, and P. D. Bates (2003), Attenuating reaches and the regional flood response of an urbanizing drainage basin, *Advances in Water Resources*, *26*(6), 673–684, doi:10.1016/S0309-1708(03)00017-4.

Valett, H. M., M. A. Baker, J. A. Morrice, C. S. Crawford, M. C. Molles Jr, C. N. Dahm, D. L. Moyer, J. R. Thibault, and L. M. Ellis (2005), Biogeochemical and metabolic responses to the flood pulse in a semiarid floodplain, *Ecology*, *86*(1), 220–234.

Van Cleave, M. (1935), *Vegetative changes in the Middle Rio Grande Conservancy District*, University of New Mexico.

Vermaas, D. A., W. S. J. Uijttewaal, and A. J. F. Hoitink (2011), Lateral transfer of streamwise momentum caused by a roughness transition across a shallow channel, *Water Resour. Res.*, *47*(2), W02530, doi:10.1029/2010WR010138.

Vivoni, E. R., R. S. Bowman, R. L. Wyckoff, R. T. Jakubowski, and K. E. Richards (2006), Analysis of a monsoon flood event in an ephemeral tributary and its downstream hydrologic effects, *Water Resources Research*, *42*(3), doi:10.1029/2005WR004036.

Ward, J. V. (1989), The Four-Dimensional Nature of Lotic Ecosystems, *Journal of the North American Benthological Society*, *8*(1), 2, doi:10.2307/1467397.

Ward, J. V., and J. A. Stanford (1995), Ecological connectivity in alluvial river ecosystems and its disruption by flow regulation, *Regulated Rivers: Research & Management*, *11*(1), 105–119.

Ward, J. V., K. Tockner, U. Uehlinger, and F. Malard (2001), Understanding natural patterns and processes in river corridors as the basis for effective river restoration, *Regulated Rivers: Research & Management*, *17*(4–5), 311–323.

Ward, J. V., F. Malard, and K. Tockner (2002), Landscape ecology: a framework for integrating pattern and process in river corridors, *Landscape Ecology*, *17*(1), 35–45, doi:10.1023/A:1015277626224.

Welcomme, R. L. (1979), *Fisheries ecology of floodplain rivers*, Longman, London; New York.

Winemiller, K. O., A. S. Flecker, and D. J. Hoeinghaus (2010), Patch dynamics and environmental heterogeneity in lotic ecosystems, *Journal of the North American Benthological Society*, *29*(1), 84–99, doi:10.1899/08-048.1.

Wohl, E., P. L. Angermeier, B. Bledsoe, G. M. Kondolf, L. MacDonnell, D. M. Merritt, M. A. Palmer, N. L. Poff, and D. Tarboton (2005), River restoration, *Water Resources Research*, *41*(10), n/a-n/a, doi:10.1029/2005WR003985.

Wohl, E., S. N. Lane, and A. C. Wilcox (2015), The science and practice of river restoration, *Water Resources Research*, *51*(8), 5974–5997, doi:10.1002/2014WR016874.

Wolff, C. G., and S. J. Burges (1994), An analysis of the influence of river channel properties on flood frequency, *Journal of Hydrology*, *153*(1), 317–337.

Woltemade, C. J., and K. W. Potter (1994), A watershed modeling analysis of fluvial geomorphologic influences on flood peak attenuation, *Water Resour. Res.*, *30*(6), 1933–1942, doi:10.1029/94WR00323.

Wong, T. H. F., and E. M. Laurenson (1983), Wave speed–discharge relations in natural channels, *Water Resour. Res.*, *19*(3), 701–706, doi:10.1029/WR019i003p00701.

Woodson, R. C., J. T. Martin, and G. Cochiti (1965), The Rio Grande comprehensive plan in New Mexico and its effects on the river regime through the middle valley, in *Symposium 1.-Land Erosion and Control*, vol. 618, p. 357.

Wyzga, B. (1996), Changes in the Magnitude and Transformation of Flood Waves Subsequent to the Channelization of the Raba River, Polish Carpathians, *Earth Surf. Process. Landforms*, *21*(8), 749–763, doi:10.1002/(SICI)1096-9837(199608)21:8<749::AID-ESP675>3.0.CO;2-5.

Yang, K., S. Cao, and D. W. Knight (2007), Flow patterns in compound channels with vegetated floodplains, *Journal of Hydraulic Engineering*, *133*(2), 148–159.

Appendices

Appendix A

The following appendix describes an investigation into the uncertainty involved with unsteady flow modeling when channel and floodplain microtopography are not known. This technical note will likely be submitted for publication in a peer-reviewed scientific journal.

Addressing uncertainty in the parameterization of hydrodynamic models for unsteady flow scenarios

Introduction

Development of two-dimensional hydrodynamic models includes substantial uncertainty most often dealing with the definition of the element specific parameters: elevation and roughness. Because elevation is typically a measured value from a given data source while roughness is often an estimate based upon user experience, roughness frequently becomes an effective parameter to account for momentum dissipation that is not captured in the process-based numerical equations and adjusted to produce optimal model performance [*Lane and Richards*, 1998; *Morvan et al.*, 2008]. A substantial amount of research has presented the implications for varying topographic inputs on flood inundation patterns [*Hardy, R.J. et al.*, 1999; *Casas et al.*, 2006; *Charrier and Li*, 2012; *Md Ali et al.*, 2015; *Witt III*, 2015], as well as flood stage [*Schumann et al.*, 2008]. Remote sensing techniques like light detection and ranging (LiDAR) are the most effective methods to produce satisfactory model results [*Casas et al.*, 2006; *Schumann et al.*, 2008; *Witt III*, 2015]. Because previous research has focused predominantly on flood inundation mapping, understanding of how topographic and roughness uncertainty influence river processes during unsteady flow events is necessary. Difficulty in calibration of a model for both inundation and wave celerity has been demonstrated in simplified raster-based modeling efforts [*Horritt and Bates*, 2001]. However, uncertainties associated with unsteady flows in fully two-dimensional flood models need to be addressed as these types of modeling efforts are now considerably more prevalent with recent increases in computational power.

Historical models can provide important insights into changes in river conditions and processes, however creation of these models produces new questions in regard to uncertainty. Previous historical model development has analyzed fish habitat [*Jacobson and Galat*, 2006] and floodplain inundation patterns [*Hesselink et al.*, 2003]. These studies both contribute to the general understanding of the ways in which rivers have changed. However, it is likely that all historical models are subject to limited data sources and data quality. In order to make appropriate conclusions from historical models in comparison with present-day models, uncertainty is important to address. Topographic uncertainty has been shown to have a substantial impact on model results even with modern data sources [*Legleiter et al.*, 2011]. Therefore, uncertainty of historical model results is likely to increase greatly. For example, if the channel and floodplain elevations lack the detail to include microtopography, defined here as topographic heterogeneity on the scale of 1 cm to 1 m [*Moser et al.*, 2007], then it is likely that roughness would need to be increased to account for the momentum dissipation of the missing microtopography. This produces an interesting link between the roughness and elevation parameterization. While previous studies have shown that smoothed topographic data produce inferior inundation mapping results to modern topographic inputs such as LiDAR [*Casas et al.*, 2006; *Witt III*, 2015], quantification of hydrodynamic processes in historical scenarios may still be achievable through manipulation of roughness parameterization.

The objective of this research was to analyze the uncertainty associated with topographic and roughness parameterization in two-dimensional modeling applications with a focus on historical data sources and unsteady flow events. These parameters are fundamental to creation of an appropriate model and are difficult to describe in historical models due to lack of accessible data or resolution of existing historical data. The objective was achieved by: (1) analyzing a historical model and defining the differences in historical parameterization data compared with current data; (2) investigating the uncertainty of these defined differences in parameterization data in a modern river reach using statistical analysis of the differences between various parameterization techniques. It is believed that this approach will be helpful in the development of historical models in the future. Historical models have the potential to inform river science regarding how systems have changed either due to natural or anthropogenic influence.

Methods

Site Description

Modeling for this study was conducted on a portion of the Rio Grande known as the Albuquerque Reach of the Middle Rio Grande (MRG) in central New Mexico. This stretch of river historically existed in a broad, alluvial valley and was described as a braided, sand-bed river. Over the past century, the river has been manipulated with modern river engineering for the purpose of water use and flood protection. With a constricted floodplain and fortified banks producing a river that is better suited for water deliveries than ecological processes, the Albuquerque Reach of the Rio Grande provides an excellent environment for a case-study on the impacts that river engineering has on hydrodynamic processes, specifically flood wave attenuation. It is in this context that a historical model was developed.

Historical Model Development

Input data were collected to represent conditions prior to significant river engineering practices. Channel cross-sections originated from survey information from 1936 while 1918 elevation contours with 0.61 m (2 foot) spacing were used to interpolate floodplain elevations. In addition, a 1918 land use map was digitized to represent general roughness classifications within the Rio Grande valley. Clearly, the use of data from different years means the constructed model does not represent any specific condition in time, but instead a representative condition of the channel and floodplain from that time period. This historical model was developed for the purpose of studying anthropogenic influences on the large-scale river process of flood wave attenuation.

Historical Model Uncertainty

If the goal of historical modeling is to provide a context or comparison for modern river process quantification, the historical model should function with a similar amount of uncertainty as the contemporary model. Because the historical model for the Albuquerque Reach of the Rio Grande was developed with the most detailed data

138

collected during that time period and the model represents a time period before stream gaging in the reach, it is impossible to test the uncertainty of the model or to calibrate the model to flow data. Therefore, this research addresses historical model uncertainty through the lens of the modern river channel and floodplain. In this way, similar attributes of the historical model can be tested in comparison with modern data sources and resolutions.

Uncertainty of topography and roughness parameterization are the main focus of this research as these are necessary parameters for each element of a two-dimensional mesh. Historical topography data sources are likely the greatest cause of increased uncertainty in historical modeling efforts. Existing roughness tables are often based upon sediment, bed form, and vegetation characteristics. With modern hydrodynamic floodplain topography based upon high resolution data, often light detection and ranging (LiDAR) sourcing, topography captured in a hydrodynamic model is complex. This is important to inundation dynamics. However, because historical data lacks the same amount of detail, flow processes are likely to be greatly impacted and inundation patterns have been shown to differ. It is anticipated that changes in small-scale flow processes associated with lack of microtopography are likely to influence the large-scale river process of attenuation as well. In comparison, uncertainty associated with roughness may not change drastically between historical and contemporary sources as roughness characterization is often lumped or distributed at an aerially digitized scale, that was possible in the creation of the historical model in this research. Roughness will, however, remain a catch-all for any momentum loss not captured by the other terms in the momentum equations [*Lane and Richards*, 1998; *Morvan et al.*, 2008].

Modeling Potential Historical Uncertainty

Because historical channel bathymetry may be difficult to obtain or be limited in extent, two alternatives for channel bathymetry were used in this study: (1) a channel described using traditional cross-sections surveys, and (2) a channel described using a planar bottom at a mean elevation. The cross-section bathymetry was created using existing United States Bureau of Reclamation (USBR) cross-section data from 2010. These cross-sections were imported into the Hydrologic Engineering Center's River

Analysis System (HEC-RAS) and 50 m cross-sections were interpolated. The cross-sections were then exported to ESRI's ArcMap where a triangular irregular network was created and converted to a digital elevation model (DEM) for the channel bottom. The simplified planar bathymetry was created using USBR cross-section data as well. Elevations from data points at each cross-section within the USBR defined active-channel were averaged to create a single elevation at each cross-section. ArcMap was again used to create a plane representative of downstream average channel elevation. The area of the active channel was then extracted from this plane. Although this method used cross-section information, it is an easier method for historical models in that a similar channel description could be made based on estimated channel depth or width-depth relationships. In addition, due to the uncertainty associated with highly dynamic channel beds of sand-bed rivers, the researchers were interested in how this simplified method influences modeled flood wave processes. The two methods constitute opposite ends of the spectrum in the representation of channel bathymetry using cross-section data.

One of the clear differences between historical topography and modern collection techniques is the lack of microtopography within historical data sources. To investigate the influences of this difference, two types of floodplain topographies were utilized: (1) floodplain topography was described with a LiDAR dataset, and (2) floodplain topography was described using a 30-m focal mean for each data point, thus creating a floodplain with minimal local microtopography. It is worth noting that the floodplain elevations derived from spatially-averaging LiDAR elevations may in fact be more precise than those elevations interpolated from historical contours. However, because there is no way of testing historical contours for accuracy, the historical elevations need to be considered representative. This method only attempts to describe the influence of effectively smoothed topography on flood wave dynamics.

With two types of channel bathymetry and two types of floodplain topography, three distinct models were created. All models used the same two-dimensional mesh with an element resolution of 40 m^2 and 725,310 total elements but with differing combinations of channel and floodplain topography to focus on one difference between historical and modern variations (Table A1). D-Flow Flexible Mesh (D-Flow FM), a finite-volume modeling program from Deltares, Inc., was chosen for mesh development

and modeling due to the ability to partition constructed meshes and perform parallel computations. Curvilinear mesh elements were created for the main sand-bed channel while vegetated islands and floodplains were represented with triangular elements. Roughness values were described in terms of Manning's n-values. Floodplain and vegetated island roughness values were distributed based upon 2008 aerial vegetation mapping [*Hink and Ohmart*, 1984; *Mussetter Engineering*, 2002] and held constant throughout the model runs (Table A2). Channel roughness was a lumped parameter which varied during steady model simulations investigating channel bathymetry and was held constant during steady investigations of floodplain topography as well as unsteady simulations (Table A3).

Table A1. Definitions of models created with differing topographic description.

Model	ID	Channel Bathymetry	Floodplain Topography
1	XSL	Cross-section	LiDAR
2	PL	Plane	LiDAR
3	XSA	Cross-section	Focal Average

Table A2. Floodplain Manning's roughness characterization.

Roughness Description	Manning's n-value
Agriculture	0.045
Open / bare ground / scattered brush-weeds	0.045
Scattered trees / light brush	0.060
Medium density trees / brush	0.080
Dense trees / brush	0.100
Urban / industrial	0.080

Table A3. Channel Manning's roughness characterization

Model	Steady Flows	Unsteady Flows
1	0.025 - 0.031	0.025
2	0.025 - 0.031	0.031
3	0.025	0.025

Modeled Hydrology

In order to investigate the hydrodynamic uncertainties of the Albuquerque Reach of the Rio Grande, both steady and unsteady discharges were modeled. All steady

simulations in this research were conducted at a moderate-high discharge of 142 m^3s^{-1} (5000 ft^3s^{-1}). This discharge is high enough to overbank in some areas of the modern river channel and remain contained within the main channel in other areas. All steady flow events were run for 96 hours. Because the amount of mass associated with a flood wave is likely to be relevant to flood wave attenuation (i.e. a smaller wave will be attenuated more quickly), six different flood waves were modeled. All flood waves had the same magnitude, 150 m^3s^{-1}, relative to the initial flow conditions, but both initial conditions and the duration of the events varied. Figure A1 displays the three flood waves with discrete durations at initial conditions of 30 m^3s^{-1}. The same flood waves were repeated for initial conditions of 150 m^3s^{-1}.
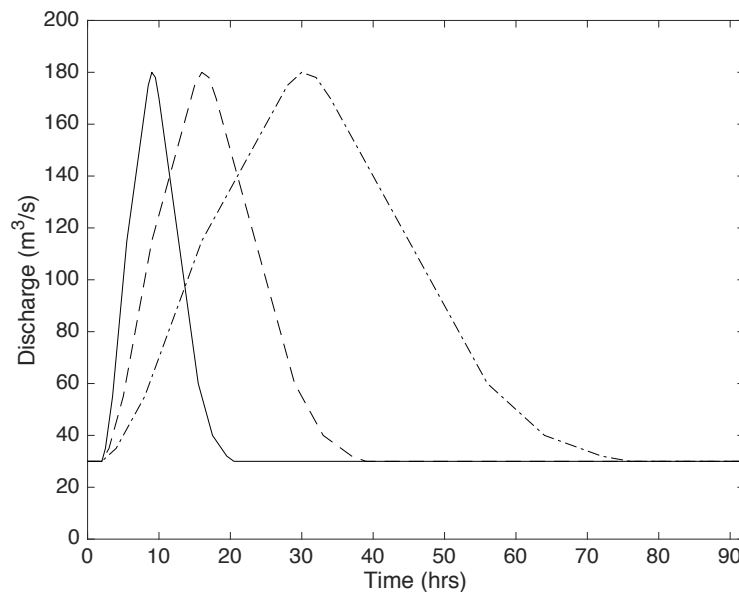

Figure A1. Small magnitude flood waves input to upstream boundary of models.

Model Output Analysis

Steady and unsteady model results were analyzed in the context of historical model uncertainty and implications for modeling river process. Floodplain inundation under steady flow scenarios was described in terms of frequency distributions and qualitative spatial representation. Implications of variable roughness values were investigated in the comparison cross-sectional and planar channel bathymetry with the goal of understanding how roughness must be adjusted to account for higher detail in

142

channel bathymetry. A one-sample t-test using the difference between cross-sectional and planar floodplain inundation predictions was used to determine which combination of roughness values assigned to the respective models produced the most similar results. Because of differences in water surface elevations due to contrasting channel bathymetry through the river reach, a mean of zero in the frequency distributions was taken to indicate the models are performing in a similar manner to produce comparable river processes. These results informed the channel roughness values for unsteady flow scenarios. Unsteady flood waves were analyzed for differences in percent attenuation and time of peak at 14 km downstream, the approximate midpoint of the modeled reach. Percent attenuation was calculated using the following equation:

$$A = \frac{(Q_{Up} - Q_{14p})}{Q_{Up}} * 100$$

where A is percent attenuation, Q_{Up} is upstream peak discharge, and Q_{14p} is measure peak discharge at 14 km downstream.

Results and Discussion

Steady Flow Scenarios

The hydrodynamic models were run under steady flow conditions to investigate the relationship between the channel bathymetry description and bed roughness parameterization. Frequency distributions between XSL and PL models show that roughness values must be considerably different depending on how channel bathymetry is described (Fig. A2). None of the distributions had a statistically significant mean of zero. However, when compared with XSL model runs that used a Manning's roughness value of 0.025, the PL model with a roughness value of 0.031 produced the mean statistically closest to zero (Table A4). In addition, the models had the smallest difference in water volume on the floodplain. Since mass transfer to the floodplain is an important process in flood wave attenuation, these results suggest a similar amount of mass transfer has occurred in the models. Therefore, 0.025 and 0.031 were used for the main channel in

unsteady model simulations for the cross-section and planar bathymetries, respectively. It should be noted that these results do not address the question regarding the correct roughness values for the modeled reach, but instead focus on how changes to model parameters can impact model results. It is clear that notably different roughness values must be used to produce similar results in terms of total floodplain inundation when different methods of channel bathymetry description are utilized. Therefore, if historical models are created using simplified techniques, care must be taken to select an appropriate roughness value for both the channel and floodplain given the chosen method.
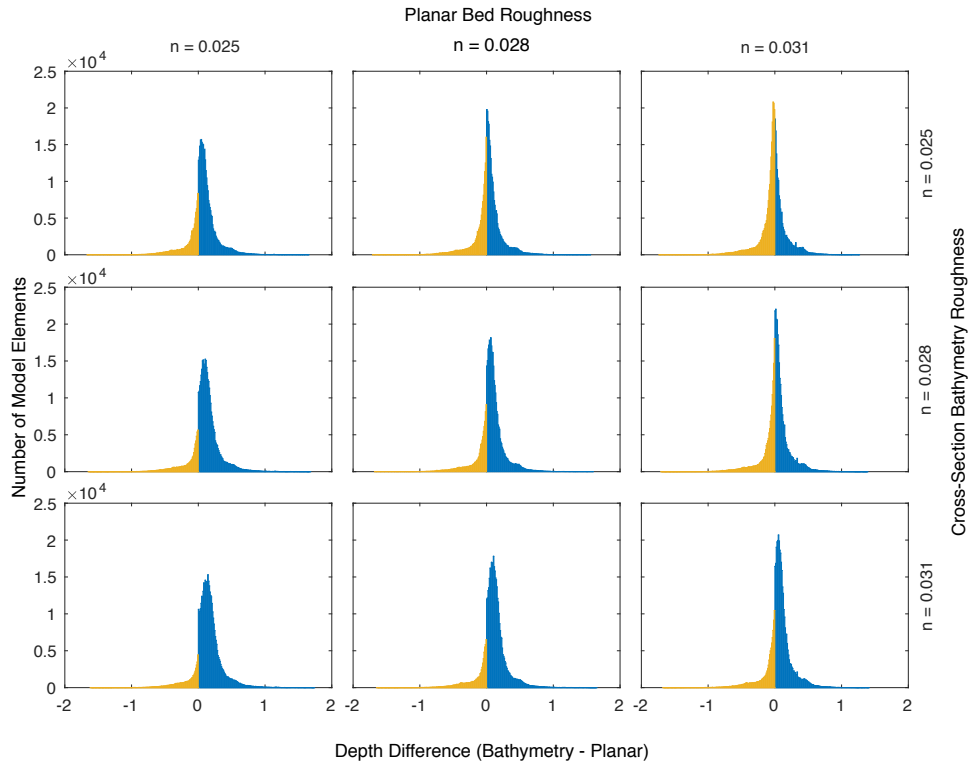

Figure A2. Frequency distributions describing floodplain inundation differences between cross-sectional and planar channel bathymetry model predictions. Yellow coloring indicates greater depth in Bathymetry model while blue coloring indicates greater depth in Planar model.

Table A4. Statistical evaluation of inundation differences between cross-sectional and planar model simulations.

Cross-sectional n-value	Planar n-value	Mean Difference in Floodplain Depth (m) (Cross-sectional - Planar)	Total Difference in Floodplain Volume (m^3)
0.025	0.025	0.0912	4.72E+05
0.025	0.028	0.0446	2.31E+05
0.025	0.029	0.0268	1.37E+05
0.025	0.030	0.0112	5.31E+04
0.025	0.031	-0.0029	-2.45E+04
0.028	0.025	0.1266	7.32E+05
0.028	0.028	0.0849	4.91E+05
0.028	0.031	0.0410	2.35E+05
0.031	0.025	0.1552	9.96E+05
0.031	0.028	0.1176	7.55E+05
0.031	0.031	0.0778	5.00E+05

Steady analysis of the XSA model compared to the XSL model yields logical results when comparing inundation patterns. Similar to previous studies, total inundated area is greater for the smooth floodplain approach than the LiDAR-derived approach. However, in the analysis of the frequency distribution comparing inundation patterns, it is clear the differences in inundation are not Gaussian in form (Fig. A3). The spike in values in which XSL inundation is greater than XSA between 0 and approximately 0.2 m likely shows the result of the 'filling' of depressions in the landscape and floodplain channels where the XSL model predicts the most significant floodplain inundation. In comparison, total area of inundation is increased and total number of elements inundated is more uniformly impacted in areas where the XSA inundation is greater than the XSL inundation.
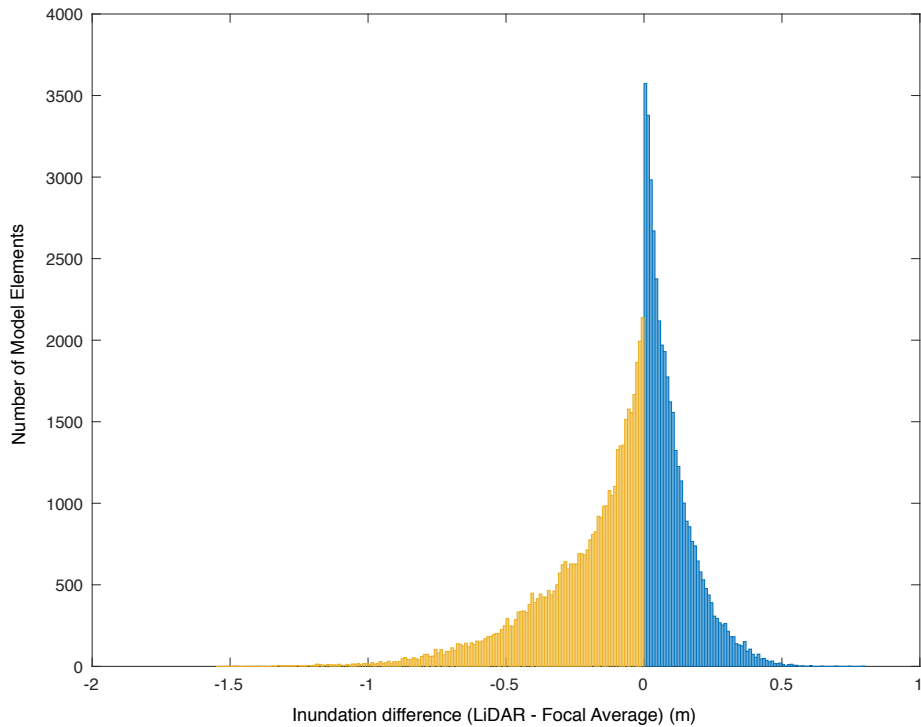
Figure A3. A frequency distribution describing floodplain inundation differences between models using LiDAR and focal average descriptions of floodplain elevation. Yellow coloring indicates greater depth in Focal Average model while blue coloring indicates greater depth in LiDAR model.

Qualitative spatial analysis displays the inundation differences of each element when comparing different model types but also the differences in large scale patterns of inundation (Fig. A4). Comparison of XSL and PL models shows floodplain inundation is similar for large portions of the floodplain, however, the greater floodplain inundation shifts from either the XSL (purple tint) or the PL model (orange tint) over large spatial trends rather than more specific microtopography influences. This is likely due to changes in predicted main channel water surface elevation for each model as floodplain elevations are the same. While inundation patterns may not be as accurate with planar bathymetry, river process may be retained when appropriate adjustments to roughness parameterization are made. In contrast, inundation patterns are considerably different when comparing XSL and XSA models. As the histogram presented above suggested, side channels and depressions have greater inundation depth in the XSL model while

averaging of floodplain elevations creates a more uniform distribution of water, as well as a larger area inundated in the XSA model. The greater volume of water being transferred to the floodplain would suggest greater mass transfer processes accruing, but lack of microtopography likely has an influence on momentum dissipation as well. In this context, unsteady flows were investigated.
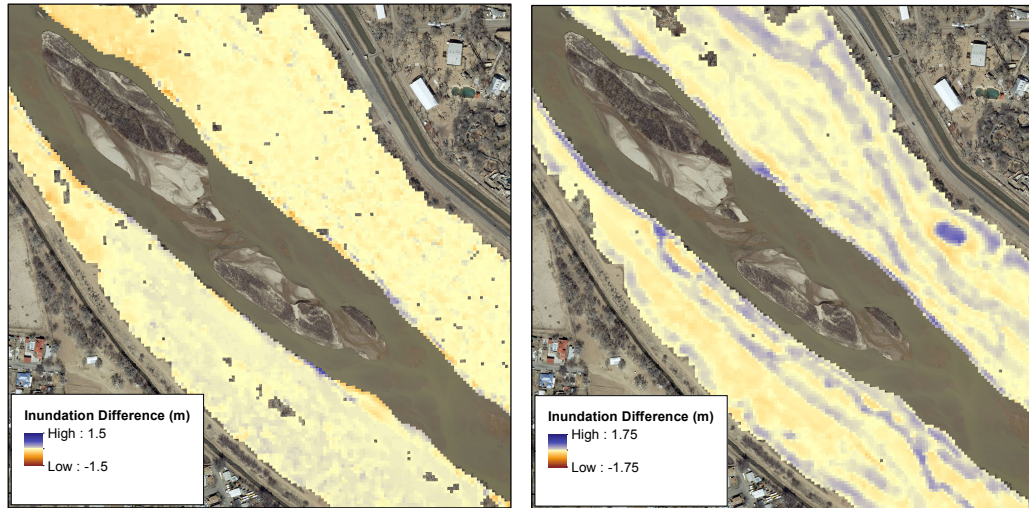

Figure A4. Spatial comparison of floodplain inundation differences between a) XSL and PL and b) XSL and XSA models.

Unsteady Flow Scenarios

Flood waves at three durations and two initial conditions were modeled for the each of the models. Results suggest that the degree of attenuation is dependent on the inclusion of floodplain microtopography included in the model (Tables A5 and A6). As expected, model results indicate a greater percent attenuation for flood waves that occurred with low initial flow than high initial flow. While this metric measures attenuation in the reach, of more interest in this paper are differences in attenuation between the three models. The first noticeable difference is that the XSA model produced less attenuation in the low magnitude scenario for the short duration event, but greater attenuation in the long duration event for the same initial flow. This reversal of which model predicts maximum attenuation is likely due to the ability of water in the long duration flood wave to spread out over the floodplain in the XSA model. In this regard,

147

total area inundated is important and mass transfer is the dominant process important to attenuation. However, when baseflow was increased the trends in attenuation change. The XSA model always has the least amount of attenuation. At the high baseflow, a considerable amount of the floodplain is inundated already. Therefore, the impact of water spreading out over a uniform floodplain is negated and microtopography in the XSL and BL models begins to have a greater impact. It is most probable in this instance that mass transfer to portions of the previously dry XSL and BL floodplains as well as increased momentum dissipation due to microtopography create greater attenuation in these models. Increases to floodplain roughness values in models created without microtopography may be necessary to generate similar quantities of river process. However, the degree of adjustment is clearly dependent on the type of flood wave and the initial conditions when the flood wave occurs.

Although to a lesser extent, results indicate that channel bathymetry also has an impact on attenuation. The PL model predicts equal or greater peak flow attenuation in all model runs when compared to the XSL model. There are two possible explanations for these differences. One possible explanation concerns the volume of water transferred to the floodplain from the main channel. In spite of the fact that the roughness value used for the channel in the unsteady PL model most closely matched inundation volumes of the XSL model during steady flow scenarios, the PL model does have slightly more water volume on the floodplain than the XSL. This additional mass transfer during unsteady simulations is likely to have an impact on flood wave attenuation, but to what degree is unknown at this time. The second possible explanation is the lack of thalweg present in the PL model. It would be expected that the thalweg in the XSL bathymetry has greater velocities than anywhere in the PL bathymetry due to the increased depth. The thalweg therefore would likely promote less attenuation than a uniform channel bottom. This alternative would also be supported by the lesser time to peak in the XSL model results for the majority of simulations.

Table A5. Unsteady flow simulation results for events having 180 m^{3}s^{-1} upstream peak discharge (PD14km – Peak discharge at 14 km downstream; PA14km – Percent attenuation at 14 km downstream; TP14km – Time of peak at 14 km downstream).

Model ID	1-day duration event			1.5-day duration event			3-day duration event		
	PD14km (m^{3}s^{-1})	PA14km	TP14km (hr)	PD14km (m^{3}s^{-1})	PA14km	TP14km (hr)	PD14km (m^{3}s^{-1})	PA14km	TP14km (hr)
XSL	158.3	12.1	13.50	170.5	5.3	20.75	176.0	2.2	35.00
PL	158.2	12.1	13.25	169.8	5.7	20.75	175.4	2.5	35.25
XSA	162.5	9.7	13.50	169.6	5.8	20.75	173.5	3.6	35.00

Table A6. Unsteady flow simulation results for events having 300 m^{3}s^{-1} upstream peak discharge (PD14km – Peak discharge at 14 km downstream; PA14km – Percent attenuation at 14 km downstream; TP14km – Time of peak at 14 km downstream).

Model ID	1-day duration event			1.5-day duration event			3-day duration event		
	PD14km (m^{3}s^{-1})	PA14km	TP14km (hr)	PD14km (m^{3}s^{-1})	PA14km	TP14km (hr)	PD14km (m^{3}s^{-1})	PA14km	TP14km (hr)
XSL	267.8	10.7	13.75	289.1	3.6	21.50	296.7	1.1	35.50
PL	266.3	11.2	14.00	286.1	4.6	21.75	296.0	1.3	35.75
XSA	283.4	5.5	13.75	294.4	1.9	20.75	298.1	0.6	35.00

Conclusions

The objective of this research was to analyze uncertainty associated with data sources used for the development of historical models and assess the impacts that these uncertainties have on steady and unsteady flow predictions. This objective was achieved by the modeling of steady and unsteady flow scenarios using three models with differing channel bathymetry and floodplain topography. Steady results show the linked nature of topographic and roughness parameterization and the necessity to adjust the roughness value considerably depending on the amount of detail included in topographic parameterization. Further, interpretation of spatial inundation patterns can help inform modeling techniques that seek to quantify river processes. The results presented in this study for different parametrization techniques should help to inform future unsteady flow studies involving the quantification of anthropogenic influences on river systems from a historical perspective as well as the development of models in systems with limited data sources.

References

Casas, A., G. Benito, V. R. Thorndycraft, and M. Rico (2006), The topographic data source of digital terrain models as a key element in the accuracy of hydraulic flood modelling, *Earth Surface Processes and Landforms*, *31*(4), 444–456.

Charrier, R., and Y. Li (2012), Assessing resolution and source effects of digital elevation models on automated floodplain delineation: A case study from the Camp Creek Watershed, Missouri, *Applied Geography*, *34*, 38–46, doi:10.1016/j.apgeog.2011.10.012.

Hardy, R.J., P. D. Bates, and M. G. Anderson (1999), The importance of spatial resolution in hydraulic models for floodplain environments, *Journal of Hydrology*, *216*(1–2), 124–136, doi:10.1016/S0022-1694(99)00002-5.

Hesselink, A. W., G. S. Stelling, J. C. J. Kwadijk, and H. Middelkoop (2003), Inundation of a Dutch river polder, sensitivity analysis of a physically based inundation model using historic data, *Water Resour. Res.*, *39*(9), 1234, doi:10.1029/2002WR001334.

Hink, V. C., and Ohmart (1984), *Middle Rio Grande Biological Survey*, U.S. Army Corps of Engineers.

Horritt, M. S., and P. D. Bates (2001), Effects of spatial resolution on a raster based model of flood flow, *Journal of Hydrology*, *253*(1–4), 239–249, doi:10.1016/S0022-1694(01)00490-5.

Jacobson, R. B., and D. L. Galat (2006), Flow and form in rehabilitation of large-river ecosystems: an example from the Lower Missouri River, *Geomorphology*, *77*(3), 249–269.

Lane, S. N., and K. S. Richards (1998), High resolution, two-dimensional spatial modelling of flow processes in a multi-thread channel, *Hydrol. Process.*, *12*(8), 1279–1298, doi:10.1002/(SICI)1099-1085(19980630)12:8<1279::AID-HYP615>3.0.CO;2-E.

Legleiter, C. J., P. C. Kyriakidis, R. R. McDonald, and J. M. Nelson (2011), Effects of uncertain topographic input data on two-dimensional flow modeling in a gravel-bed river, *Water Resour. Res.*, *47*(3), W03518, doi:10.1029/2010WR009618.

Md Ali, A., D. P. Solomatine, and G. Di Baldassarre (2015), Assessing the impact of different sources of topographic data on 1-D hydraulic modelling of floods, *Hydrol. Earth Syst. Sci.*, *19*(1), 631–643, doi:10.5194/hess-19-631-2015.

Morvan, H., D. Knight, N. Wright, X. Tang, and A. Crossley (2008), The concept of roughness in fluvial hydraulics and its formulation in 1D, 2D and 3D numerical simulation models, *Journal of Hydraulic Research*, *46*(2), 191–208, doi:10.1080/00221686.2008.9521855.

Moser, K., C. Ahn, and G. Noe (2007), Characterization of microtopography and its influence on vegetation patterns in created wetlands, *Wetlands*, *27*(4), 1081–1097.

Mussetter Engineering, M. E. (2002), *Hydraulic and Sediment Continuity Modeling of the San Joaquin River from Friant Dam to Mendota Dam, California*, U.S. Bureau of Reclamation, U.S. Bureau of Reclamation.

Schumann, G., P. Matgen, M. E. J. Cutler, A. Black, L. Hoffmann, and L. Pfister (2008), Comparison of remotely sensed water stages from LiDAR, topographic contours and SRTM, *ISPRS Journal of Photogrammetry and Remote Sensing*, *63*(3), 283–296, doi:10.1016/j.isprsjprs.2007.09.004.

Witt III, E. C. (2015), Evaluation of the U.S. Geological Survey standard elevation products in a two-dimensional hydraulic modeling application for a low relief coastal floodplain, *Journal of Hydrology*, *531*, *Part 3*, 759–767, doi:10.1016/j.jhydrol.2015.10.051.

Appendix B

Methodology for Creation of Topographic Surfaces

The following text and figures describes the creation of all topographic surfaces used in hydrodynamic modeling within Chapters 2 through 4, with the exception of the historical topography modeled in Chapter 2. Methods for the creation of the historical elevation surface can be found in Adair [2016]. All contemporary topography data was acquired courtesy of the Mid-Region Council of Governments. Restoration sites and contemporary vegetation mapping were acquired from the Middle Rio Grande Endangered Species Collaborative Program.

Chapter 2 included four topographic surfaces: historical [*Adair*, 2016], pre-restoration LiDAR (Light Detection and Ranging), contemporary contour, and contemporary LiDAR model. Figure B1 displays the steps employed to create each topographic surface.

Chapter 3 included five topographic surfaces: the contemporary LiDAR model described in Chapter 2 and Figure B1, two surfaces in which the channel bed was raised or lowered by 0.3048 m (1 foot), and two surfaces in which channel banks of 10-meter width were adjusted between 0 and 0.3048 m (1 foot). Figure B2 displays the workflow for creating the topographic surfaces in which channel and bank roughness were adjusted.

Chapter 4 used only one topographic surface which was the same as the contemporary, LiDAR model presented in Chapters 2 and 3.
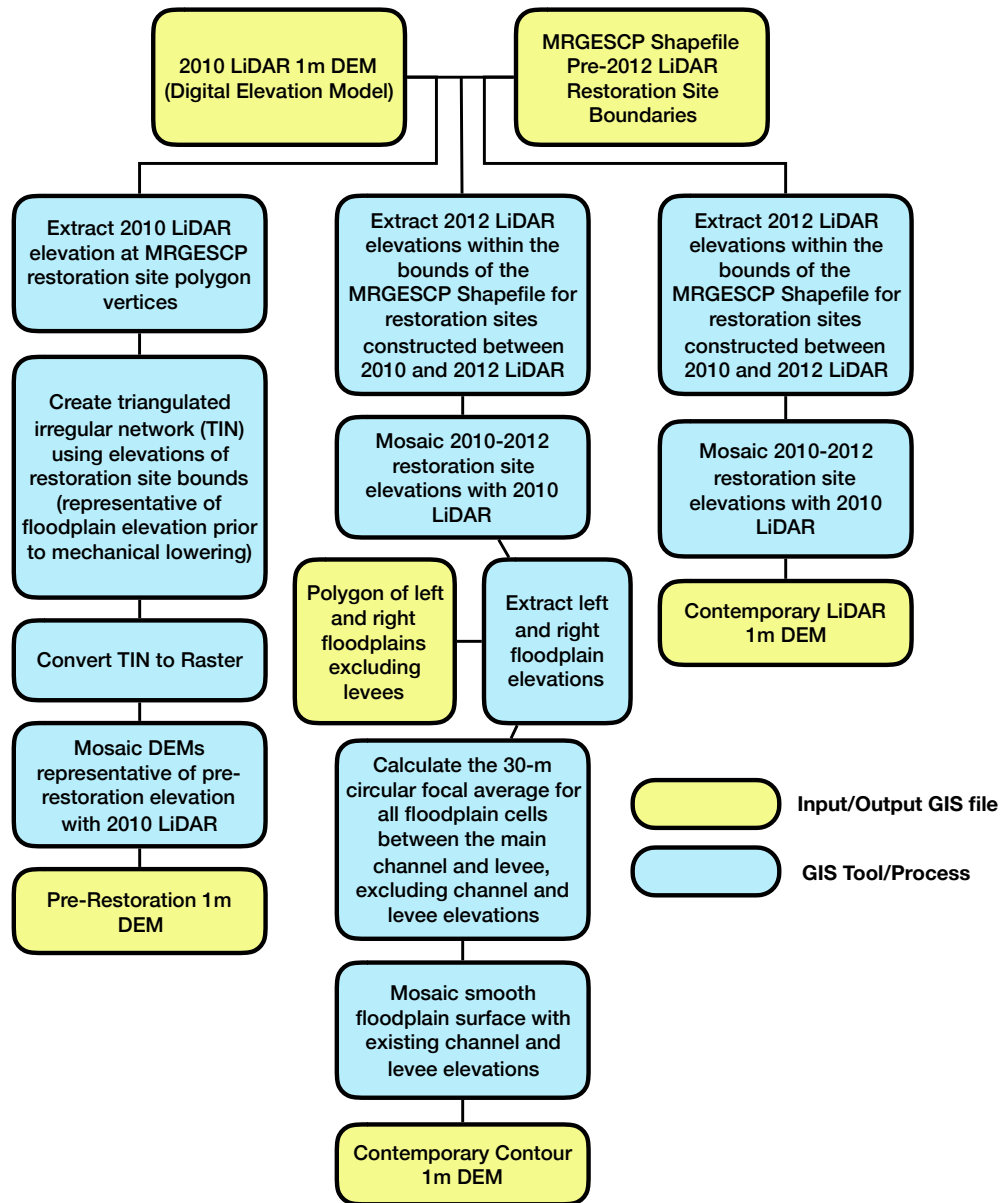
Figure B1. Workflow for pre-restoration, contemporary contour, and contemporary LiDAR topographic surfaces in Chapter 2.
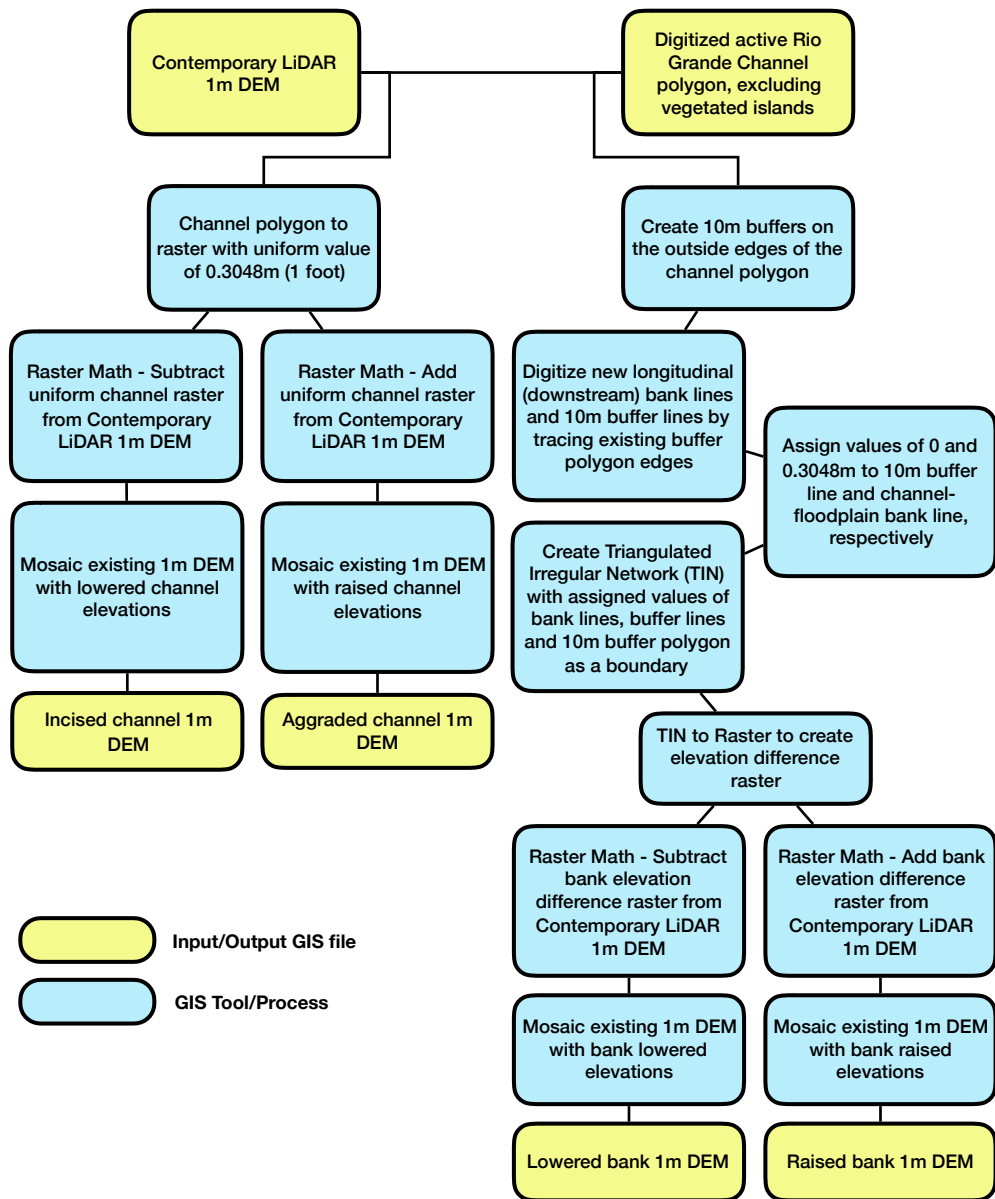
Figure B1. Workflow for incised channel, aggraded channel, lowered bank, and raised bank topographic surfaces in Chapter 3.

Appendix C

Models, Data, and Post-Processing Scripts

All models, data, and post-processing scripts are available electronically at the following link:

http://digitalrepository.unm.edu/eng_etd_data/1/